

1. Report No. FHWA/TX-06/0-4468-3		2. Government Accession No.		3. Recipient's Catalog No.	
4. Title and Subtitle APPLICATION OF CALIBRATED MECHANISTIC FATIGUE ANALYSIS WITH AGING EFFECTS				5. Report Date November 2006 Resubmitted: May 2006 Published: July 2006	
				6. Performing Organization Code	
7. Author(s) Lubinda F. Walubita, Amy Epps Martin, Sung Hoon Jung, Charles J. Glover, and Eun Sug Park				8. Performing Organization Report No. Report 0-4468-3	
9. Performing Organization Name and Address Texas Transportation Institute The Texas A&M University System College Station, Texas 77843-3135				10. Work Unit No. (TRAIS)	
				11. Contract or Grant No. Project 0-4468	
12. Sponsoring Agency Name and Address Texas Department of Transportation Research and Technology Implementation Office P. O. Box 5080 Austin, Texas 78763-5080				13. Type of Report and Period Covered Technical Report: September 2004-August 2005	
				14. Sponsoring Agency Code	
15. Supplementary Notes Project performed in cooperation with the Texas Department of Transportation and the Federal Highway Administration. Project Title: Evaluate the Fatigue Resistance of Rut Resistance Mixes URL: http://tti.tamu.edu/documents/0-4468-3.pdf					
16. Abstract The work contained in this report constitutes Phase II of TxDOT Project 0-4468. Phase I is documented in Reports 0-4468-1 and 0-4468-2. The primary objective of Phase II was to provide additional laboratory validation and sensitivity analysis of the calibrated mechanistic with (CMSE) and without (CM) surface energy measurements fatigue analysis approaches recommended in Report 0-4468-2. The second objective was to provide a better understanding of the binder-mixture relationships and effects of binder oxidative aging on both mixture fracture properties and fatigue life (N_f). The third objective was to explore the possibility of establishing a surrogate fatigue test protocol based on the CMSE approach. These objectives were achieved through fatigue characterization of additional hot-mix asphalt concrete (HMAC) mixtures with different mix-design parameters and materials under varying laboratory aging exposure conditions. Analysis of the results indicated that the CMSE approach provides a promising and rational methodology for fundamentally characterizing the fatigue resistance of HMAC mixtures. The results obtained were reasonable and exhibited low statistical variability. Compared to the CMSE, the simplified CM approach has a reduced laboratory test program and analysis time, but it is less versatile. For the materials and test conditions considered in the project, N_f was observed to be dependent on both mix-design parameters and material properties. Generally, an increase in binder content improved the mixture fracture properties and N_f . The results further indicated that binders and mixtures do stiffen due to oxidative aging and that the N_f decline is characteristic of each mixture type. The application of Miners' cumulative damage concept also provided a fundamentally promising basis for quantifying N_f decline as a function of both aging and traffic loading effects and should be explored further. With respect to CMSE laboratory testing, although the repeated direct-tension test provided the best correlation with CMSE N_f predictions, the tensile strength test was preliminarily proposed as the surrogate fatigue test protocol based on practicality and simplicity. However, additional validation of the CMSE and CM approaches together with the surrogate fatigue test protocols and software development are recommended.					
17. Key Words Asphalt, Asphalt Concrete, Fatigue, Aging, Fracture, Microcracking, Healing, Mechanistic Empirical, Calibrated Mechanistic, Surface Energy, Surrogate			18. Distribution Statement No restrictions. This document is available to the public through NTIS: National Technical Information Service Springfield, Virginia 22161 http://www.ntis.gov		
19. Security Classif.(of this report) Unclassified		20. Security Classif.(of this page) Unclassified		21. No. of Pages 196	22. Price

**APPLICATION
OF CALIBRATED MECHANISTIC FATIGUE ANALYSIS
WITH AGING EFFECTS**

by

Lubinda F. Walubita
Assistant Transportation Researcher, Texas Transportation Institute

Amy Epps Martin
Associate Research Engineer, Texas Transportation Institute

Sung Hoon Jung
Graduate Research Assistant, Texas Transportation Institute

Charles J. Glover
Research Engineer, Texas Transportation Institute

and

Eun Sug Park
Assistant Research Scientist, Texas Transportation Institute

Report 0-4468-3

Project 0-4468

Project Title: Evaluate the Fatigue Resistance of Rut Resistance Mixes

Performed in cooperation with the
Texas Department of Transportation
and the
Federal Highway Administration

November 2005

Resubmitted: May 2006

Published: July 2006

TEXAS TRANSPORTATION INSTITUTE
The Texas A&M University System
College Station, Texas 77843-3135

DISCLAIMER

The contents of this report reflect the views of the authors, who are responsible for the facts and the accuracy of the data presented herein. The contents do not necessarily reflect the official view or policies of the Federal Highway Administration (FHWA) and the Texas Department of Transportation (TxDOT). This report does not constitute a standard, specification, or regulation, nor is it intended for construction, bidding, or permit purposes. Trade names were used solely for information and not for product endorsement. The engineers in charge were Amy Epps Martin, P.E. (Texas No. 91053), and Charles J. Glover, P.E. (Texas No. 48732).

ACKNOWLEDGMENTS

This project was conducted for TxDOT, and the authors thank TxDOT and FHWA for their support in funding this research project. In particular, the guidance and technical assistance provided by the project director (PD) Magdy Mikhail of TxDOT and his predecessor Gregory Cleveland, the project coordinator (PC) James Travis of the FHWA, the project monitoring committee (PMC) member Zhiming Si of TxDOT, and German Claros of the Research and Technology Implementation (RTI) office are greatly appreciated. Special thanks also go to Lee Gustavus, Rick Canatella, and Gerry Harrison from the Texas Transportation Institute (TTI) for their help in specimen/sample preparation, laboratory testing, and data analysis. The various TxDOT district offices that provided the material mix designs and assistance in material procurement are also thanked.

TABLE OF CONTENTS

LIST OF FIGURES	xii
LIST OF TABLES	xiv
LIST OF ABBREVIATIONS AND SYMBOLS	xv
CHAPTER 1. INTRODUCTION	1-1
RESEARCH OBJECTIVES	1-3
WORK PLAN	1-4
SCOPE OF WORK	1-5
RESEARCH METHODOLOGY	1-5
DESCRIPTION OF CONTENTS	1-7
SUMMARY	1-7
CHAPTER 2. EXPERIMENTAL DESIGN AND MATERIALS SELECTION	2-1
BINDERS	2-1
AGGREGATE	2-1
MIX DESIGN AND HMAC MIXTURES	2-3
HMAC SPECIMEN FABRICATION	2-4
LABORATORY AGING EXPOSURE CONDITIONS	2-5
HMAC MIXTURES AND FACTORIAL EXPERIMENTAL DESIGN	2-6
LABORATORY TESTING	2-7
PAVEMENT STRUCTURES AND TRAFFIC	2-7
ENVIRONMENTAL CONDITIONS AND RELIABILITY LEVEL	2-8
SUMMARY	2-10
CHAPTER 3. MIXTURE CHARACTERIZATION AND FATIGUE RESISTANCE	3-1
AGGREGATE PROPERTIES	3-1
BINDER PG PROPERTIES	3-2
HMAC MIXTURE PROPERTIES	3-4
Surface Energy	3-4
Tensile Strength	3-7
Relaxation Modulus	3-9
Dissipated Pseudo Strain Energy	3-11

TABLE OF CONTENTS (continued)

Shift Factors Due to Anisotropy and Healing.....	3-12
Shift Factor Due to Aging.....	3-13
HMAC MIXTURE FATIGUE RESISTANCE	3-17
CMSE N_f Prediction	3-18
N_f Comparison (CMSE versus CM).....	3-20
CMSE N_f Prediction versus Pavement Structure and Environment	3-21
CMSE/CM SENSITIVITY ANALYSIS	3-23
SUMMARY	3-23
 CHAPTER 4. MIXTURE VERSUS NEAT-FILM BINDER OXIDATION AND HARDENING AND THE IMPACT OF BINDER OXIDATION ON MIXTURE FATIGUE	
OBJECTIVES.....	4-2
EXPERIMENTAL DESIGN	4-2
THE CALIBRATED MECHANISTIC WITH SURFACE ENERGY FATIGUE MODEL	4-4
CMSE Fatigue Analysis Models.....	4-4
HMAC Mixture Tests	4-6
BINDER TESTS.....	4-6
Extraction and Recovery.....	4-6
Size Exclusion Chromatography.....	4-8
Dynamic Shear Rheometer	4-8
Fourier Transform Infrared Spectrometer.....	4-9
RESULTS AND DISCUSSION.....	4-9
Mixture Oxidative Aging and Fatigue Resistance	4-9
Mixture versus Neat-Film Binder Oxidation and Hardening	4-12
The Impact of Binder Aging on Mixture Fatigue Life	4-17
SUMMARY	4-23

TABLE OF CONTENTS (continued)

CHAPTER 5. BINDER-MIXTURE CHARACTERIZATION	5-1
MATERIALS AND METHODS.....	5-1
Binders and Tests.....	5-2
HMAC Mixtures and Tests.....	5-3
RESULTS	5-5
Effect of Mixture Oxidation on Binder Rheology	5-5
Effect of Mixture Oxidation on Mixture Rheology	5-9
Binder-Mixture Relationships.....	5-13
SUMMARY	5-24
CHAPTER 6. PROPOSAL FOR A SURROGATE FATIGUE TEST PROTOCOL	6-1
METHODOLOGY	6-1
Step 1: Laboratory Testing and Material Property Characterization.....	6-2
Step 2: CMSE N_f Prediction.....	6-2
Step 3: Analysis of Material Properties as a Function of Predicted CMSE N_f	6-2
Step 4: Establishment of Limiting Fatigue Threshold Values	6-3
Step 5: Proposal of a Surrogate Fatigue Test Protocol	6-3
MATERIAL PROPERTIES AND N_f PREDICTION	6-4
Tensile Strength Criteria.....	6-5
Relaxation Modulus Criteria.....	6-7
Repeated Direct-Tension Criteria	6-8
Limiting Fatigue Threshold Values	6-9
Pavement Service Life and the SF_{aging} Method.....	6-11
SELECTION OF A SURROGATE FATIGUE TEST PROTOCOL.....	6-11
Ranking of the Test Protocols.....	6-12
RDT Testing and Data Analysis	6-13
Recommendation for a Proposed Surrogate Fatigue Test Protocol.....	6-15
TS-RDT Preliminary Validation.....	6-16
SUMMARY	6-17

TABLE OF CONTENTS (continued)

CHAPTER 7. DISCUSSION AND SYNTHESIS OF RESULTS	7-1
STATISTICAL ANALYSES	7-1
Comparison of the CMSE and CM Approaches	7-2
Comparison of HMAC Mixtures	7-2
AGING EFFECTS	7-3
The SF _{ag} Method – DSR _f Concept	7-3
The SF _{aging} Method – Miners’ Cumulative Damage Hypothesis	7-6
Comparison and Integration of the SF _{ag} and SF _{aging} Methods	7-7
Binder-HMAC Relationships	7-10
SURROGATE FATIGUE TEST PROTOCOLS	7-10
The TS Test Protocol	7-11
The RDT Test Protocol	7-11
The TS-RDT Test Protocol	7-11
N _f RESULTS AND FIELD PERFORMANCE	7-12
CMSE VALIDATION AND MODIFICATION	7-12
Incorporation of Other Influencing Variables	7-12
Incorporation of Multiple Distress Analyses	7-13
SUMMARY	7-14
CHAPTER 8. CONCLUSIONS AND RECOMMENDATIONS	8-1
CONCLUSIONS	8-1
The CMSE and CM Fatigue Analysis Approaches	8-1
HMAC Mixture Fatigue Resistance	8-2
Binder-HMAC Mixture Relationships and Effects of Aging	8-3
Exploration of Methods to Quantitatively Incorporate Aging in N _f Prediction	8-3
Surrogate Fatigue Test Protocols	8-4
RECOMMENDATIONS	8-5
CLOSURE AND PRODUCT DELIVERABLES	8-6
REFERENCES	9-1

TABLE OF CONTENTS (continued)

APPENDICES

APPENDIX A: CMSE FATIGUE ANALYSIS MODELS.....	10-3
APPENDIX B: CMSE/CM LABORATORY TESTS.....	10-6
APPENDIX C: MATERIAL PROPERTIES.....	10-34
APPENDIX D: HMAC MIXTURE FATIGUE LIFE.....	10-37
APPENDIX E: LIMITING FATIGUE THRESHOLD VALUES: PAVEMENT SERVICE LIFE (X_{PSL}) AND THE SF_{aging} METHOD	10-39

LIST OF FIGURES

Figure	Page
2-1 Gravel Aggregate Gradation Curve.....	2-2
2-2 Standard SGC Compactor and HMAC Cylindrical Test Specimen.....	2-5
2-3 Texas Environmental Zones.....	2-9
3-1 Binder High Temperature Properties ($G^*/\sin [\delta \cong \delta]$).....	3-2
3-2 Binder Low Temperature Properties (Flexural Creep Stiffness).....	3-2
3-3 Binder Low Temperature Properties (m-value).....	3-3
3-4 HMAC Mixture Adhesive Bond Strength (Fracture).....	3-6
3-5 HMAC Mixture Adhesive Bond Strength (Healing).....	3-6
3-6 Tensile Failure Strength versus Binder Content.....	3-8
3-7 Relaxation Modulus (Tension) versus Binder Content.....	3-9
3-8 m (Tension) versus Binder Content.....	3-10
3-9 The b Value versus Binder Content.....	3-11
3-10 Plot of SF_{ag} as a Function of Time.....	3-15
3-11 HMAC Mixture N_f Comparison (CMSE versus CM).....	3-20
3-12 Mixture (A10) N_f versus Pavement Structure and Environment.....	3-22
4-1 Decline of Field N_f with Oxidative Aging.....	4-11
4-2 DSR Function versus Carbonyl Area for Bryan Binder (PG 64-22).....	4-14
4-3 DSR Function versus CA for Yoakum Binder (PG 76-22).....	4-15
4-4 DSR Function versus CA for C1 Mixture Binder (PG 76-22 TR).....	4-16
4-5 Decline of Mixture Field N_f with Binder DSR Function Hardening.....	4-19
4-6 DSR Function Hardening Rate of Neat Binder after Initial Jump.....	4-20
4-7 The Effect of Oxidative Aging on Estimated Pavement Service Life.....	4-22
5-1 Binder Oxidative Aging and Testing.....	5-2
5-2 Binder-Mixture Characterization Test Procedure.....	5-4
5-3 Recovered Binder Master Curves for $G^* (\omega)$ (Bryan Mixture).....	5-6
5-4 Recovered Binder Master Curves for $G^* (\omega)$ (Yoakum Mixture).....	5-7
5-5 DSR Function of Binders for Bryan Mixture.....	5-8

LIST OF FIGURES (Continued)

5-6	DSR Function of Binders for Yoakum Mixture	5-8
5-7	Master Curves of Bryan Mixture for $E(t)$	5-10
5-8	Master Curves of Yoakum Mixture for $E(t)$	5-10
5-9	Master Curves of Bryan Mixture for $G^* (\omega)$	5-11
5-10	Master Curves of Yoakum Mixture for $G^* (\omega)$	5-11
5-11	VE Function of Bryan Mixture.....	5-12
5-12	VE Function of Yoakum Mixture.....	5-13
5-13	VE Function versus DSR Function	5-15
5-14	Hirsch Model from Bryan PP2 Binder	5-16
5-15	Comparison between Bryan Mixture PP2 Hirsch Model.....	5-17
5-16	Comparison between Yoakum Mixture PP2 Hirsch Model	5-18
5-17	Mixture Stiffening for Bryan Mixture: Oxidation versus Temperature	5-19
5-18	Mixture Stiffening for Yoakum Mixture: Oxidation versus Temperature	5-20
5-19	Binder Stiffening for Bryan Mixture: Oxidation versus Temperature	5-21
5-20	Binder Stiffening for Yoakum Mixture: Oxidation versus Temperature	5-21
5-21	Fatigue Life Decline with Binder Hardening	5-23
6-1	Tensile Strength (σ_t) versus N_f	6-5
6-2	Failure Strain (ε_f) versus N_f	6-6
6-3	Relaxation Modulus (Tension) (E_t) versus N_f	6-7
6-4	Stress Relaxation Rate (m) (Tension) versus N_f	6-7
6-5	Rate of Fracture Damage Accumulation (b) versus N_f	6-8
6-6	The RDT Loading Sequence	6-14
7-1	The SF_{ag} Method.....	7-5
7-2	The SF_{aging} Method	7-6

LIST OF TABLES

Table	Page
2-1 Binder Types	2-1
2-2 Gravel Aggregate Gradation	2-2
2-3 HMAC Mixtures	2-3
2-4 HMAC Mixture Mixing and Compaction Temperatures	2-4
2-5 Factorial Experimental Design for HMAC Mixtures	2-6
2-6 Laboratory Tests	2-7
2-7 Selected Pavement Structures and Traffic Levels	2-8
3-1 Crushed River Gravel Aggregate Properties	3-1
3-2 Binder Intermediate Temperature Properties at 25 °C (77 °F)	3-3
3-3 SE Components for the Crushed River Gravel Aggregate	3-4
3-4 Binder SE Components (Advancing \approx Wetting \approx Healing)	3-5
3-5 Binder SE Components (Receding \approx Dewetting \approx Fracturing)	3-5
3-6 HMAC Mixture Tensile Strength Test Data	3-8
3-7 Shift Factors Due to Anisotropy (SF_a) and Healing (SF_h)	3-13
3-8 Material Regression Constants for the Shift Factor Due to Aging	3-16
3-9 Lab N_f ($N_i + N_p$) Results (PS#1 under the WW Environment)	3-18
3-10 CMSE N_f Predictions (PS#1 and WW Environment)	3-19
4-1 Summary of CMSE Laboratory Tests	4-7
4-2 Summary of Shift Factors, Lab N_f , and Field N_f Results	4-10
4-3 Chemical and Physical Properties of Binders	4-13
4-4 Summary of Pavement Fatigue Life Parameters	4-21
6-1 Limiting Fatigue Threshold Values	6-10
6-2 Ranking Results of the Test Protocols	6-12
6-3 Comparison of HMAC Mixture Results (TS-RDT, BB, OT, and MEPDG)	6-16
7-1 Ranking of the HMAC Mixtures Using the SF_{ag} and SF_{aging} Methods	7-8

LIST OF ABBREVIATIONS AND SYMBOLS

FATIGUE ANALYSIS APPROACHES

CMSE	Calibrated mechanistic with surface Energy measurements
CM	Calibrated mechanistic without surface energy measurements
ME	Mechanistic-empirical
MEPDG	NCHRP 1-37A 2002 <i>Design Guide</i> or the <i>M-E Pavement Design Guide</i>

CMSE FATIGUE ANALYSIS PARAMETERS

N_f	HMAC mixture fatigue resistance (or field fatigue life) expressed in terms of the number of allowable traffic ESALs to fatigue failure
$N_{f(ti)}$	HMAC mixture fatigue resistance predicted over a given design period at time t_i in terms of aging exposure period (years)
SF_a	Shift factor due to HMAC anisotropy
SF_{ag}	Shift factor due to binder aging
SF_h	Shift factor due to healing
N_i	Number of load cycles to crack initiation
N_p	Number of load cycles to crack propagation
Q	Reliability factor
PS	Pavement structure (e.g., PS#1 = pavement structure number 1)

CMSE HMAC MIXTURE TESTS

TS	Tensile strength test
RM	Relaxation modulus test
RDT	Uniaxial repeated-direct tension test

HMAC MIXTURE PROPERTIES

σ_t	Tensile strength of HMAC mixture (psi)
ε_f	Failure tensile strain at break under tensile loading (in/in)
$\mu\varepsilon$	Microstrain (1 E-06)
E_1	HMAC elastic relaxation modulus at 1 s reduced loading time (psi)
m	Stress relaxation rate of the HMAC mixture
b	Rate of fracture damage accumulation under repeated direct-tension test

CHAPTER 1

INTRODUCTION

The work contained in this report constitutes Phase II of Texas Department of Transportation (TxDOT) Project No. 0-4468 “Evaluate the Fatigue Resistance of Rut Resistance Mixes,” whose two primary objectives were (Walubita et al., 2005a, b):

- (1) To evaluate and recommend a fatigue hot-mix asphalt concrete (HMAC) mixture design and analysis system for TxDOT to ensure adequate mixture performance in a particular pavement structure under specific environmental and traffic loading conditions and account for the effects of binder oxidative aging.
- (2) To comparatively evaluate and establish a database of fatigue resistance of commonly used TxDOT HMAC mixtures.

In Phase I (Reports 0-4468-1 and 0-4468-2), four fatigue analysis approaches (the mechanistic empirical [ME], the calibrated mechanistic with surface energy measurements [CMSE], the calibrated mechanistic without surface energy measurements [CM], and the new 2002 *M-E Pavement Design Guide* [MEPDG]) were comparatively evaluated based on two HMAC mixtures (TxDOT Type C and 12.5 mm Superpave) and three laboratory aging exposure conditions (0, 3, and 6 months at 60 °C [140 °F]) (Walubita et al., 2005b). The TxDOT Type C mixture denoted as the Bryan mixture was a typical TxDOT basic mixture designed with a performance-graded (PG) binder (PG 64-22) and limestone aggregate. The 12.5 mm Superpave mixture denoted as the Yoakum mixture was a rut resistant mixture designed with 5 percent styrene-butadiene-styrene versus modified PG 76-22 binder and gravel aggregate. The 0, 3, and 6 months laboratory aging conditions at 60 °C (140 °F) represent approximately up to 12 years of Texas HMAC field aging exposure (Glover et al., 2005, Walubita et al., 2005a, b).

Based on a value engineering assessment criteria and considering the test conditions in the project, the CMSE fatigue analysis approach was selected and recommended for predicting HMAC mixture fatigue life (N_f). Details of this analysis including a description of all four fatigue analysis approaches (ME, CMSE, CM, and the new 2002 M-E Pavement Design Guide) are documented in Report 0-4468-2 (Walubita et al., 2005b).

The CM approach which was modified based on the CMSE results was recommended as the second alternative approach in lieu of the CMSE, particularly in the absence of surface energy (SE) data. This CM approach is potentially promising in terms of analysis simplicity, practicality, and cost considerations over the CMSE, but further validation through additional HMAC mixture fatigue characterization is needed.

With respect to the second objective, a limited database of N_f values for the two HMAC mixtures (the Bryan mixture and the Yoakum mixture) in tabular format was established based on prediction by the four fatigue analysis approaches considered in the project. These N_f values were predicted for five hypothetical standard field TxDOT HMAC pavement structures in two Texas environmental conditions, wet-warm (WW) and dry-cold (DC) that are considered critical to HMAC fatigue cracking ([Walubita et al., 2005b](#), [TxDOT, 2003](#)).

In terms of HMAC mixture comparison, the Yoakum mixture designed with a stiffer modified binder exhibited less sensitivity to binder oxidative aging and better fatigue resistance measured in terms of N_f magnitude. This was attributed to the higher binder (5.6 percent by weight of aggregate) and 1 percent hydrated lime content in the mixture compared to the Bryan mixture (4.6 percent binder by weight of aggregate).

Overall, this finding suggested that binder stiffness alone may not be used as a sole indicator or measure of fatigue resistance, especially in performance comparison studies of this nature. A mixture designed with a stiffer binder may not necessarily perform poorly in fatigue compared to a mixture designed with a softer binder. The mix-design characteristics and other material properties need to be comparatively evaluated. Note that the mix-design characteristics and material types for these two mixtures were different. Consequently, the effect of binder oxidative aging and subsequent comparative fatigue resistance of the two mixtures were not fully realized due to many variable parameters.

In terms of statistical analysis, higher variability was observed for the Yoakum mixture than for the Bryan mixture. This statistical variability was measured in terms of the coefficient of variation (COV) of $\ln N_f$ and 95 percent prediction interval (PI) at 95 percent reliability level.

The results in Phase I (Reports [0-4468-1](#) and [0-4468-2](#)) also showed that both binders and mixtures do stiffen with aging and that these changes quantitatively correlated with each other. A visco-elastic function, defined as the ratio of the dynamic shear modulus (G') and dynamic viscosity (η') was successfully utilized to track these changes.

The results further indicated that binder oxidative aging exponentially reduces HMAC fatigue resistance and that the rate of N_f decay due to aging is mixture dependent. From the binder shear properties based on the dynamic shear rheometer (DSR) function and binder-HMAC mixture relationships, CMSE/CM aging shift factors (SF_{ag}) were developed and utilized to estimate N_f beyond the laboratory aging exposure periods. A second method (SF_{aging}) utilized the predicted N_f , the DSR properties, and a cumulative damage hypothesis to quantitatively estimate the decline in N_f caused by both trafficking and binder aging. Both methods produced promising results. However, further validation of the SF_{ag} and SF_{aging} concepts with more binders and HMAC mixture testing including additional laboratory aging conditions was recommended to better quantify the N_f -aging relationship and develop more representative aging shift factors.

RESEARCH OBJECTIVES

Based on the findings and recommendations from Phase I (Reports [0-4468-1](#) and [0-4468-2](#)), the objectives of the research work (Phase II) contained in this report were as follows ([Walubita et al., 2005a, b](#)):

1. Through fatigue characterization of additional HMAC mixtures:
 - Provide confidence and validation in the selected CMSE fatigue analysis approach.
 - Populate the N_f database of commonly used TxDOT rut resistant mixtures.
 - Provide additional data to adequately model and incorporate the effects of binder oxidative aging.
2. Through a systematic approach, facilitate a sensitivity analysis necessary to streamline the CMSE approach and reduce/eliminate redundant or less sensitive variables by:
 - Simplifying and reducing the time required for the CMSE fatigue analysis process.
 - Facilitating a quicker and more convenient way to validate and, if need be, modify the CMSE approach based on characterization of additional HMAC mixtures.
3. With additional HMAC mixtures and using the CMSE results as a benchmark:
 - Provide further validation of the CMSE-CM relationship.
 - Validate and, if need be, modify the CM- N_f models based on the CMSE results.

- If possible provide a credible basis for recommending the CM approach over the CMSE approach due to analysis simplicity, practicality, and cost considerations among other factors.
4. With additional binders, HMAC mixtures, and laboratory aging conditions:
 - Provide a better understanding and quantification of the binder-HMAC mixture relationships and effects of binder oxidative aging.
 - Further validate the SF_{ag} and SF_{aging} concepts and if possible develop representative aging shift factors for the materials under consideration.
 - Quantify the N_f -aging relationship.
 - Investigate the effects of binder type, binder content, and modification on both HMAC mixture fatigue resistance and aging.
 5. Explore the possibility of establishing a surrogate fatigue test protocol for mix design and HMAC mixture screening for fatigue resistance based on the CMSE fatigue analysis approach.

WORK PLAN

To accomplish these objectives, the research team expanded the number of HMAC mixtures characterized in Phase I, but with a focus on modified binders which provide rut resistant mixtures. Consequently, only 12.5 mm Superpave HMAC mixtures with gravel (Report [0-4468-2](#)) aggregate were used ([Walubita et al., 2005b](#)). PG 64-22 and PG 76-22 binders with two modifiers (SBS and tire rubber (TR)) were used.

Two binder content levels, optimum and optimum plus 0.5 percent, consistent with TxDOT recommendations, were utilized to investigate the effect of binder content on the fatigue resistance of these rut resistant mixtures. In terms of laboratory aging conditions, only two (0 and 6 months at 60 °C [140 °F]) aging exposure conditions were addressed to supplement the 0, 3, and 6 months aging conditions from Phase I (Reports [0-4468-1](#) and [2](#)). With these mix-design combinations and aging conditions, the total number of HMAC mixtures characterized with respect to fatigue in this report was twelve, two from Phase I and ten from Phase II.

For ease of comparison and to provide a better understanding of the effects of mix-design parameters and material type on mixture fatigue resistance, excerpts from the results in Reports [0-4468-1](#) and [0-4468-2](#) are also presented in this report ([Walubita et al., 2005a, b](#)).

SCOPE OF WORK

The general scope of the research work (Phase II) contained in this report was limited to:

- twelve 12.5 mm Superpave rut resistant HMAC mixtures;
- one aggregate type: gravel;
- three binder types: PG 64-22, PG 76-22 versus, and PG 76-22 (TR);
- two design binder content levels: optimum and optimum plus 0.5 percent;
- two laboratory aging exposure conditions: 0 and 6 months at 60 °C (140 °F) that simulate Texas field HMAC aging conditions;
- five hypothetical field HMAC pavement structures under representative traffic loading conditions;
- two Texas environmental conditions: WW and DC which are critical to fatigue cracking;
- one typical reliability level for statistical analysis: 95 percent; and
- two fatigue analysis approaches: CMSE and CM.

RESEARCH METHODOLOGY

The research methodology in Phase II involved both binder testing and fatigue characterization of 10 12.5 mm Superpave HMAC mixtures at both 0 and 6 months aging conditions using the CMSE and CM test protocols and analysis procedure. Thereafter, the results were analyzed and compared with the binder and Yoakum mixture results reported in Reports [0-4468-1](#) and [0-4468-2](#) from Phase I ([Walubita et al., 2005a, b](#)). Note that the Bryan mixture results are also presented to supplement the comparative analysis.

This laboratory characterization of more HMAC mixtures in terms of fatigue increased the TxDOT Field N_f database for rut resistant mixtures and brought the total to 12 including the Yoakum mixture analyzed in Phase I (Report [0-4468-2](#)). These results provided a validation platform for the CMSE and CM approaches including modifications and sensitivity analysis.

The results also provided more data for understanding the important phenomenon of binder oxidative aging and its impact on HMAC mixture fatigue resistance as well as developing more representative SF_{ag} factors to account for aging in N_f analysis. With these additional mixtures, the effects of binder type, binder content, and modification on both HMAC mixture fatigue resistance and aging were also investigated and demonstrated.

The major tasks associated with this work included:

- experimental design and materials selection,
- laboratory testing and data analysis,
- material property characterization (for binders, HMAC mixtures, and binder-HMAC mixture relationships),
- prediction and comparative evaluation of HMAC mixture N_f ,
- validation and sensitivity analysis of the CMSE and CM approaches,
- development and exploration of methods to quantitatively incorporate aging in N_f prediction,
- investigation of surrogate fatigue tests,
- conclusions and recommendations, and
- data documentation/report writing.

These tasks were accomplished consistent with CMSE and CM test protocols and analysis procedures based on the recommendations in Reports [0-4468-1](#) and [0-4468-2](#) from Phase I ([Walubita et al., 2005a, b](#)). The CMSE and CM laboratory test protocols and analysis models/procedures are attached as Appendices [A](#) and [B](#), respectively, of this report. Further details of the CMSE and CM fatigue analysis approaches, laboratory tests, and analysis models/procedures can be found in Reports [0-4468-1](#) and [0-4468-2](#) ([Walubita et al., 2005a, b](#)).

DESCRIPTION OF CONTENTS

This report consists of eight chapters including this chapter ([Chapter 1](#)) that provides the background of the research, the overall objectives, the work plan, the scope of work, and the research methodology including the associated tasks. [Chapter 2](#) is the experimental design that briefly describes the materials selection and mix-design parameters including specimen fabrication, aging conditions, pavement structures, environmental conditions, and the selected analysis reliability level. [Chapter 3](#) presents the laboratory test results and subsequent analyses categorized in terms of aggregate properties, binder PG properties, HMAC mixture property characterization, prediction of mixture N_f , and a CMSE/CM sensitivity analysis. Chapters [4](#) and [5](#) present and discuss the impact of binder oxidation on mixture fatigue resistance and the impact of binder aging on mixture properties, respectively. [Chapter 6](#) discusses the exploration and proposal for a surrogate fatigue test, and [Chapter 7](#) is a comparative synthesis and discussion of the results and research findings.

The report concludes in [Chapter 8](#) with a summary of findings and recommendations. Appendices of detailed laboratory test results and other important data are also included. This includes the CMSE and CM analysis models/procedures and laboratory test protocols in Appendices [A](#) and [B](#), respectively. Laboratory test results are in Appendices [C](#) through [E](#).

SUMMARY

In this introductory chapter, the background and the research objectives are discussed. The work plan, scope of work, and research methodology are described followed by a description of the report contents.

CHAPTER 2

EXPERIMENTAL DESIGN AND MATERIALS SELECTION

The experimental design and materials selection for Phase II of this project are discussed in this chapter. This includes selection of binders, aggregate, mix-design and HMAC mixtures, HMAC specimen fabrication, aging conditions, laboratory testing, pavement structures and traffic, environmental conditions, and reliability level.

BINDERS

One unmodified and two modified binders (modified with 5 percent SBS and TR, respectively) were used in this project. These three binders are listed in [Table 2-1](#). Note that the PG 76-22 binder modified with TR also contained some SBS in it.

Table 2-1. Binder Types.

Binder Notation	Binder PG Grade	Modifier	Source
A	PG 64-22	None	Eagle Asphalt (Marlin Asphalt), Inc., Texas (TX)
B	PG 76-22	≅ 5% SBS	Eagle Asphalt (Marlin Asphalt), Inc., TX
C	PG 76-22	≅ 5% TR with SBS	Wright Asphalt, Inc., Houston, TX

AGGREGATE

One aggregate type (crushed river gravel) with a combined dense gradation shown in [Figure 2-1](#) and [Table 2-2](#) was used. This crushed gravel was obtained from the Fordyce Materials plant in Victoria, Texas. The bulk specific gravity for the combined aggregate gradation was 2.591. The combined gradation included 14 percent limestone screenings and 1 percent hydrated lime.

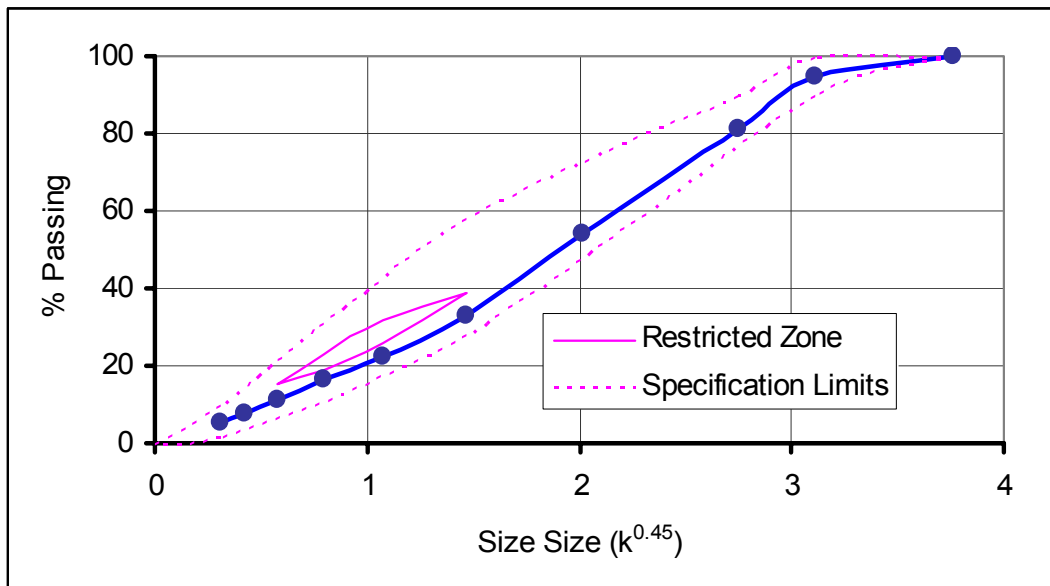


Figure 2-1. Gravel Aggregate Gradation Curve.

Table 2-2. Gravel Aggregate Gradation.

Sieve Size		TxDOT Specification (TxDOT, 2004)		% Passing
		Upper Limit (%)	Lower Limit (%)	
	mm			
³ / ₄ inches	19.00	100		100.0
¹ / ₂ inches	12.50	100	90	94.6
³ / ₈ inches	9.50	90		81.0
#4	4.75			54.4
#8	2.36	58	28	32.9
#16	1.18			22.4
#30	0.60			16.2
#50	0.30			11.0
#100	0.150			7.6
#200	0.075	10	2	5.5

MIX DESIGN AND HMAC MIXTURES

Consistent with the objectives of this project, mix design was limited to a 12.5 mm Superpave mixture that provides a rut resistant HMAC mixture. The optimum binder contents were determined consistent with the TxDOT Tex-204-F test procedures and specifications (TxDOT, 2005). By allowing binder content and binder type to vary, six HMAC mixtures were produced as shown in Table 2-3.

Table 2-3. HMAC Mixtures.

HMAC Mixture Notation	Binder + Aggregate	Binder	
		Design	Content (%)
A1	PG 64-22 + Gravel	Optimum	5.3 (5.0)
B1	PG 76-22 (SBS) + Gravel	Optimum	5.6 (5.3)
C1	PG 76-22 (TR)+ Gravel	Optimum	5.5 (5.2)
A2	PG 64-22 + Gravel	Optimum + 0.5%	5.8 (5.5)
B2	PG 76-22 (SBS) + Gravel	Optimum + 0.5%	6.1 (5.8)
C2	PG 76-22 (TR)+ Gravel	Optimum + 0.5%	6.0 (5.7)

The design binder contents in Table 2-3 are by weight of aggregate, and the values in parentheses represent the binder content by total weight of mix. The Rice specific gravity (G_t) and voids in mineral aggregates (VMA) that were determined at optimum design binder content were: 2.425 and 15.48 percent for A1, 2.410 and 15.90 percent for B1, and 2.411 and 15.31 percent for C1, respectively.

In terms of HMAC mixture notations in column 1 (Table 2-3), the first letters “A,” “B,” and “C” stand for a 12.5 mm Superpave HMAC mixture designed with a “PG 64-22,” “PG 76-22 (SBS),” and “PG 76-22 (TR)” binder, respectively. The numbers “1” and “2” stand for “optimum” and “optimum plus 0.5 percent” design binder content, respectively.

HMAC SPECIMEN FABRICATION

The basic HMAC specimen fabrication procedure involved aggregate batching, binder-aggregate mixing, short-term oven aging, compaction, sawing and coring, and finally volumetric analysis to determine the specimen air void (AV) content. These processes are described in greater details in Reports [0-4468-1](#) and [0-4468-2](#) and were consistent with Superpave, American Association of State Highway and Transportation Officials (AASHTO), and TxDOT standards ([Walubita et al., 2005a, b](#)). [Table 2-4](#) contains a list of the binder-aggregate mixing and compaction temperatures as utilized in this project consistent with the TxDOT specifications for PG 64-22 and PG 76-22 modified binders ([TxDOT, 2005](#)).

Table 2-4. HMAC Mixture Mixing and Compaction Temperatures.

Process	Temperature (°C)	
	PG 64-22	PG 76-22
Aggregate pre-heating	144 (291 °F)	163 (325 °F)
30 minutes binder pre-heating	144 (291 °F)	163 (325 °F)
Binder-aggregate mixing	144 (291 °F)	163 (325 °F)
4 hrs short-oven aging	135 (275 °F)	135 (275 °F)
Compaction	127 (261 °F)	149 (300 °F)

[Figure 2-2](#) shows the standard Superpave gyratory compactor (SGC) that was used for molding HMAC cylindrical specimens to final dimensions of 150 mm (6 inches) in height by 100 mm (4 inches) in diameter. Compaction parameters included a 1.25° compaction angle and 600 kPa (87 psi) vertical pressure at a rate of 30 gyrations per minute. For all HMAC mixtures, the target specimen fabrication AV content was 7±0.5 percent to simulate the in situ field AV after pavement construction and traffic when HMAC fatigue resistance is considered critical.



Figure 2-2. Standard SGC Compactor and HMAC Cylindrical Test Specimen.

LABORATORY AGING EXPOSURE CONDITIONS

Two laboratory aging exposure conditions, 0 and 6 months at 60 °C (140 °F), for both binders and HMAC mixtures were considered to supplement the 0, 3, and 6 months aging conditions of Phase I discussed in Reports [0-4468-1](#) and [0-4468-2](#) ([Walubita et al., 2005a, b](#)). Allowing heated air at 60 °C (140 °F) to circulate freely around the specimens in an environmentally temperature controlled room induced accelerated oxidative aging of the binder within the HMAC specimens. These aging conditions simulate up to approximately 12 years of Texas HMAC field aging exposure at a critical pavement service temperature for HMAC binder oxidative aging ([Glover et al., 2005](#), [Walubita et al., 2005a, b](#)).

Additionally, neat binders were also aged in a standard stirred air flow test (SAFT) and in 1 mm thin films in a pressure aging vessel (PAV*). These aging processes simulate both short-term aging that occurs during the HMAC hot-mixing process and construction operations and HMAC long-term aging during service, respectively, and are different from the standard PAV aging conditions ([Vassiliev et al., 2002](#)). These aging conditions were SAFT + PAV* 0 hrs, SAFT + PAV* 16 hrs, and SAFT + PAV* 32 hrs and simulate approximately up to 6 years of Texas HMAC field aging exposure ([Glover et al., 2005](#), [Vassiliev et al., 2002](#), [Walubita et al., 2005b](#)).

HMAC MIXTURES AND FACTORIAL EXPERIMENTAL DESIGN

Table 2-5 summarizes the 12 HMAC mixtures based on a full factorial design experiment that can estimate the main influencing factors including binder type-modifier type (BTMT), binder content (BC), and aging condition (AC); and the three two-way interactions. These three two-way interactions are BTMT versus AC (BTMT*AC), BTMT versus BC (BTMT*BC), and BC versus AC (BC*AC).

Table 2-5. Factorial Experimental Design for HMAC Mixtures.

#	HMAC Mixture	Binder Type-Modifier Type	Binder Content	Aging Condition
1	A10	PG 64-22	Optimum	0 Months @ 60 °C (140 °F)
2	A20	PG 64-22	Optimum + 0.5%	0 Months @ 60 °C (140 °F)
3	<i>B10</i>	PG 76-22 (SBS)	Optimum	0 Months @ 60 °C (140 °F)
4	B20	PG 76-22 (SBS)	Optimum + 0.5%	0 Months @ 60 °C (140 °F)
5	C10	PG 76-22 (TR)	Optimum	0 Months @ 60 °C (140 °F)
6	C20	PG 76-22 (TR)	Optimum + 0.5%	0 Months @ 60 °C (140 °F)
7	A16	PG 64-22	Optimum	6 Months @ 60 °C (140 °F)
8	A26	PG 64-22	Optimum + 0.5%	6 Months @ 60 °C (140 °F)
9	<i>B16</i>	PG 76-22 (SBS)	Optimum	6 Months @ 60 °C (140 °F)
10	B26	PG 76-22 (SBS)	Optimum + 0.5%	6 Months @ 60 °C (140 °F)
11	C16	PG 76-22 (TR)	Optimum	6 Months @ 60 °C (140 °F)
12	C26	PG 76-22 (TR)	Optimum + 0.5%	6 Months @ 60 °C (140 °F)

The HMAC mixtures *B10* and *B16* in italics (# 3 and 9) in Table 2-5 are the HMAC mixtures that were characterized in Phase I and described in Report 0-4468-2 (Walubita et al., 2005b). For HMAC mixture notation description (Table 2-5, column 2), the first letters A, B, and C stand for binder type (i.e., A for PG 64-22, B for PG 76-22 (SBS), and C for PG 76-22 (TR), respectively). The second numbers 1 and 2 stand for the design binder content (i.e., 1 for optimum and 2 for optimum plus 0.5 percent, respectively). The third numbers 0 and 6 stand for the laboratory aging conditions (i.e., 0 and 6 months aging at 60 °C [140 °F], respectively).

LABORATORY TESTING

Laboratory testing of both binders and HMAC mixtures was conducted consistent with the CMSE and CM test protocols utilized in Phase I of this project and listed in [Table 2-6](#). Further details of these laboratory tests can be found in Report [0-4468-2](#) and [Appendix B](#) of this report ([Walubita et al., 2005b](#)). For simplicity and because HMAC fatigue damage is generally more prevalent at intermediate pavement service temperatures, most of these laboratory tests were conducted at 20 °C (68 °F). Otherwise, the test data were normalized to 20 °C (68 °F) during the analysis phase.

Table 2-6. Laboratory Tests.

Binder and Aggregate Tests (Walubita et al., 2005a, b)	HMAC Mixture Tests (Walubita et al., 2005a, b)
<ul style="list-style-type: none"> • PG Grading • Wilhelmy Plate (WP) • Dynamic Shear Rheometer • SAFT & PAV* • Fourier Transform Infrared Spectroscopy (FTIR) • Size Exclusion Chromatography (SEC) • Universal Sorption Device (USD) (for aggregates) 	<ul style="list-style-type: none"> • Tensile Strength (TS) • Relaxation Modulus (RM) Tension & Compression • Uniaxial Repeated Direct-Tension (RDT)

PAVEMENT STRUCTURES AND TRAFFIC

[Table 2-7](#) displays a list of the five selected hypothetical TxDOT pavement structures (PS) and five associated traffic levels ranging from 0.25 to 11.00×10^6 ESALs that were considered in this project. These pavement structures represent actual material properties and layer thicknesses that have been used on various Texas highways. Typical traffic conditions consisted of an 80 kN (18 kip) axle load, 690 kPa (100 psi) tire pressure, and 97 km/hr (60 mph) speed over a design life of 20 years ([Walubita et al., 2005b](#)).

Table 2-7. Selected Pavement Structures and Traffic Levels.

P S	Surfacing	Base	Subbase	Subgrade	ESALs (1 E+06)	% Trucks
1	HMAC, 6 inches, 500,000 psi	Flex, 14 inches, 28,000 psi	-	9,000 psi	5.00	25.0
2	HMAC, 2 inches, 500,000 psi	Flex, 10 inches, 60,000 psi	Lime stabilized, 6 inches, 35,000 psi	12,400 psi	1.40	23.7
3	HMAC, 2 inches, 500,000 psi	Asphalt Stab., 7 inches, 500,000 psi	Flex, 8 inches, 24,000 psi	Silt-clay, 9,600 psi	7.22	13.0
4	HMAC, 2 inches, 500,000 psi	Flex, 6 inches, 50,000 psi	Stab. subgrade, 5 inches, 30,000 psi	10,000 psi	0.39	10.7
5	US 290 HMAC, 4 inches, 500,000 psi	Cemented, 14 inches, 150,000 psi	-	15,000 psi	10.75	15.2

ENVIRONMENTAL CONDITIONS AND RELIABILITY LEVEL

Two Texas environmental conditions, WW and DC, that are considered critical to HMAC mixture fatigue performance in terms of fatigue (alligator) cracking were considered (TxDOT, 2003). These environmental locations are shown in [Figure 2-3](#). A typical 95 percent reliability level was selected for the analysis.

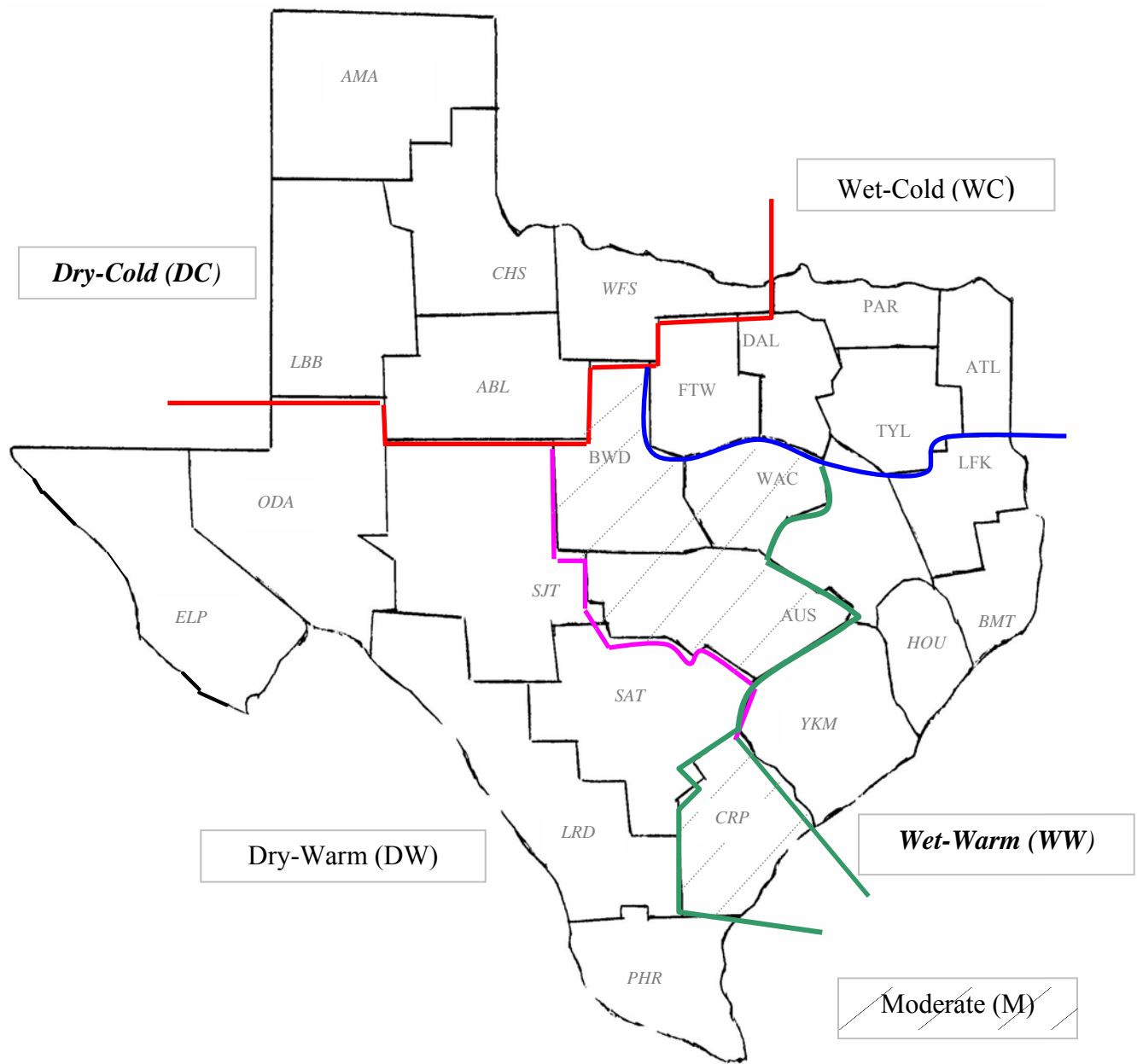


Figure 2-3. Texas Environmental Zones.

SUMMARY

The bullets below summarize the important points from the experimental design and materials selection discussed in this chapter:

- Three binder types (PG 64-22, PG 76-22 (SBS), and PG 76-22 (TR)) and one aggregate type (crushed river gravel) were used for Phase II of this project. Two design binder content levels, optimum and optimum plus 0.5 percent, were utilized.
- Two laboratory aging exposure conditions, 0 and 6 months at 60 °C (140 °F), that simulate approximately up to 12 years of Texas field HMAC aging exposure were utilized to investigate the effects of oxidative aging on both binders and HMAC mixture properties including fatigue resistance. These two aging conditions were a supplement to the Phase I aging conditions of 0, 3, and 6 months, respectively.
- Twelve rut resistant 12.5 mm Superpave mixtures were used in this project based on a comprehensive factorial design experiment that incorporated the main influencing variables including binder type, modifier type, design binder content, and aging condition and the three two-way interactions. These three two-way interactions are binder type-modifier type versus aging condition (BTMT*AC), binder type-modifier type versus binder content (BTMT*BC), and binder content versus aging condition (BC*AC).
- The standard SGC compactor was utilized for molding HMAC cylindrical specimens. The target specimen fabrication AV content was 7 ± 0.5 percent to simulate the in situ field AV after pavement construction and traffic when HMAC fatigue resistance is considered critical.
- Both binder and HMAC mixture laboratory testing was conducted consistent with the CMSE/CM test protocols utilized in Phase I of this project. These tests include binder PG grading, surface energy (WP and USD), DSR, SEC, FTIR, SAFT + PAV*, TS, RM, and RDT ([Walubita et al., 2005b](#)).
- Five commonly used TxDOT HMAC pavement structures with corresponding traffic levels of 0.25 to 11.00 million ESALs were selected for analysis.
- Two Texas environmental conditions (wet-warm and dry-cold) considered critical to fatigue associated (alligator) cracking in HMAC pavements and a 95 percent reliability level were selected for the analysis.

CHAPTER 3

MIXTURE CHARACTERIZATION AND FATIGUE RESISTANCE

The laboratory test results for the HMAC mixture properties are presented and analyzed in this chapter. These results include aggregate properties, binder PG properties, and HMAC mixture properties. CMSE/CM aging shift factors and the predicted HMAC mixture fatigue resistance in terms of N_f magnitude including a CMSE/CM sensitivity analysis are also presented in this chapter. A summary of the findings is presented at the end of the chapter.

Note that for most of the binder test results, metric units were used consistent with the PG specifications used by TxDOT for binders ([AASHTO, 1994](#), [TxDOT, 2005](#)). English (U.S.) units and/or unit conversions are provided in parentheses to meet TxDOT requirements for other units including length (1 mm \cong 0.039 inches), temperature ($^{\circ}\text{F} = 32 + 1.8 [^{\circ}\text{C}]$), and stress (1 MPa \cong 145 psi, 1 kPa \cong 0.145 psi, and 1 Pa \cong 1.45×10^{-4} psi).

AGGREGATE PROPERTIES

The material properties for the crushed river gravel aggregate used in this project are summarized in [Table 3-1](#). These results indicate that the aggregate met the specification consistent with the respective test methods ([Walubita et al., 2005b](#), [TxDOT, 2005](#)).

Table 3-1. Crushed River Gravel Aggregate Properties.

Test Parameter	Measured Value	Specification	Test Method (TxDOT, 2005)
Soundness	20%	$\leq 30\%$	Tex-411-A
Crushed faces count (two faces)	100%	$\geq 85\%$	Tex-460-A
Los Angeles (LA) abrasion	25%	$\leq 40\%$	Tex-410-A
Sand equivalent	77%	$\geq 45\%$	Tex-203-F

BINDER PG PROPERTIES

PG laboratory test characterization of the binders based on the AASHTO PP1, PP6, T313, and T315 test protocols produced the results shown in Figures 3-1 through 3-3 and Table 3-2, respectively (AASHTO, 1994, 1996, Walubita et al., 2005a, b). These results represent mean values of at least two binder test samples per binder type. For unit conversions in Figure 3-1 through 3-3 and Table 3-2: $^{\circ}\text{F} = 32 + 1.8(^{\circ}\text{C})$, $1 \text{ MPa} \cong 145 \text{ psi}$, $1 \text{ kPa} \cong 1.45 \times 10^{-1} \text{ psi}$, and $1 \text{ Pascal} \cong 1.45 \times 10^{-4} \text{ psi}$.

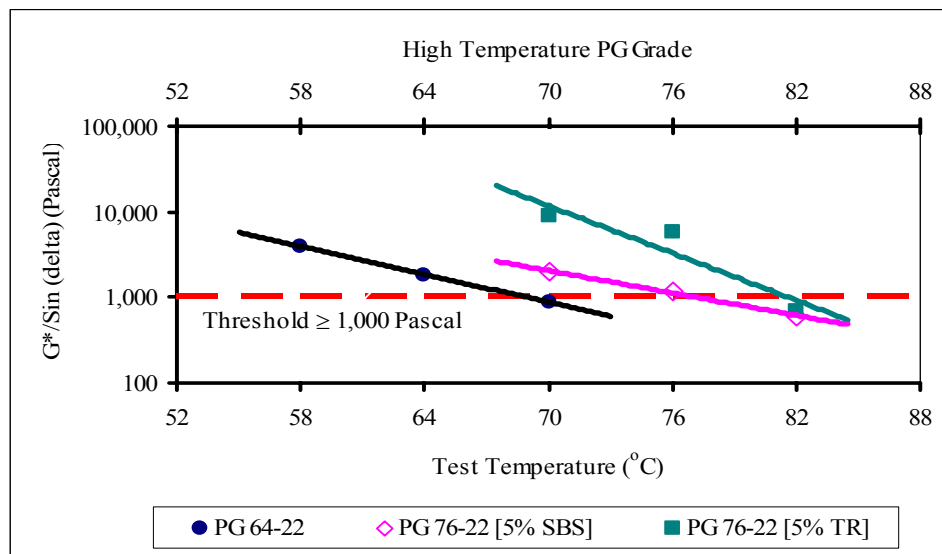


Figure 3-1. Binder High Temperature Properties ($G^*/\text{Sin} [\delta \cong \delta]$).

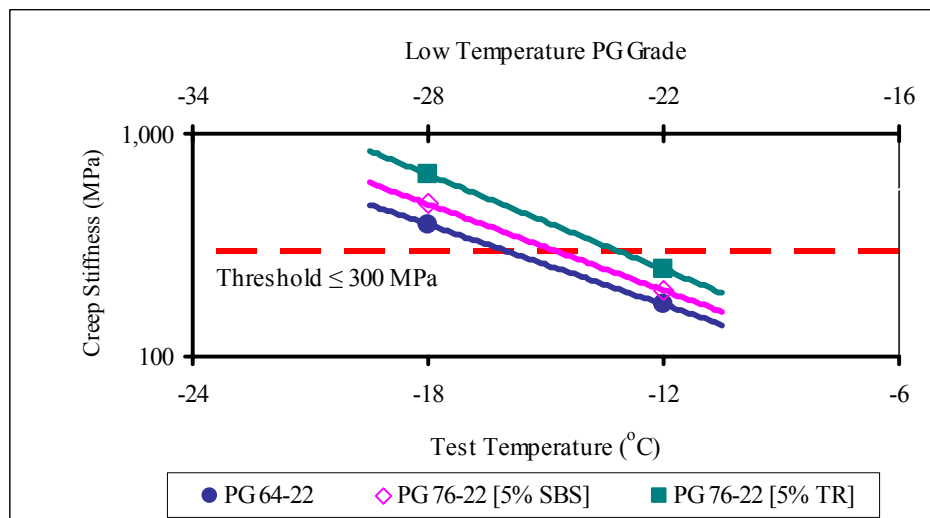


Figure 3-2. Binder Low Temperature Properties (Flexural Creep Stiffness).

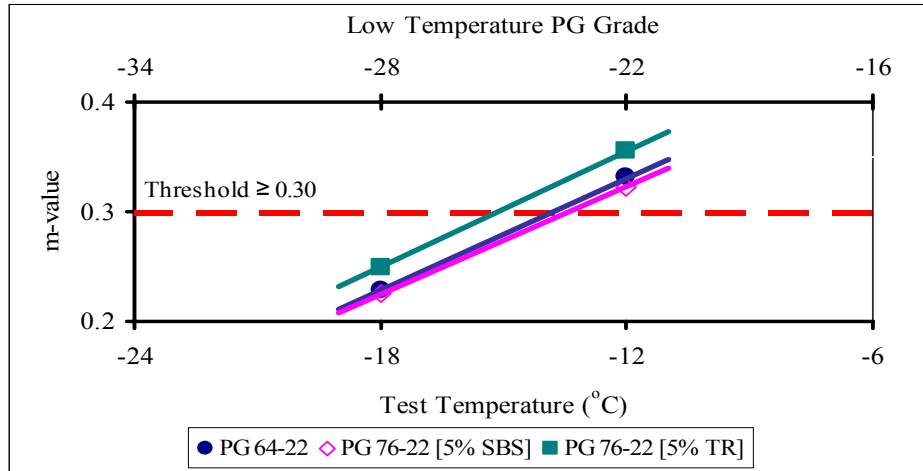


Figure 3-3. Binder Low Temperature Properties (m-value).

The verification results shown in Figures 3-1 through 3-3 indicate that the binders met the PG specification consistent with the material properties for PG 64-22 and PG 76-22 binders (AASHTO, 1994, 1996, Walubita et al., 2005a, b). Table 3-2 shows the measured intermediate temperature properties of the binders at 25 °C (77 °F) in terms of the complex shear modulus (G^*) and the phase angle (δ). The results represent average values of three tests on three different binder samples per binder type. As shown in Table 3-2, all three binders met the required maximum PG specified threshold $G^* \sin \delta$ value of 5000 kPa (AASHTO, 1994, 1996).

Table 3-2. Binder Intermediate Temperature Properties at 25 °C (77 °F).

Binder	δ (°)	$G^* \sin \delta$ (kPa)	Stdev (kPa)	COV ($G^* \sin \delta$)	PG Specification
A: PG 64-22	65	600	10.91	1.82 %	≤ 5000 kPa
B: PG 76-22 [SBS]	62	1019	70.03	6.90 %	≤ 5000 kPa
C: PG 76-22 [TR]	58	2028	115.39	5.69 %	≤ 5000 kPa

Notice also from both Figures 3-1 and 3-2 and Table 3-2 that the PG 76-22 (TR) binder exhibited greater stiffness than the PG 76-22 (SBS) at similar test temperatures. This difference in stiffness was attributed to the differences in the modifier type and impacted the HMA mixture fatigue resistance as discussed subsequently. As theoretically expected, the unmodified PG 64-22 binder exhibited the lowest stiffness value, particularly at high test temperatures.

HMAC MIXTURE PROPERTIES

The HMAC mixture property results presented in this section include surface energy, tensile strength, relaxation modulus, dissipated pseudo strain energy, and the shift factors due to anisotropy and healing. Laboratory tests and data analysis for these HMAC mixture properties were conducted consistent with the CMSE and CM test protocols and analysis procedures described in Report 0-4468-2 and attached as Appendices A and B of this report (Walubita et al., 2005b).

In general, these laboratory test results represent mean values of at least two replicate measurements per test per mixture type per aging condition. For simplicity and because HMAC fatigue damage is generally more prevalent at intermediate pavement service temperatures, most of these laboratory tests were conducted at 20 °C (68 °F). Otherwise, the test data were normalized to 20 °C (68 °F) during the analysis phase. Note that in this report, mixtures Bryan and B10 represent the Bryan and Yoakum mixtures described in Report 0-4468-2 (Walubita et al., 2005b).

Surface Energy

The measured surface energy components for the aggregate and binders are listed in Table 3-3 through 3-5. These SE components were measured using the universal sorption device and the Wilhelmy plate test methods for aggregate and binder, respectively (Walubita et al., 2005a, b).

Table 3-3. SE Components for the Crushed River Gravel Aggregate.

SE Component	Value (ergs/cm ²)
Γ^+	1.1
Γ^-	426.85
Γ^{AB}	43.31
Γ^{LW}	81.34
Γ^{Total}	124.65
SSA (m ² /gm)	1.57

Table 3-4. Binder SE Components (Advancing \approx Wetting \approx Healing).

SE (ergs/cm ²)	PG 64-22		PG 76-22 (SBS)		PG 76-22 (TR)	
	0 Months	6 Months	0 Months	6 Months	0 Months	6 Months
Γ_s^{LW}	4.28	9.78	13.63	44.16	38.36	43.92
Γ_s^-	4.43	8.21	2.28	4.47	1.01	1.52
Γ_s^+	1.83	2.35	1.15	1.94	2.49	3.28
Γ_s^{AB}	8.87	6.57	4.23	3.43	3.17	4.47
Γ_s^{Total}	13.15	16.35	17.86	47.59	41.53	48.39

Table 3-5. Binder SE Components (Receding \approx Dewetting \approx Fracturing).

SE (ergs/cm ²)	PG 64-22		PG 76-22 (SBS)		PG 76-22 (TR)	
	0 Months	6 Months	0 Months	6 Months	0 Months	6 Months
Γ_s^{LW}	20.01	15.54	26.92	31.53	46.12	53.98
Γ_s^-	7.05	15.04	9.42	58.81	1.26	7.32
Γ_s^+	2.06	3.08	4.48	11.05	2.56	0.04
Γ_s^{AB}	10.58	16.53	5.98	25.27	3.60	1.14
Γ_s^{Total}	30.59	32.07	32.90	56.80	49.72	55.12

Figures 3-4 and 3-5 are a plot of the HMAC mixture adhesive bond strengths measured in terms of fracture (ΔG_f) and healing (ΔG_h) SEs, respectively, under dry conditions (assuming no moisture damage) at 20 °C (68 °F). From Figure 3-4, the decreasing rank order of mixture bond strength in terms of resistance to fracture damage as indicated by the ΔG_f magnitude is mixture B, C, and A. In terms of the potential to self-heal, the decreasing rank order is mixture B, A, and C (Figure 3-5). For the materials evaluated in this project, these SE results indicate that a combination of PG 76-22 (SBS) binder and gravel aggregate will result in a mixture with the best fracture damage resistance and potential to self-heal as compared to any other combination.

Based on energy theory concepts, the higher the ΔG_f value in magnitude, the greater the resistance to fracture damage. The lower the ΔG_h value in magnitude, the greater the potential to self-heal. In simpler terms, SE is a representative measure of the bond strength between the binder and aggregate (Walubita et al., 2005b).

ΔG_f is associated with the energy required to break the bond between the binder and aggregate and cause fracture or cracking. ΔG_h is associated with the energy required to create a bond between the binder and aggregate and close the cracks (healing). With these relationships, mixture B (PG 76-22 [SBS] + gravel) has a better adhesive bond strength to resist fracture damage and a stronger potential to self-heal compared to mixtures A and C.

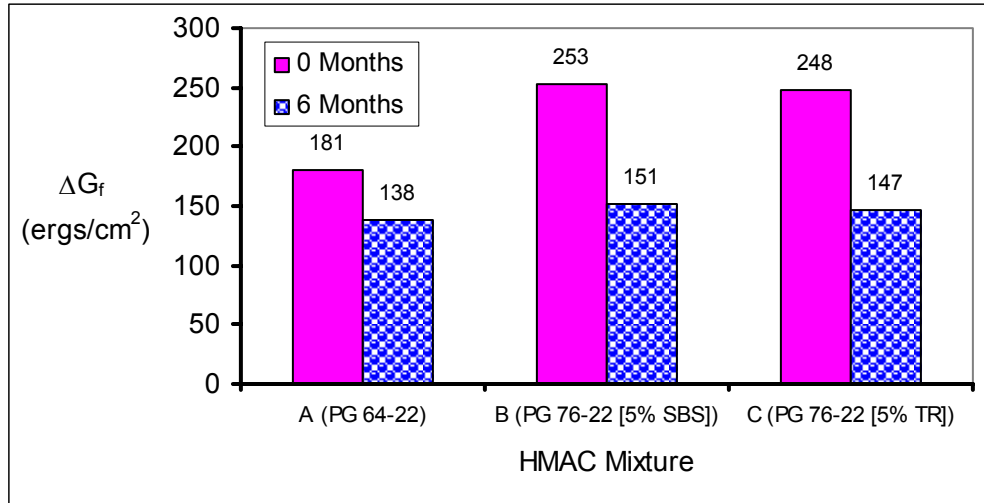


Figure 3-4. HMAC Mixture Adhesive Bond Strength (Fracture).

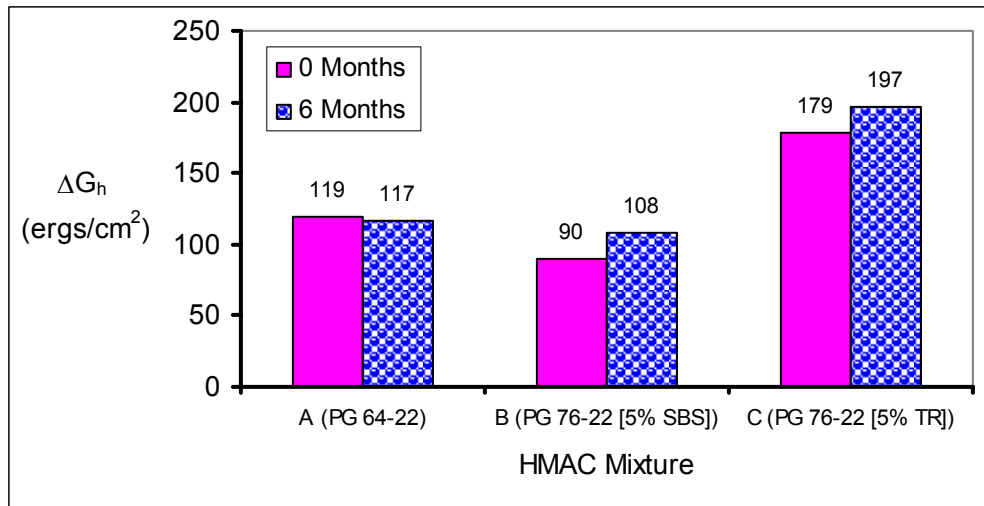


Figure 3-5. HMAC Mixture Adhesive Bond Strength (Healing).

Interestingly, the fracture bond strength expressed in terms of ΔG_f magnitude did not differ significantly for the two mixtures B and C (Figure 3-4) with modified binders. However, a significant difference is noted in the ΔG_h values (Figure 3-5) or potential to self-heal for the two mixtures. This difference is theoretically expected due to the differences in the modifier type.

For all mixtures, the detrimental effect of aging on ΔG_f and ΔG_h is clearly evident when comparing the 0 and 6 months data. Generally, there is a decrease in ΔG_f magnitude and an increase in ΔG_h magnitude after 6 months of binder oxidative aging at 60 °C (140 °F). These results indicate a decreased resistance to fracture damage and potential to self-heal after aging. Based on the SE changes in Figures 3-4 and 3-5, ΔG_f appears to be more sensitive to aging than ΔG_h .

Tensile Strength

Table 3-6 is a summary of the mixture tensile strength characteristics in terms of the tensile stress (σ_t) and strain (ε_f) at break measured at 20 °C (68 °F). A graphical representation of these results is included in Appendix C.

Table 3-6 shows that both σ_t and ε_f are sensitive to binder type and aging condition. While changes in the parameter σ_t with aging were within the test variability (Medani et al. 2004), the ε_f at break decreased significantly by more than 30 percent due to an increase in HMAC mixture brittleness from oxidative aging of the binder. In general, as the HMAC mixture ages, it becomes more brittle (less ductile) and breaks under tensile loading at a lower ε_f level. Thus aging reduces HMAC mixture ductility and increases brittleness at the expense of fracture damage resistance under tensile loading.

Note also that the σ_t and ε_f values of mixtures B and C with modified binders do not differ significantly, although mixture C with PG 76-22 (TR) appears to be more brittle based on the relatively lower ε_f values. Figure 3-6 is a plot of the ε_f values as a function of binder content for all the mixtures including the Bryan mixture from Report 0-4468-2 (Walubita et al., 2005a, b).

Table 3-6. HMAC Mixture Tensile Strength Test Data.

HMAC Mixture	Binder + Aggregate	σ_t (psi)	ϵ_f ($\mu\epsilon$)
Bryan	PG 64-22 + Limestone	105 (725 kPa)	1245
A10	PG 64-22 + Gravel	76 (525 kPa)	5099
A20		68 (470 kPa)	5630
B10 (Yoakum)	PG 76-22 (SBS) + Gravel	123 (849 kPa)	3483
B20		115 (795 kPa)	6103
C10	PG 76-22 (TR) + Gravel	125 (861 kPa)	3057
C20		112 (770 kPa)	5387
A16	PG 64-22 + Gravel	168 (1159 kPa)	1090
A26		171 (1179 kPa)	2078
B16	PG 76-22 (SBS) + Gravel	184 (1270 kPa)	851
B26		177 (1221 kPa)	1651
C16	PG 76-22 (TR) + Gravel	193 (1332 kPa)	954
C26		198 (1366 kPa)	1454

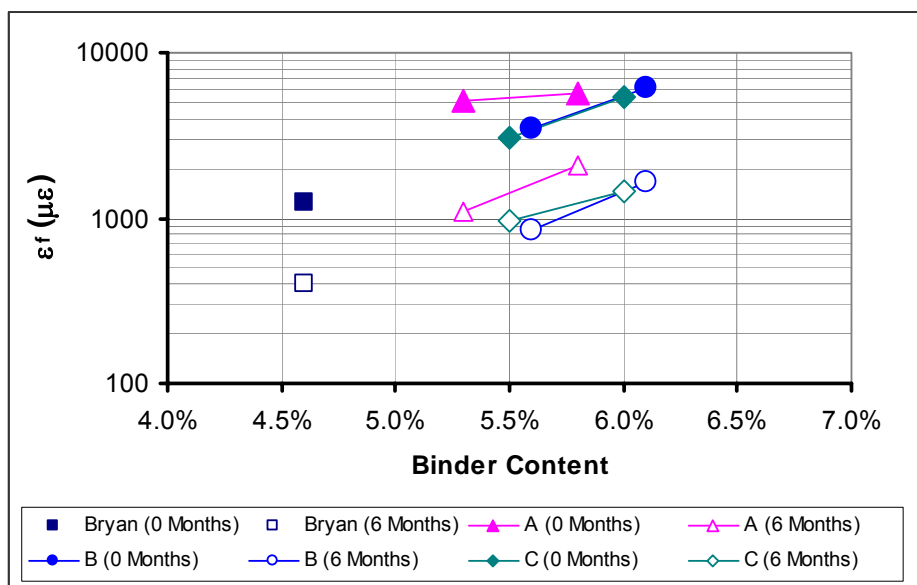


Figure 3-6. Tensile Failure Strain versus Binder Content.

Figure 3-6 shows an increasing trend in the mixture ductility with an increase in the binder content based on the ϵ_f magnitude. Generally, a high ϵ_f at break indicates that a particular HMAC mixture is more ductile and can tolerate higher strains before failing. Thus increasing the binder content improves mixture ductility and possibly fatigue resistance under tensile loading. Based on Figure 3-6, the decreasing rank order of mixture ductility in terms of ϵ_f magnitude is A (more ductile), B, C, and Bryan (more brittle). Consequently, the Bryan mixture with PG 64-22 and limestone aggregate would be considered the most brittle followed by mixture C with PG 76-22 (TR) and gravel aggregates, based on these results. Between mixtures A and B, mixture A appears to be more ductile compared to mixture B at optimum binder content, while the opposite is true at optimum plus 0.5 percent binder content.

Relaxation Modulus

The relaxation modulus test results in terms of $E(t)$ at 1.0 s and m values are summarized in Figures 3-7 and 3-8 as a function of binder content for each mixture type (including the Bryan mixture from Report 0-4468-2). These results were derived from RM master curves that were generated at a reference temperature of 20 °C (68 °F) from RM test data that were measured at three test temperatures of 10 °C (50 °F), 20 °C (68 °F), and 30 °C (86 °F) in tension (Walubita et al., 2005a, b).

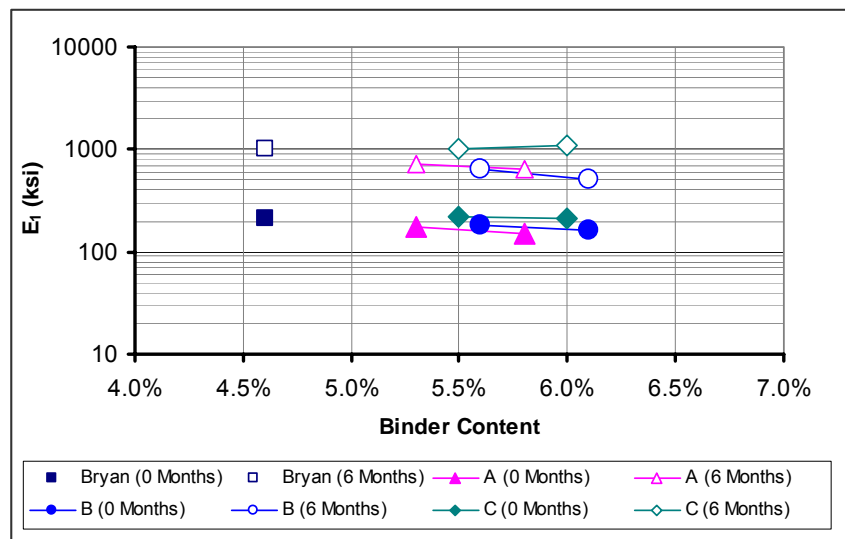


Figure 3-7. Relaxation Modulus (Tension) versus Binder Content.

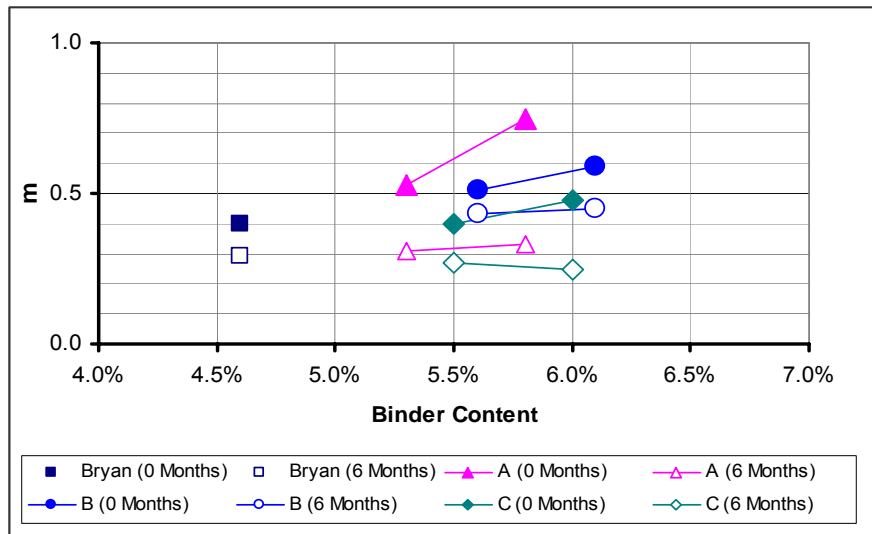


Figure 3-8. m (Tension) versus Binder Content.

Figures 3-7 and 3-8 indicate a general decrease in E_I and an increase in m , with an increase in binder content and vice versa with aging. As the binder content is increased, the mixture becomes relatively less stiff (small E_I value) with a greater potential to relax the applied stress as indicated by the increasing m value. By contrast, the mixture becomes stiffer with a high E_I value and a decreased potential to relax the applied stress (small m value) with increased aging. Based on Figures 3-7 and 3-8, the 0 months E_I values are smaller in magnitude compared to the 6 months E_I values and vice versa for the m values. For visco-elastic materials like HMAC, the higher the m value, the better the ability of the mixture to relax the applied stress and the greater the resistance to fracture damage. Thus, an increase in binder content increases mixture resistance to fracture damage, but this resistance declines with aging (under strain-controlled testing conditions).

In comparison, Bryan and mixture C (with PG 76-22 [TR]) exhibited the least potential to relax the applied stress based on the small m values. These two mixtures would thus be theoretically expected to exhibit less resistance to fracture damage compared to mixtures A (PG 64-22 with gravel aggregates) and B (PG 76-22 [SBS] with gravel aggregates). Comparing mixtures A and B, both Figures 3-7 and 3-8 indicate that mixture A is more susceptible to binder oxidative aging than mixture B based on the higher E_I values and smaller m values after 6 months of laboratory aging.

Dissipated Pseudo Strain Energy

Figure 3-9 is a plot of the dissipated pseudo strain energy (DPSE) expressed in terms of the parameter b during uniaxial repeated direct-tension testing at 30 °C (86 °F) with the test data normalized to 20 °C (68 °F) (Walubita et al., 2005a, b). This parameter b , which is the slope of a plot of DPSE versus $\log N$ (where N is the number of laboratory RDT load cycles), is an indicator of the rate of fracture damage accumulation under RDT testing.

In the CMSE analysis, the use of DPSE to characterize fracture damage under RDT testing allows for non-linearity and visco-elasticity corrections of the HMAC behavior. These corrections are achieved through the use of pseudo strain and a non-linearity correction factor, $\psi(t)$, when calculating for the parameter b (Walubita et al., 2005a, b). Figure 3-9 is a plot of the parameter b as a function of binder content.

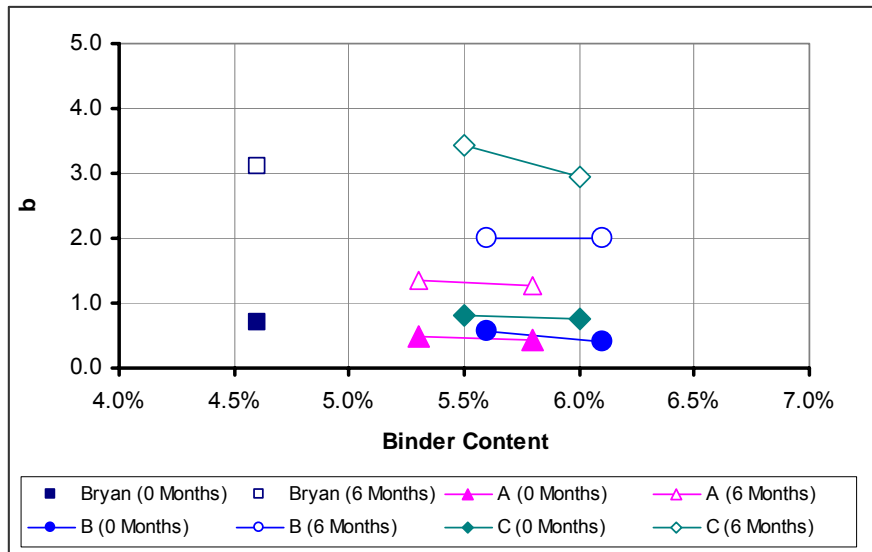


Figure 3-9. The b Value versus Binder Content.

Generally, the higher the b value, the greater the rate of accumulation of fracture damage, and thus a smaller value of b is desired. Consequently, Figure 3-9 shows that increasing the binder content improves the mixture fracture damage resistance, but this resistance declines with aging. Figure 3-9 shows a decreasing trend for the b value with an increase in binder content and higher b values for the 6 months aged mixtures.

According to [Figure 3-9](#), the Bryan mixture (PG 64-22 plus limestone from Report [0-4468-2](#)) and mixture C (PG 76-22 [TR] plus gravel) are the most susceptible to fracture damage based on the higher b values, particularly after aging. Mixture A (PG 64-22 plus gravel aggregate) would be the least susceptible to fracture damage. On a comparative basis and considering the same PG 64-22 binder, this result indicates that aggregate type and aggregate gradation play a significant role in the fracture behavior of HMAC mixtures. On this basis, these results ([Figure 3-9](#)) indicate that the combination of PG 64-22 plus gravel aggregates (mixture A) provides better fracture resistant properties than the combination of PG 64-22 plus limestone aggregates (Bryan mixture). Consequently, mixture A would be expected to perform better in terms of fracture resistance compared to the Bryan mixture. In terms of binder content, [Figure 3-9](#) shows that an increase in binder content improves the fracture behavior of HMAC mixtures based on the decreasing b value. Comparing the modified binders, it is obvious that mixture B (with PG 76-22 [SBS]) provides better fracture resistant properties than mixture C with PG 76-22 (TR), at both aging conditions.

Shift Factors Due to Anisotropy and Healing

[Table 3-7](#) summarizes the computed SF_a and SF_h shift factors used in this project. For all the HMAC mixtures (including Bryan and B10 [Yoakum] from Report [0-4468-2](#)), a similar SF_a value of 2.0 was used in this report as shown in [Table 3-5](#). This is consistent with the findings reported in Report [0-4468-2](#) which indicated that a value of 2.0 was appropriate for the mixtures under consideration within a ± 15 percent error tolerance ([Medani et al., 2004](#), [Walubita et al., 2005a, b](#)).

A difference in the SF_h values across the mixtures as a function of both binder content and aging is noted; mixture B (PG 76-22 [SBS] plus gravel) exhibited the greatest potential to self-heal and mixture C (PG 76-22 [TR] plus gravel) the least potential to self-heal, based on the lower SF_h magnitude. As theoretically expected, [Table 3-7](#) shows that aging reduces the mixtures' potential to self-heal based on the significantly smaller SF_h values in magnitude after 6 months of laboratory aging. In general, the higher the SF_h value in magnitude, the greater the potential to self-heal. This SF_h was computed as described in [Appendix A](#) and takes into account traffic loading and environment effects ([Walubita et al., 2005a, b](#)).

Table 3-7. Shift Factors Due to Anisotropy (SF_a) and Healing (SF_h).

HMAC Mixture	Binder + Aggregate	SF _a	SF _h
Bryan	PG 64-22 + Limestone	2.0	6.73
A10	PG 64-22 + Gravel	2.0	7.18
A20		2.0	7.28
B10	PG 76-22 (SBS) + Gravel	2.0	7.26
B20		2.0	7.32
C10	PG 76-22 (TR) + Gravel	2.0	5.91
C20		2.0	6.53
A16	PG 64-22 + Gravel	2.0	3.63
A26		2.0	3.66
B16	PG 76-22 (SBS) + Gravel	2.0	3.81
B26		2.0	3.98
C16	PG 76-22 (TR) + Gravel	2.0	2.97
C26		2.0	2.95

Shift Factor Due to Aging

The CMSE/CM SF_{ag} factors were developed based on neat binder SAFT+PAV* aging and DSR testing. The hypothesis is that practical implementation of the CMSE and CM approaches will involve only laboratory aging of neat binders (not HMAC mixtures) to develop shift factors due to aging. Thereafter, these SF_{ag} factors would be used as input variables to predict the HMAC mixture fatigue resistance in terms of N_f for any desired aging exposure period.

In this project, the DSR function was used because it provides a better representation of the binder shear properties in terms of ductility and durability, properties that are considered critical to fatigue performance for field aged HMAC pavements (Glover et al., 2005).

Equation 3-1 is the formulation of the SF_{ag} based on the DSR function.

$$SF_{ag} = u[\chi(t)]^w \quad (3-1)$$

$$\chi(t) = \left(\frac{m' @ t_i}{m' @ t_0} \right) \left(\frac{DSR_{f(1)} @ t_0}{DSR_{f(1)} @ t_i} \right) \quad (3-2)$$

$$DSR_f = [G' / (\eta' / G')], \quad DSR_f(\omega) = DSR_{f(1)}(\omega)^{m'} \quad (3-3)$$

where:

SF_{ag}	=	Shift factor due to binder oxidative aging
$\chi(t)$	=	Material property ratio that relates the aged to the unaged binder shear properties as a function of time
u, w	=	Material regression constants
m'	=	Slope of the binder $DSR_f(\omega)$ plot within a reduced angular frequency range of 1 E-06 to 1 E+02 rad/s at 20 °C (68 °F)
ω	=	Reduced angular frequency (rad/s)
$DSR_{f(1)}$	=	The value of $[G' / (\eta' / G')]$ at 1 rad/s (Pa·s)
G'	=	Elastic dynamic shear modulus (MPa)
η'	=	Dynamic viscosity (Pa·s)

The plot of the binder DSR graph on a log-log scale is represented in the form of a power function as shown in [Appendix C \(Walubita et al., 2005b\)](#). These graphs ([Appendix C](#)) were generated from neat binder DSR test data that were measured at three test temperatures of 20 °C (68° F), 40 °C (104 °F), and 60 °C (140 °F) per aging condition within an angular frequency of 0.1 to 100 rad/s. The three laboratory aging conditions for these binders were SAFT+PAV*, SAFT+PAV* 16 hrs, and SAFT+PAV* 32 hrs. These aging conditions simulate approximately up to 6 years of Texas field HMAC aging exposure ([Glover et al., 2005](#); [Walubita et al., 2005a, b](#); [Vassiliev et al., 2002](#)). [Figure 3-10](#) is a plot of the computed SF_{ag} values as a function of aging exposure period expressed in years (with $w \cong u \cong 1.0$).

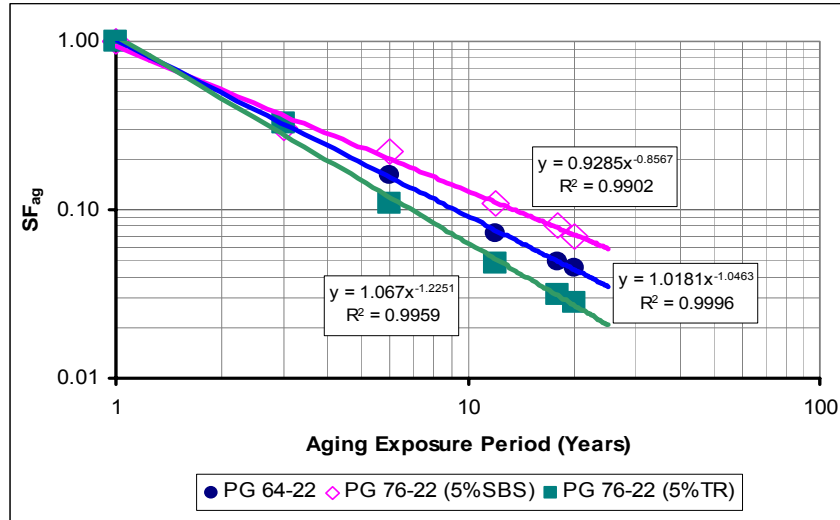


Figure 3-10. Plot of SF_{ag} as a Function of Time.

Based on [Figure 3-10](#), the binders in order of increasing sensitivity to oxidative aging are PG 76-22 (SBS), PG 64-22, and PG 76-22 (TR). Consequently, mixture C with PG 76-22 (TR) binder would be theoretically expected to perform poorly in fatigue in terms of N_f magnitude, which is consistent with the material properties reported previously in this chapter. By contrast, mixture B (PG 76-22 [SBS]) is expected to exhibit superior fatigue resistance in terms of N_f magnitude.

From [Figure 3-10](#), the SF_{ag} values considering a 20-year aging exposure period were estimated to be approximately 0.045, 0.07, and 0.028 for PG 64-22, PG 76-22 (SBS), and PG 76-22 (TR) binders, respectively. These SF_{ag} values clearly indicate a comparatively greater sensitivity to oxidative aging for the mixture with PG 76-22 (TR) binder based on the smaller SF_{ag} value while the mixture with PG 76-22 (SBS) binder is the least sensitive to oxidative aging based on the relatively larger SF_{ag} value. When plotted as a function of time as shown in [Figure 3-10](#), SF_{ag} exhibits a simple power functional relationship with time as expressed by [Equation 3-4](#).

$$SF_{ag} = u_1 [t]^{w_1} \quad (3-4)$$

where:

- u_1, w_1 = Material regression constants
- t = Aging exposure period in years

Using this SF_{ag} -time relationship, the SF_{ag} value for each respective binder/mixture can be predicted for any aging exposure period. As illustrated by Equation 3-5, this allows for prediction of N_f for any aging exposure period without having to age the HMAC mixtures:

$$N_{f(t_i)} = SF_{ag(t_i)} \times [N_{f(t_0)}] \quad (3-5)$$

where:

- $N_{f(t_i)}$ = HMAC mixture fatigue resistance at time t_i in terms of aging exposure exposure period (years)
- $N_{f(t_0)}$ = HMAC mixture fatigue resistance at assumed zero aging exposure just after construction
- $SF_{ag(t_i)}$ = Shift factor due to binder oxidative aging at time t_i in terms of aging exposure period (years)

The material regression constants u_1 and w_1 in Equation 3-4 are characteristic of each binder type and will generally vary as a function of binder/mixture type. Table 3-8 summarizes these material regression constants based on Figure 3-10.

Table 3-8. Material Regression Constants for the Shift Factor Due to Aging.

Binder	u_1	w_1
PG 64-22	1.0181	-1.0463
PG 76-22 (SBS)	0.9285	-0.8567
PG 76-22 (TR)	1.0670	-1.2251

Using a SF_{ag} based on binder properties implies that any HMAC mixture using a particular binder type would always have the same SF_{ag} value, which is a desirable concept because it is only the binder that oxidizes in any given HMAC mixture. Under similar traffic loading and environmental conditions, such a SF_{ag} should therefore vary only as a function of mix-design parameters (binder content, AV, and aggregate gradation) and volumetric properties. However, these mix-design parameters and volumetric properties are not taken into account in the current SF_{ag} derived in this report.

Furthermore, although traffic loading and environmental effects are taken into account through the SF_h , these factors also need to be considered in the SF_{ag} (Walubita et al., 2005a, b). In particular, effects of temperature variations are hypothesized to play a significant role in the oxidative aging of the binder within the HMAC mixtures.

HMAC MIXTURE FATIGUE RESISTANCE

For both the CMSE and CM approaches, the mixture N_f was predicted as expressed by Equation 3-6. However, some differences between the CMSE and CM approaches arise in the computation of SF_h and Paris' Law fracture coefficient A (Appendix A). In computing these parameters, the CM approach does not incorporate SE data due to healing nor RM data in compression (Walubita et al., 2005b). Instead, the CM approach uses modified models that were adjusted based on CMSE results from Phase I of this project (Walubita et al., 2005a, b).

$$N_f = SF_i (N_i + N_p) \geq Q \times TrafficDesign_{ESALs} \quad (3-6)$$

$$SF_i = SF_{ag} (SF_a \times SF_h) \quad (3-7)$$

where:

- N_f = HMAC mixture fatigue resistance (or field fatigue life) expressed in terms of the number of allowable traffic ESALs to fatigue failure
- N_i = Number of fatigue load cycles (N) to microcrack initiation
- N_p = Number of fatigue load cycles (N) to microcrack propagation through the HMAC layer
- SF_i = Composite shift factor that discretely accounts for HMAC anisotropy, healing, and aging
- SF_a = Shift factor due to HMAC anisotropy, ranging between 1 and 5
- SF_h = Shift factor due to healing, ranging between 1 and 10, at temperatures around 20 °C (68 °F)
- SF_{ag} = Shift factor due to binder oxidative aging, ranging between 0.001 and 1 at a reference temperature of 20 °C (68 °F) (see Figure 3-10)

Q = Reliability factor (a value of 1.0 was used in this project)

Equations 3-6 and 3-7 are the basic CMSE and CM fatigue analysis models. Detailed description of these equations and their component variables is contained in Appendix A and Report 0-4468-2 (Walubita et al., 2005a, b). In Equation 3-6, the sum ($N_i + N_p$) represents Lab N_f and the product ($SF_i [N_i + N_p]$) represents Field N_f . In these analyses, the aging effects are incorporated through the SF_{ag} , while all other variables are based on material properties measured from virgin HMAC mixtures that have only been subjected to AASHTO PP2 short-term oven aging (AASHTO, 1994).

CMSE N_f Prediction

Table 3-9 is the predicted Lab $N_f (N_i + N_p)$ results for both 0 and 6 months aged mixtures. According to Table 3-9, all mixtures exhibited a declining trend in Lab N_f magnitude in response to binder oxidative aging. The 0 months Lab N_f values are larger than the 6 months Lab N_f values. Thus aging reduces mixture fatigue resistance under strain-controlled repeated tension testing. Table 3-9 also shows that response to binder oxidative aging in terms of the decrease of Lab N_f (fatigue resistance) is characteristic of each mixture type

Table 3-9. Lab $N_f (N_i + N_p)$ Results (PS#1 under the WW Environment).

HMAC Mixture	Lab $N_f (N_i + N_p)$	Aging Period @ 60 °C (140 °F)
Bryan	06.31 E+06	0 Months
A10	12.95 E+06	0 Months
A20	14.86 E+06	0 Months
B10	07.88 E+06	0 Months
B20	09.01 E+06	0 Months
C10	04.92 E+06	0 Months
C20	06.12 E+06	0 Months
A16	04.98 E+06	6 Months
A26	05.26 E+06	6 Months
B16	03.23 E+06	6 Months
B26	04.12 E+06	6 Months
C16	02.73 E+06	6 Months
C26	02.71 E+06	6 Months

Table 3-10 is an example of the mixture Field N_f results for PS#1 under the WW environment predicted over a 20-year design period (considering a 20-year aging exposure period) according to the CMSE approach based on Equation 3-6. Detailed Field N_f results for other pavement structures and environmental conditions including those for the CM approach are included in Appendix D.

Table 3-10 shows Field N_f results computed with a SF_a value of 2.0 applied to all the mixtures including Bryan and B10 (Yoakum) mixtures (from Report 0-4468-2 [Walubita et al., 2005b]). Therefore, the Bryan and B10 (Yoakum) N_f results may differ slightly from the N_f results originally reported in Report 0-4468-2 (Walubita et al., 2005a, b). For easy and quick reference, the Field N_f results for the Bryan and Yoakum (B10) mixtures excerpted from Report 0-4468-2 are given in parentheses in Table 3-10 (Walubita et al., 2005a, b). Note also that the mixtures Bryan, A10, B10, and C10 were designed at optimum binder content and mixtures A20, B20, and C20 at optimum plus 0.5 percent binder content.

Table 3-10. CMSE Field N_f Predictions (PS#1 and WW Environment).

Parameter	HMAC Mixture						
	Bryan	A10	A20	B10	B20	C10	C20
SF_a	2.0	2.0	2.0	2.0	2.0	2.0	2.0
SF_h	6.73	7.18	7.28	7.26	7.32	5.91	6.53
SF_{ag}	0.045	0.045	0.045	0.07	0.07	0.028	0.028
Lab N_f (1E+06)	6.31	12.95	14.86	7.88	9.01	4.92	6.12
Field N_f (1E+06)	3.82 (3.11)	8.37	9.74	8.01 (8.40)	9.23	1.63	2.29
Legend:							
Mixtures Bryan, A10, B10, & C10 = optimum binder content							
Mixtures A20, B20, & C20 = optimum plus 0.5 percent binder content							
Field $N_f = SF_{ag} \times [SF_a \times SF_h] \times [Lab N_f]$							
() = Field N_f values from Report 0-4468-2 (Walubita et al., 2005b).							

Considering 5 E+06 design traffic ESALs over a 20-year design period at a 95 percent reliability level for this particular pavement structure (PS#1), it is clear that only mixtures A and B will adequately sustain the estimated traffic without premature fatigue failure.

From Table 3-10, the Field N_f sensitivity to binder type and binder content is also evident. An increase in binder content increases the Field N_f in all the mixtures. In terms of binder type, mixture C with PG 76-22 (TR) appears to be the worst in terms of Field N_f magnitude. When comparing Bryan and mixture A, for the same PG 64-22 binder, mixture A with gravel aggregates exhibited better Field N_f than the corresponding Bryan mixture with limestone aggregates. This result is consistent with the material property results reported previously in this chapter and confirms that material type/combination plays a significant role in the fatigue performance of HMAC mixtures.

N_f Comparison (CMSE versus CM)

Figure 3-11 is a comparative plot of the mixture Field N_f as a function of binder content based on both the CMSE and CM approaches. These results represent Field N_f predictions for PS#1 under the WW environment based on a 20-year design period with aging incorporated through the SF_{ag} considering a 20-year aging exposure period.

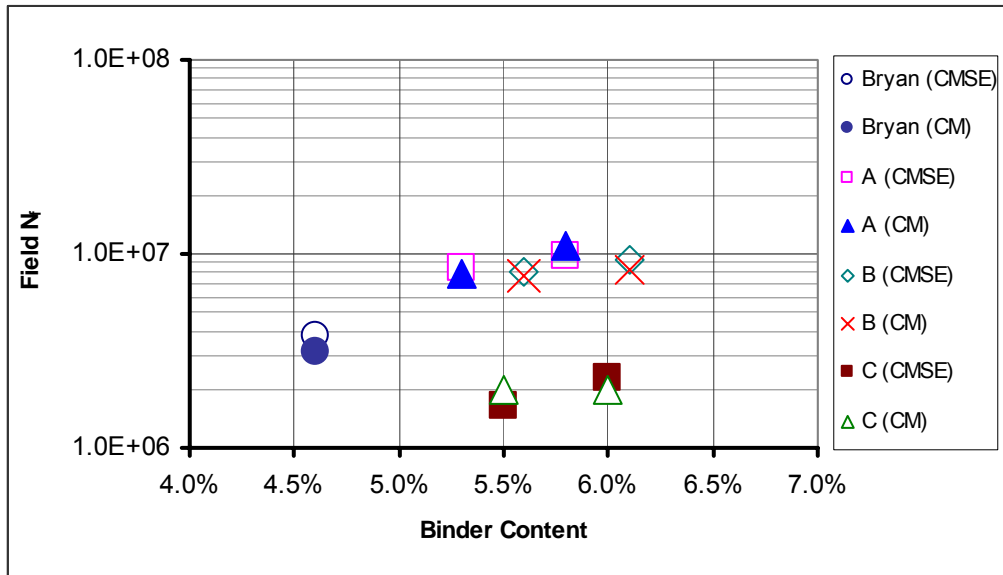


Figure 3-11. HMAC Mixture N_f Comparison (CMSE versus CM).

Although there was a marginal difference with the modified binders, it is clear from [Figure 3-11](#) that the CM results are comparable to the CMSE approach. Despite this correlation and the fact that the CM is relatively cheaper in terms of laboratory testing and data analysis time, the CM approach is recommended over the CMSE only if fatigue is the only primary distress of concern or SE and RM (compression) data are unavailable. Otherwise the CMSE is preferred because, unlike the CM, the CMSE approach has the potential to simultaneously model other distresses such as moisture damage (with the use of SE data under wet conditions with water) and permanent deformation (rutting). Practical HMAC pavement structural designs are often based on a compromise among all the prevalent distresses such as fatigue, rutting, moisture damage, and permanent deformation. Therefore, an approach that has the potential or whose input data can also be utilized to simultaneously characterize other HMAC pavement distresses is preferred.

Note from [Figure 3-11](#) the poor fatigue performance of mixture C in terms of Field N_f magnitude, followed by the Bryan mixture. This was expected of mixture C based on the material property results reported previously in this chapter. In summary these results indicated that mixture C was the most susceptible to fracture damage, had the least potential to self-heal, and most susceptible to binder oxidative aging.

On the other hand, the Field N_f results for mixtures A and B are comparable in terms of magnitude. However, a detailed review of [Table 3-7](#) and [Figure 3-11](#) suggests that mixture A would have performed better than mixture B based on the Lab N_f , but the PG 64-22 binder appears to be more susceptible to oxidative aging than the PG 76-22 (SBS) binder based on the smaller SF_{ag} value (i.e., 0.045 versus 0.07). As a result, the final Field N_f values for both mixtures are comparable. Generally, [Figure 3-11](#) also shows an increasing trend in Field N_f magnitude with an increase in binder content for all mixtures, similar to the results in [Table 3-7](#).

CMSE N_f Prediction versus Pavement Structure and Environment

[Figure 3-12](#) is a plot of Field N_f for mixture A10 as a function of pavement structure and environmental location. These results represent Field N_f values predicted over a 20-year design period using the CMSE approach with aging effects incorporated through the SF_{ag} .

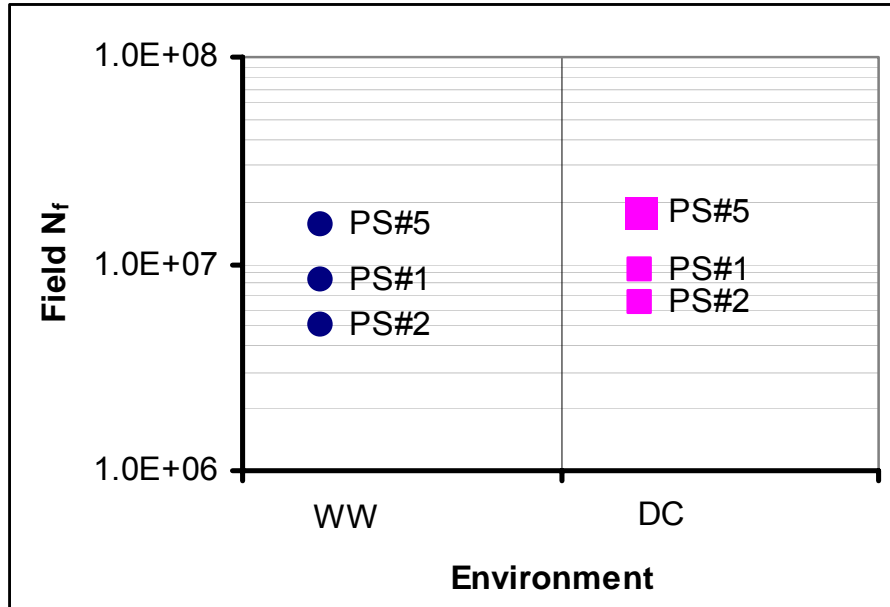


Figure 3-12. Mixture (A10) N_f versus Pavement Structure and Environment.

Figure 3-12 clearly shows that the fatigue resistance and subsequent fatigue performance of any given HMAC mixture is also dependent on the pavement structure and the environment where it is used. For example, Figure 3-12 shows that mixture A10 exhibits relatively better fatigue resistance (measured in terms of Field N_f magnitude) in PS#5 and the DC environment. That is, this particular mixture (A10) would theoretically perform better in fatigue if used in pavement structure PS#5 under the DC environment.

These results stem from the stress-strain response of the HMAC layer, which constitutes an input parameter in N_f prediction, that is dependent on the entire pavement structure and the environment. The environment (primarily temperature and moisture variations) impacts the material properties of both the HMAC and underlying layers differently. In other words, N_f prediction is dependent on pavement structure and the environment. On the same basis, a surrogate fatigue test protocol can only be established for mix-design and HMAC mixture screening, but not for a comprehensive N_f prediction analysis. Investigation of surrogate fatigue tests for mix design and HMAC mixture screening for fatigue resistance are discussed in Chapter 6 of this report.

CMSE/CM SENSITIVITY ANALYSIS

A sensitivity analysis of the CMSE and CM approaches was conducted to remove redundant variables and simplify the analysis models. This procedure involved an iterative change of the input variables and observation of their effect on N_f (both Lab and Field). For a 95 percent reliability level, the sensitivity analysis was set to a 5 percent threshold for the input variables and arbitrarily to 2.5 percent for the output N_f . If changing an input variable by 5 percent (while holding the other variables constant) caused a change of more than 2.5 percent in N_f , then the variable was considered significant and kept in the model. Otherwise, it was considered insignificant and removed from the model.

Also, where applicable, variable parameters were replaced with numerical values in the models. For example, C_{max} ([Appendix A](#)) has been replaced by 1.75 mm (0.03 inches) based on the CMSE/CM failure criterion. With aging accounted for through the use of the SF_{ag} , some variables such as n_{BD} (brittle-ductile characterization) ([Appendix A](#)) become redundant and were thus removed from the models ([Walubita et al., 2005b](#)).

Additionally, the CM models were re-adjusted and modified accordingly within a ± 15 percent error tolerance based on a wide spectrum of HMAC mixtures to match the CMSE results. The final CMSE and CM models after sensitivity analysis are shown in [Appendix A](#). Note that in these models, aging effects are incorporated through the SF_{ag} , and all other variables are based on virgin HMAC mixtures subjected to AASHTO PP2 short-term oven aging only.

SUMMARY

The following list summarizes the important findings of this chapter based on the HMAC mixture N_f results:

- At comparable test temperatures, the PG 76-22 (TR) binder was found to be much stiffer than the second modified binder (PG 76-22 (SBS)) based on the DSR $G^*/\sin \delta$ property.

- Mixture fatigue resistance (N_f) (at an assumed constant AV content) is a complex function of mix-design parameters (binder content) and material properties (binder, aggregate, and HMAC). These parameters and properties affect various HMAC mixtures differently and should be discretely taken into account when modeling HMAC mixture fatigue resistance. In addition, N_f is dependent on the pavement structure and environment; thus mix design and HMAC fatigue characterization must be integrated with pavement structural design and analysis to ensure adequate fatigue performance.
- Increase in binder content improves HMAC fracture properties and increases mixture N_f .
- For the same gravel aggregate and gradation, the mixture with PG 76-22 (SBS) exhibited superior fracture properties and N_f compared to the second modified mixture with PG 76-22 (TR). In fact, the PG 76-22 (TR) mixture exhibited the worst N_f compared to all other HMAC mixtures considered in Phase II of this project.
- For the same PG 64-22 binder, the gravel mixture exhibited better N_f than the corresponding limestone mixture.
- Under strain-controlled testing, binder oxidative aging reduces mixture fatigue resistance, and the response to binder oxidative aging is characteristic of each mixture type.
- While the SF_{ag} methodology utilized in this report produced reasonable results, validation of these concepts is still required through testing of additional binders and HMAC mixtures, possibly with longer laboratory aging periods that realistically simulate current HMAC pavement design practices. Furthermore, there is a need to incorporate mixture volumetric properties (such as AV and binder content) and effects of temperature variations and traffic loading in the SF_{ag} model. These factors are hypothesized to play a significant role in the aging phenomenon of HMAC mixtures due to binder oxidation.
- The CMSE approach provides a promising and rational methodology for fundamentally characterizing mixture N_f . The approach:
 - interactively utilizes fundamental material properties to estimate N_f and discretely accounts for HMAC non-linearity, visco-elasticity (through DPSE), anisotropic, healing, and binder oxidative aging effects;
 - utilizes relatively simple laboratory tests and a realistic failure criterion; and
 - provides a rational basis for comparatively evaluating the effects of mix-design parameters, volumetric properties, and material type on mixture N_f .

- Although there was a marginal difference for mixtures with modified binders, the CM results were nonetheless comparable to those of the CMSE approach. However, the CM approach is only recommended over the CMSE if fatigue is the only primary distress of concern or there is limited data; otherwise the CMSE is preferred.

CHAPTER 4

MIXTURE VERSUS NEAT-FILM BINDER OXIDATION AND HARDENING AND THE IMPACT OF BINDER OXIDATION ON MIXTURE FATIGUE

Hot-mix asphalt concrete is a heterogeneous complex composite material of air, binder, and aggregates used in pavement construction. Approximately 500 million tons of HMAC (valued at about \$11.5 billion) is used in pavement construction annually in the United States (Si, 2001). Despite this widespread usage, the fatigue characterization of HMAC mixtures to ensure adequate performance is not well established, and fundamental fatigue predictive models still remain to be developed. Under traffic loading and changing environmental conditions, HMAC exhibits nonlinear elasto-viscoplastic and anisotropic behavior. Its mechanical properties and performance are loading rate, temperature, and directional dependent (Kim et al., 1997b, Lee, 1996, Lytton et al., 1993). With time, HMAC also ages but has the potential to heal (closure of fracture surfaces) during traffic loading rest periods (Cheng, 2002, Kim et al., 1997a, Si, 2001). Inevitably, this complex nature of HMAC response behavior under changing traffic loading and environmental conditions makes it harder to adequately model HMAC mixture properties, particularly with respect to fatigue cracking. Complicating mixture resistance to fatigue are the effects of binder oxidative aging (as a function of time) that increase both the binder viscosity and elastic modulus over time, thus reducing its ductility and increasing the HMAC mixture's susceptibility to fatigue cracking (Glover et al., 2005).

Note that in this chapter, materials from Report 0-4468-2 (Walubita et al., 2005b) and Chapters 2 and 3 of this report are discussed. Most of the HMAC mixture results including the N_f are based on data from Chapters 2 and 3 and from Report 0-4468-2.

OBJECTIVES

In this project, the effects of binder oxidative aging on HMAC fatigue resistance were investigated using a continuum micromechanics-based calibrated mechanistic fatigue analysis approach with surface energy measurements. The objectives of this part of the project were:

- (1) to compare neat-film binder aging to laboratory compacted mixture binder aging,
- (2) to quantify the effects of oxidative binder aging on controlled-strain mixture fatigue,
- (3) to compare different mixture designs with respect to fatigue and the impact of aging, and
- (4) to develop a cumulative damage understanding of fatigue decline that utilizes both mixture and binder characteristics.

EXPERIMENTAL DESIGN

Two commonly used TxDOT HMAC mixtures termed Basic and Rut Resistant were utilized. The basic mixture (defined as a Bryan mixture) was a dense graded TxDOT Type C mixture designed with a PG 64-22 binder and limestone aggregate ([TxDOT, 2005](#)). The Rut Resistant mixture was a 12.5 mm Superpave mixture designed with a PG 76-22 binder modified with polymer modifiers and crushed river gravel aggregate. The 12.5 mm Superpave HMAC mixture designed with a PG 64-22, a PG 76-22 modified with SBS, and a PG 76-22 modified with tire rubber and SBS is defined as A, B, and C mixtures, respectively. And, they have two binder content levels (optimum [1] and optimum + 5 percentage points [2]). Note that each letter and number represents binder type and binder content. Additionally, the A, B and C mixtures used 14 percent limestone screenings and 1 percent hydrated lime. The optimum design binder contents were 4.6 percent, 5.3 percent, 5.6 percent, and 5.5 percent for Bryan, A1, B1 (also called Yoakum), and C1 mixtures, respectively, by weight of aggregate. The target specimen fabrication air void content for both mixtures was 7 ± 0.5 percent to simulate the in situ AV field compaction during HMAC pavement construction. The standard Superpave gyratory compactor was used for compacting cylindrical HMAC specimens for CMSE testing to final dimensions of 4 inch diameter by 6 inch height ([AASHTO, 1994, 1996; 2004, TxDOT, 2003](#)).

Three aging exposure conditions (0, 3, and 6 months) at 60 °C that simulate approximately up to 12 years of Texas field HMAC aging at the critical pavement service temperature were selected to investigate the effects of aging on binder and HMAC mixture fatigue properties and N_f (Glover et al., 2005).

The oxidative aging process involved keeping the compacted HMAC specimens in a temperature-controlled room at 60 °C and allowing the heated air to circulate freely around the specimens. This allowed for accelerated oxidative aging of the binder within the HMAC specimens. Note that all loose HMAC mixtures were subjected to the standard AASHTO PP2 4-hr short-oven aging process at 135 °C prior to 60 °C aging (AASHTO, 1994). After HMAC mixture testing, aged binders were extracted for testing to characterize the binder chemical and physical properties. In addition, some binders were also aged in a stirred air flow test to simulate the hot-mix process for short-term aging comparisons with the AASHTO PP2 aging procedure (Glover et al., 2005, Vassiliev et al., 2002). For each test type, at least two replicate HMAC specimens were tested per aging condition per mixture type. Because HMAC fatigue cracking is generally more prevalent at intermediate pavement service temperatures, most of the laboratory tests were conducted at 20 °C (68 °F). Otherwise, the data were normalized to 20 °C (68 °F) during the analysis phase.

For hypothetical field conditions, a standard TxDOT pavement structure consisting of 6 inches HMAC (500 ksi, $\nu = 0.33$), 14 inches flex (granular) base (28 ksi, $\nu = 0.40$), and a subgrade with an elastic modulus of 9 ksi ($\nu = 0.45$) was utilized. Typical traffic conditions consisted of an 80 kN (18 kip) axle load, 690 kPa (100 psi) tire pressure, and 5 million ESALs with about 25 percent trucks over a design life of 20 years and a 95 percent reliability level in a wet-warm Texas environment considered critical to HMAC pavement fatigue performance (Huang, 1993, TxDOT, 2003). Shear strains (γ) which constitute the input failure load-response parameters for the CMSE fatigue analysis approach discussed in the subsequent section were computed using an elastic multi-layered ELSYM5 software, but were adjusted based on Finite Element (FEM) simulations to account for more realistic HMAC behavior (Park, 2004, Walubita et al., 2005b).

THE CALIBRATED MECHANISTIC WITH SURFACE ENERGY FATIGUE MODEL

The CMSE is a continuum micromechanics approach based upon the fundamental theory that HMAC is a complex composite material that behaves in a nonlinear elasto-viscoplastic manner, exhibits anisotropic behavior, ages, heals, and requires that energy be expended to cause load-induced damage in the form of cracking. Equally, energy must be expended to close up these fracture surfaces, a process called healing. The approach utilizes the visco-elastic correspondence principle, Paris' Law fracture mechanics, and the work potential theory described by Schapery (1984) to remove viscous effects and monitoring of accumulated fracture damage through changes in dissipated pseudo strain energy under repeated uniaxial tensile tests (Kim et al., 1997a; Kim et al., 1997b; Lytton et al., 1993; Si, 2001). The CMSE approach considers that HMAC micro-fatigue damage consists of two components, resistance to fracture under repeated loading and the ability to heal during rest periods, processes that both change over time. The approach further considers that resistance to fracture is governed by two processes, namely the number of repetitive load cycles for microcracks to coalesce to macrocrack initiation (N_i) and the number of repetitive load cycles for macrocrack propagation through the HMAC layer (N_p) that add to N_f .

The HMAC is thus characterized in terms of fracture (ΔG_f) and healing (ΔG_h) processes, and requires only uniaxial relaxation tests (tension and compression), strength, repeated load tests in uniaxial tension, and fracture and healing surface energy components of binders and aggregates measured separately (Table 4-1).

CMSE Fatigue Analysis Models

Equations 3-5, 4-1, and 4-2 are the fundamental principles of CMSE fatigue modeling of HMAC mixtures as utilized in this study.

$$N_f = SF_i (N_i + N_p) \geq Q \times \text{TrafficDesign}_{\text{ESALS}} \quad (3-6)$$

$$SF_i = SF_a \times SF_h \quad (4-1)$$

$$N_p = k_1 \gamma^{-k_2} \quad (4-2)$$

The CMSE approach considers the fact that HMAC is not an isotropic material and introduces an anisotropic shift factor SF_a to account for the differences in the vertical and lateral elastic modulus that result from the differences in the particle orientation during compaction/construction. Due to traffic rest periods and temperature variations, the binder has a tendency to heal, which often results in improvement in the HMAC mixture fatigue performance. A shift factor SF_h is thus introduced in the analysis to account for this healing process. This SF_h is a function of the rest periods, pavement design life, field temperature correction factor, HMAC elastic relaxation modulus in compression, surface energy due to healing (ΔG_h), and fatigue field calibration constants.

N_i is defined as the number of load cycles required to initiate and grow a microcrack of 7.5 mm in length in the HMAC layer and is a function of crack density, specimen cross-sectional area, Paris' Law fracture coefficients (A and n), and the rate of damage accumulation (b) as indicated by DPSE in the uniaxial repeated-direct tension test. Crack density calculations in this project were based on the cavitation analysis by [Marek and Herrin \(1968\)](#), assuming a brittle-adhesive mode of crack failure for the HMAC specimens. N_p refers to the number of load cycles required to propagate a 7.5 mm microcrack through the HMAC layer thickness. N_p is calculated as a function of the maximum microcrack length, HMAC layer thickness, shear modulus, Paris' Law fracture coefficients (A and n), and a design shear strain (γ) ([Cheng, 2002](#), [Lytton et al., 1993](#), [Si, 2001](#)). Other CMSE input parameters include non-linearity correction factor (ψ), stress intensity, regression and shear coefficient factors, healing constants, and field calibration constants.

Q is a reliability factor that accounts for mixture and traffic prediction variability and the anticipated uncertainties in the mixture fatigue performance during service. A Q value of 1.0 was used in this project. However, further CMSE research should inevitably explore the derivation of Q as a function of reliability level so as to adequately account for HMAC mixture and traffic prediction variability in N_f analysis.

HMAC Mixture Tests

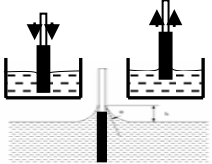
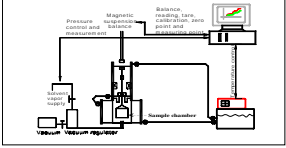
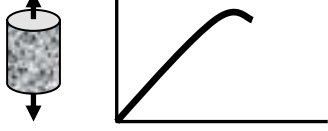
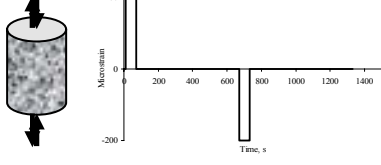

The CMSE laboratory tests conducted in this study are summarized in [Table 4-1](#). Output data from these laboratory tests served as input data for predicting mixture N_f using [Equation 3-5](#) ([Cheng, 2002](#), [Lytton et al., 1993](#), [Si, 2001](#)). Fatigue failure for the CMSE approach was defined as crack initiation and propagation through the HMAC layer thickness with a 7.5 mm microcrack length as the selected failure threshold value based on the work by [Tseng and Lytton \(1990\)](#) and [Lytton et al. \(1993\)](#).

BINDER TESTS

Extraction and Recovery

The extraction used three successive washes: one wash of 100 percent toluene followed by two washes of a mixture of 15 percent ethanol plus 85 percent toluene by volume. After the extraction, the solvent was filtered to remove all aggregate particles from the binder solution using a centrifuge. The binder was recovered from the solvent with a Büchi, RE 111 rotovap ([Burr et al., 1993](#)). During recovery, nitrogen gas was introduced to the vessel to drive off any remaining solvent and to prevent contact with oxygen. Before the removal of the solvent from the last batch of the solution, the bath temperature was kept at 100 °C (212 °F) to avoid hardening or softening of the asphalt in dilute solution ([Burr et al., 1994](#), [Burr et al., 1991](#)). When no more solvent could be detected visually, the temperatures was increased to 173.9 °C (345 °F) for an additional 30 minutes to ensure sufficient solvent removal ([Burr et al., 1990](#)).

Table 4-1. Summary of CMSE Laboratory Tests.

Test	Loading Configuration, Test Parameters, and Output Data	Application
Wilhelmy Plate-CMSE	 <p>Automatic immersion and withdrawal of binder-coated glass plates into/from liquid solvents up to approx. 5 mm depth @ 20±2 °C. Test time: ≈45 minutes. Measurable & output data are dynamic contact angle (θ) and surface energy (SE) components for the binder ($\Gamma_{i-binder}$)</p>	Computation of HMAC mixture fracture (ΔG_f) and healing (ΔG_h) energies, respectively (Cheng, 2002, Si, 2001)
Universal Sorption Device- CMSE	 <p>Clean oven dried 50 g aggregate of fraction size (4.75 mm < aggregate size < 2.63 mm) . Measurable parameters are vapor pressure & adsorbed gas mass of liquid solvents @ 25±2 °C. Test time: 60 to 70 hrs. Output data is SE components for the aggregates ($\Gamma_{i-aggregate}$).</p>	
Tensile Strength-CMSE	 <p>Tensile loading until break @ 0.05 mm/min @ 20 °C. Test time: ≈5 minutes. Output data are HMAC mixture tensile strength (σ_T) and failure strain (ϵ_f).</p>	Computation of Paris' Law fracture coefficient A
Uniaxial Relaxation Modulus- CMSE	 <p>Trapezoidal shaped strain-controlled @ 200 microstrain (tension & compression), 60 s loading & 600 s rest period @ 10, 20, & 30 °C. Test time: ≈ 25 minutes. Output data are HMAC mixture elastic relaxation modulus (E_i), stress relaxation rate (m), and temperature correction factors (a_T).</p>	Computation of healing shift factor (SF_h) and Paris' Law fracture coefficients A and n (Si, 2001)
Uniaxial Repeated Direct- Tension-MSE	 <p>Haversine strain-controlled @ 1 Hz, 30 °C, & 350 microstrain level for 1,000 load cycles. Test time: ≈20 minutes. Output data are dissipated pseudo strain energy and rate of fracture damage accumulation (b).</p>	Computation of load cycle to crack initiation (N_i) (Si, 2001)

Size Exclusion Chromatography

After the binder was extracted and recovered, it was analyzed by SEC to ensure complete solvent removal using the previously reported methodology (Burr et al., 1990, Leicht et al., 2001). Without this feedback on the recovery process, it is likely that residual solvent will be left in the binder, especially the more heavily aged binders (Burr et al., 1990). Test samples were prepared by dissolving 0.2 ± 0.005 g of binder in 10 mL of carrier. The sample of interest was then sonicated to ensure complete dissolution. The sonicated sample was then filtered through a $0.45 \mu\text{m}$ polytetrafluoro ethylene (PTFE) syringe filter. Samples of $100 \mu\text{L}$ were injected into 1000, 500, and 50 \AA columns in series with tetrahydrofuran (THF) carrier solvent flowing at 1.0 mL/min . Incomplete solvent removal is indicated by a peak located at 38 minutes on the chromatogram.

Dynamic Shear Rheometer

After complete solvent removal, the rheological properties of the binder were determined. The DSR used in this research was a Carri-Med CSL 500 Controlled Stress Rheometer.

The rheological properties of interest were the complex viscosity (η_o^*) measured at $60 \text{ }^\circ\text{C}$ ($140 \text{ }^\circ\text{F}$) and 0.1 rad/s (approximately equal to the low-shear rate limiting viscosity) and the storage modulus (G') and the dynamic viscosity (η'), both at $44.7 \text{ }^\circ\text{C}$ ($112.5 \text{ }^\circ\text{F}$) and 10 rad/s in time sweep mode. A 2.5 cm (0.98 inch) composite parallel plate geometry was used with a $500 \mu\text{m}$ gap between the plates.

DSR measurement was also important for deciding whether the binder was chemically altered in some way by the extraction and recovery process (Burr et al., 1990, Burr et al., 1994, Burr et al., 1991, Cipione et al., 1991). If two extraction and recovery processes yielded binders with matching SEC chromatograms but significantly different complex viscosities, then at least one of the binders was suspected of having undergone solvent hardening or softening.

Fourier Transform Infrared Spectrometer

Carbonyl area was measured using a Galaxy 5000 FTIR spectrometer with an attenuated total reflectance (ATR) zinc selenide prism (Jemison et al., 1992). The absorption band from 1650 to 1820 cm^{-1} relates directly to oxygen content (Liu et al., 1998) and thus provides a good measure of binder oxidation.

RESULTS AND DISCUSSION

Mixture Oxidative Aging and Fatigue Resistance

As noted above, mixtures were aged for 0, 3, and 6 months beyond PP2 conditioning in an environmental room (ER), temperature controlled at 60 °C (140 °F). These mixtures were subjected to the tests in Table 4-1 to determine the various CMSE parameters from which mixture fatigue under strain-controlled testing was determined. Table 4-2 is a summary of the SF_i , $[N_i + N_p]$, and Field N_f calculated results from laboratory tested mixtures.

While Table 4-2 shows some degree of SF_a dependence on mixture type due to the differences in the aggregate gradation, this parameter did not vary significantly as a function of aging condition based on a $\pm 15\%$ error tolerance. This SF_a insensitivity to aging was theoretically expected because anisotropy is predominantly controlled by particle orientation due to compaction and will therefore be insignificantly affected by aging. Therefore, the same SF_a for the other mixtures were used for the Field N_f calculations.

SF_h on the other hand is dependent on both mixture type and aging condition. In terms of SF_h magnitude, the higher the value, the greater the potential to self-heal. Table 4-2 shows that SF_h decreases with oxidative aging and increases with binder content at PP2 level aging. As mentioned earlier, the A1, B1, and C1 mixtures have optimum binder content, and the A2, B2, and C2 mixtures have optimum + 0.5 percentage point binder content. Therefore, mixtures lose their healing ability with aging and show better SF_h with more binder content at initial aging time. However, SF_h does not increase significantly with the increase of binder content at 6 months beyond PP2 level aging.

Table 4-2. Summary of Shift Factor, Lab N_f , and Field N_f Results.

Mixture	Parameter	Aging Condition (Months in 60 °C [140 °F] ER beyond PP2)		
		0	3	6
Bryan	SF_a	1.63	1.65	2.09
	SF_h	6.73	4.74	3.07
	Lab N_f	6.31E+06	2.42E+06	0.94E+06
	Field N_f	69.2E+06	18.9E+06	6.03E+06
Yoakum (or B1)	SF_a	2.10	2.08	2.40
	SF_h	7.26	4.76	3.81
	Lab N_f	7.88E+06	4.95E+06	3.23E+06
	Field N_f	1.20E+08	4.91E+07	2.95E+07
A1, A2, B2, C1, C2	SF_a	2.0	2.0	2.0
A1	SF_h	7.18	-	3.63
	Lab N_f	1.30E+07	-	4.98E+06
	Field N_f	1.86E+08	-	3.62E+07
A2	SF_h	7.28	-	3.66
	Lab N_f	1.49E+07	-	5.26E+06
	Field N_f	2.16E+08	-	3.85E+07
B2	SF_h	7.32	-	3.98
	Lab N_f	9.01E+06	-	4.12E+06
	Field N_f	1.32E+08	-	3.28E+07
C1	SF_h	5.91	-	2.97
	Lab N_f	4.92E+06	-	2.73E+06
	Field N_f	5.82E+07	-	1.62E+07
C2	SF_h	6.53	-	2.95
	Lab N_f	6.12E+06	-	2.71E+06
	Field N_f	7.99E+07	-	1.60E+07

* SF_a ($1 \leq SF_a \leq 5$), SF_h ($1 \leq SF_h \leq 10$), Lab $N_f = (N_i + N_p)$

Binder oxidative aging in mixtures significantly decreases controlled-strain fatigue performance. Figure 4-1 shows the decline of Field N_f as the result of binder aging, and the deterioration is significant in all cases. Fatigue life decline with binder oxidation is also characteristic of each mixture type. Mixtures from different mixture designs show different fatigue decline rates, which is independent of Field N_f at PP2 level aging. Even though the A mixture has a higher N_f than the other mixtures at PP2 level aging, the B and C mixtures have a slower fatigue decline rate than the A mixture over the period of aging time. This difference is significant with respect to the expected pavement fatigue performance. The reasons for this difference are not as yet understood, but are important and merit further research.

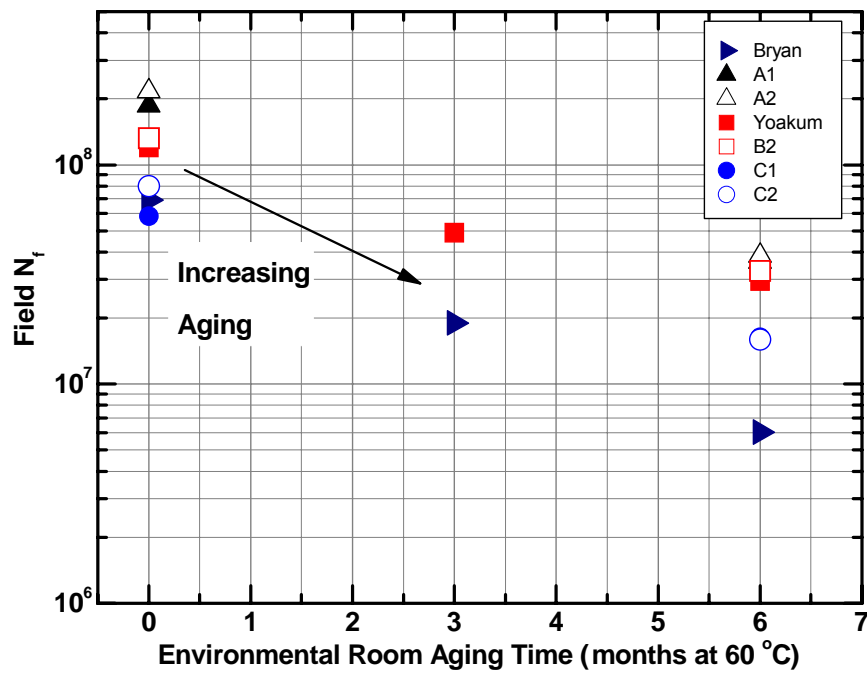


Figure 4-1. Decline of Field N_f with Oxidative Aging.

Mixture versus Neat-Film Binder Oxidation and Hardening

As noted earlier, mixtures were prepared using the PP2 short-term aging protocol and then compacted to produce one aging level (PP2+0M). Second and third levels were obtained by aging the compacted laboratory mixture in the ER for 3 and 6 months beyond PP2 conditioning (PP2+3M and PP2+6M), respectively. Here, the “0 months,” “3 months,” and “6 months” refer to environmental room aging *beyond* PP2 aging so that 0 months aging still has a significant level of aging beyond hot-mix aging. Note that Yoakum mixtures with only optimum binder content (B1) have one more aging level- 9 months beyond PP2 (PP2+9M), and the C mixtures do not have PP2+3M. The two binders were extracted and recovered from their laboratory prepared mixtures only with optimum binder content at several levels of aging and evaluated. Neat binders were aged in an HMAC simulation, the stirred air-flow test (Vassiliev et al., 2002), to give one level of aging (designated SAFT). Then these binders were further aged in the 60 °C (140 °F) environmental room in thin films (approximately 1 mm thick) for 3, 6, and 9 months to obtain second, third, and fourth aging levels (SAFT+3M, SAFT+6M, and SAFT+9M).

The aged binders were characterized by DSR and FT-IR measurements. Aging increases carbonyl area (CA, oxygen content), viscosity, and the elastic modulus, but decreases the ductility. Data for CA, η_o^* , and the DSR function for both binders and for the three mixture aging levels are shown in Table 4-3. Neat binder aging beyond SAFT also is shown.

CA increases with aging level for both the neat binders and for the recovered binders from Bryan, Yoakum, and C1 mixtures. SAFT aging leaves the binder within the initial jump (higher aging rate) region, whereas PP2 aging is more severe than the SAFT and produces a binder that seems to be aged beyond this region. Thus the PP2 data show a more uniform aging rate, whereas the SAFT points show a higher aging rate (slope) between 0 and 3 months than among 3, 6, and 9 months.

Table 4-3. Chemical and Physical Properties of Binders.

ER	CA					
Aging						
(months)	Bryan		Yoakum		C1	
	SAFT	PP2	SAFT	PP2	SAFT	PP2
0	0.620	0.807	0.556	0.720	0.708	0.7175
3	0.857	0.923	0.914	0.884	0.863	-
6	0.957	0.970	1.033	0.958	1.045	1.0225
9	1.138	-	1.194	1.067	1.217	-
ER	η_0^*					
Aging	(dPa-s @ 60 °C, 0.1 rad/s)					
(months)	Bryan		Yoakum		C1	
	SAFT	PP2	SAFT	PP2	SAFT	PP2
0	10500	37550	-	-	-	-
3	45760	78000	-	-	-	-
6	106400	119050	-	-	-	-
9	-	-	-	-	-	-
ER	DSR Function x 10 ⁴					
Aging	(MPa/s @ 15 °C, 0.005 rad/s)					
(months)	Bryan		Yoakum		C1	
	SAFT	PP2	SAFT	PP2	SAFT	PP2
0	0.43	2.11	0.80	2.78	1.41	1.63
3	3.11	6.05	8.83	7.87	9.48	-
6	8.30	9.45	16.1	12.0	22.5	15.3
9	19.79	-	49.3	25.5	39.7	-

Similar to the CA data, η_0^* for the Bryan binder also increases with aging level. The PP2-aged binder also seems to have passed the initial jump period, as the data for all three aging levels show essentially the same hardening rate. The DSR function ($G'/(G'/G')$) for the Bryan binder, shown in [Figure 4-2](#) versus the CA, also increases with aging. The DSR function is plotted on a logarithmic scale against the CA which represents the amount of aging. Thus, aging time is removed as a factor and PP2-aged binder and SAFT-aged binder show the same relation between CA and DSR function. The fact that PP2+0M is more aged than SAFT+0M is evident in both CA and DSR function values.

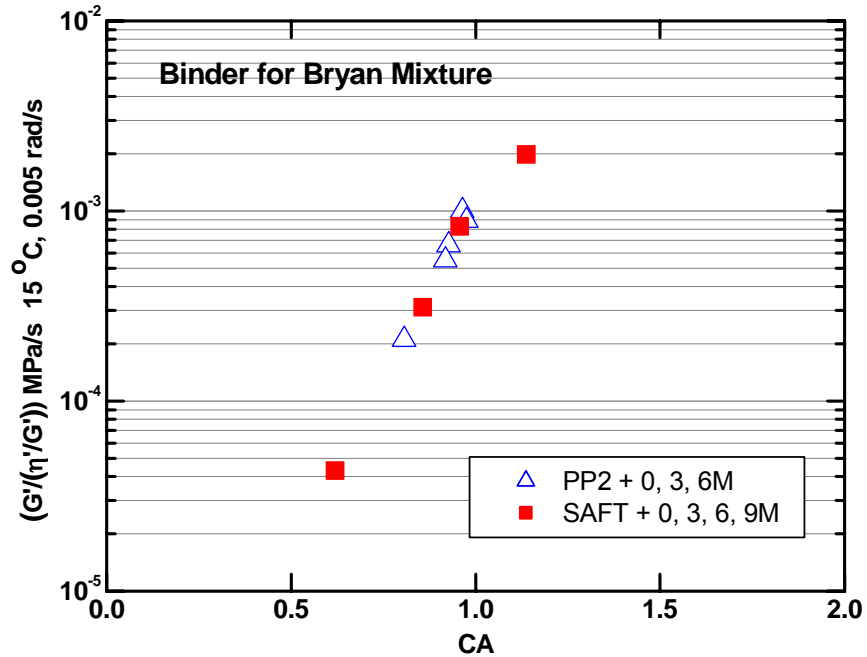


Figure 4-2. DSR Function versus Carbonyl Area for Bryan Binder (PG 64-22).

The Yoakum (B1) and C1 mixture binders are polymer modified binders (PG76-22 modified with SBS and PG76-22 modified with tire rubber and SBS), for which the zero shear viscosity is not appropriate for characterizing hardening rate (polymer modified binders typically do not exhibit a low shear rate limiting viscosity). Instead, the DSR function (at a defined temperature and frequency) hardening rate is used to represent changes of binder physical properties with aging.

The DSR function of the Yoakum binder increases with aging time, and the PP2 aging process (PP2+0M) aged the Yoakum binder more than the SAFT process (SAFT+0M). However, after 3, 6, and 9 months additional aging in the 60 °C (140 °F) room, the neat-thin film aged Yoakum binder was harder than the mixture-aged binder. Figure 4-3 shows the increase in DSR function with CA for the Yoakum binder. Again, both neat binder and mixture-aged binder show the same relation, suggesting the same aging mechanism is followed in both cases.

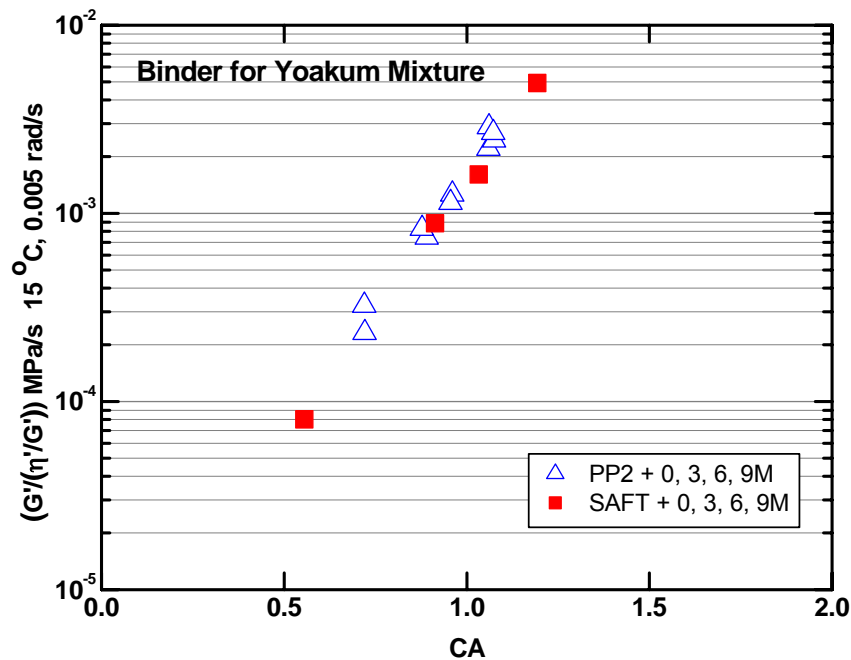


Figure 4-3. DSR Function versus CA for Yoakum Binder (PG 76-22).

The DSR function of the C1 mixture binder also increases with aging time, but the PP2 aging process (PP2+0 M) aged the C1 mixture binder slightly more than the SAFT process (SAFT+0M) in Figure 4-4. Normally, SAFT-aged binder is much less aged than PP2-aged binder in most cases. C1 mixture binder has an exceptionally higher physicochemical property at SAFT aging level and slower hardening rate than the other two binders after the initial jump period. More data are recommended for certainty.

However, this result provides possible criteria for designing more durable pavement. Higher initial stiffness could provide a high rut-resistant ability in early pavement service and slower hardening rate could improve long-term fatigue performance. More research is recommended to determine the fundamental reason for the different behavior of the C1 mixture

binder. After 6 month additional aging in the 60 °C (140 °F) room, the neat thin film aged C1 mixture binder is harder than the mixture aged binder.

The thin film binder aging catches up with the mixture binder partly because, after SAFT, it is still in the higher aging-rate initial jump period, but also because binder aging in thin films has more access to oxygen than binder in compacted mixtures. In the case of the Bryan binder, it appears that the same process is occurring but that the neat binder takes longer to catch up to the mixture-aged binder.

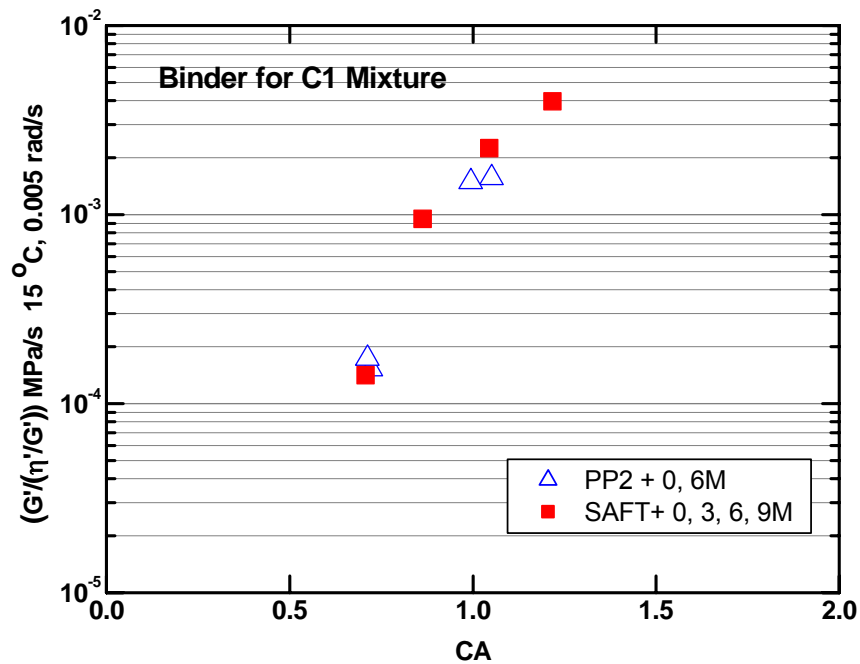


Figure 4-4. DSR Function versus CA for C1 Mixture Binder (PG 76-22 TR).

The Impact of Binder Aging on Mixture Fatigue Life

In [Figure 4-1](#), the effect of binder oxidative aging on mixture fatigue resistance was presented. The decrease in fatigue life with aging is striking, and significant differences in the rate of decline were noted among all mixtures. The reasons for these differences are as yet unknown. The discussion in this section elaborates on the possible impact of this decline in fatigue resistance on a pavement's service life and its relationship to binder mixture characteristics.

The approach discussed below utilizes the binder DSR function, attempts to incorporate the significant aspect of traffic loading, and is based on Field N_f . First, the following definitions are made:

$$\begin{aligned} N_f &= \text{Field fatigue life, ESALs} \\ R_L &= \text{Pavement loading rate, ESALs/yr} \end{aligned}$$

Then $N_f/R_L = \text{Pavement Fatigue Life Expectancy}$, in years, assuming that the fatigue is the only factor consuming the pavement life (no decline due to aging, for example). If, however, Field N_f is a function of time due to a decline with binder oxidative aging, for example, then this decline must be taken into account when estimating the pavement fatigue life. This process is typically quantified by calculating cumulative damage by Miner's hypothesis as:

$$D = \sum \frac{n_i}{N_i} \quad (4-3)$$

where D is the total damage (as a fraction) and N_i is the fatigue life when n_i loads are applied.

In this work, damage and hardening rates due to oxidation are related by the same approach but expressed in terms of time rather than loads. For a differential time period dt , during which the field fatigue life is $N_f(t)$, the fraction of a pavement's total available fatigue life consumed during dt is calculated as:

$$\text{Fraction of Life Expended during Time } dt = \frac{dt}{N_f(t)/R_L} \quad (4-4)$$

Then, Miner's hypothesis is used to sum over the pavement's entire life, defined to be the amount of time to reach an integrated fraction equal to unity:

$$\int_0^{t_{\text{end}}} \frac{dt}{N_f(t)/R_L} = 1 \quad (4-5)$$

From the experimental data for the decline of Field N_f with binder oxidative aging, $N_f(t)$ can be represented by an exponential relation:

$$N_f(t) = N_{f0} e^{-K_1 K_2 t} \quad (4-6)$$

where K_1 is the magnitude of the power law slope that relates the decline of N_f to the increase in the DSR function $G'/(η'/G')$ with aging and K_2 is the (exponential) rate of the increase of the DSR function with aging time in the pavement. N_{f0} is the initial fatigue life at $t = 0$. Solving this integral for t_{end} gives:

$$t_{\text{end}} = \frac{\ln(K_1 K_2 N_{f0} / R_L + 1)}{K_1 K_2} \quad (4-7)$$

Equation 4-5 also can be solved numerically for t_{end} if an analytical expression is not available.

An aging shift factor can be defined as the ratio of the age-shortened fatigue life to the unaged fatigue life expectancy:

$$SF_{\text{aging}} = \frac{\text{Age-shortened Life}}{\text{Unaged Life Expectancy}} = \frac{\ln(K_1 K_2 N_{f0} / R_L + 1)}{K_1 K_2 N_{f0} / R_L} \quad (4-8)$$

From this relationship, the bigger K_1 and K_2 are, the smaller the aging shift factor, i.e., the shorter the pavement's fatigue life expectancy. Equation 4-8 also shows that K_1 and K_2 have an identical effect on this shift factor. That is, the impact of aging on the DSR function and the response of the fatigue life to these changes in DSR function produce the same effect on the final aging shift factor.

The decline of mixture fatigue life with increasing DSR function is shown in Figure 4-5. Values of N_{fp} (here equal to the fatigue life of the PP2-aged compacted mixtures) were reported in Table 4-2, and K_2 , the $\ln(\text{DSR function})$ hardening rate, was taken from a lab-to-field hardening rate conversion factor of 15 field months per one ER month obtained in Project 0-1872 (Glover et al., 2005) and applied to the DSR function hardening rate, Figure 4-6.

Hardening rates of course vary from pavement to pavement and depend principally upon the climate but also on air voids and binder content. Consequently, the value used here gives only an approximate indication for any specific pavement.

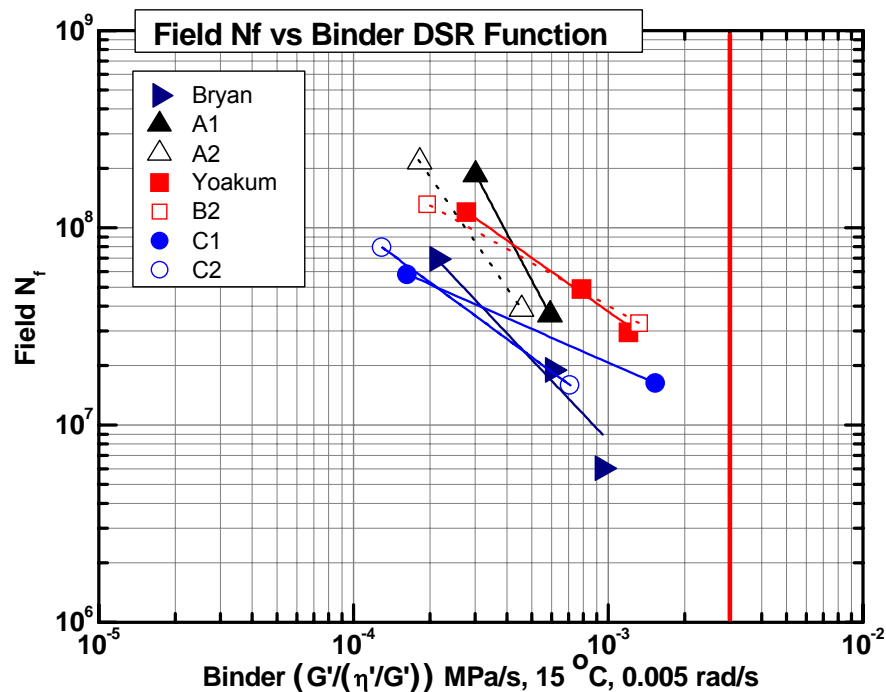


Figure 4-5. Decline of Mixture Field N_f with Binder DSR Function Hardening.

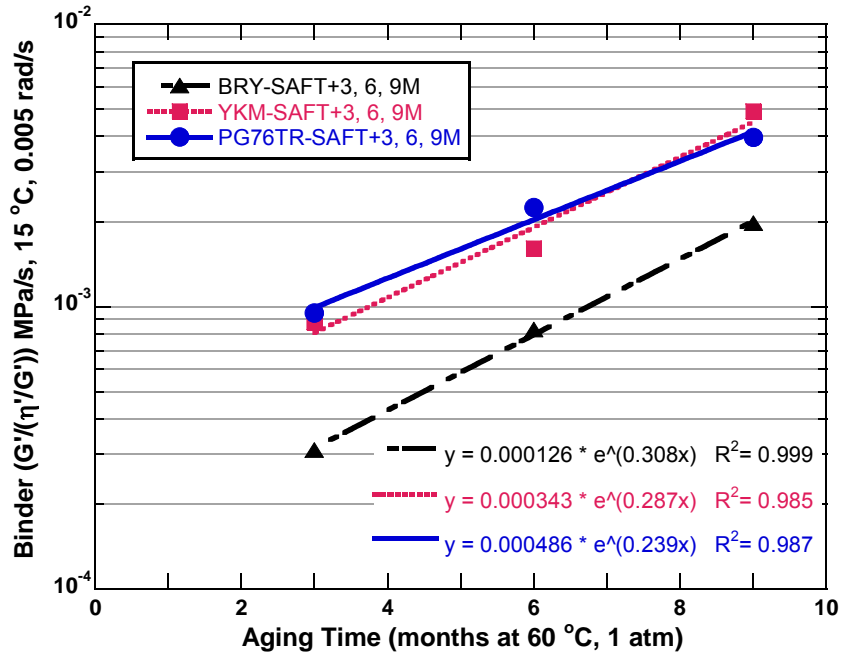


Figure 4-6. DSR Function Hardening Rate of Neat Binder after Initial Jump.

Table 4-4 summarizes the parameters and calculations for the mixtures. A loading rate of 0.25 million ESALs/year was selected for these calculations, consistent with the hypothetical field condition discussed in the "Experimental Design" section of this chapter. These calculations are intended primarily to represent a calculation procedure that shows the differences in fatigue life that might be expected between different mixtures, based upon laboratory measurements that account for binder oxidative aging. More laboratory and field data are needed to verify this approach.

Table 4-4. Summary of Pavement Fatigue Life Parameters.

Mixture	N_{fo}	R_L	K_1	K_2	SF_{aging}	Pavement Life
	10^6 ESALs	10^6 ESALs/yr				(yrs after PP2)
Bryan	69	0.25	1.37	0.25	0.049	13.5
A1	186	0.25	2.44	0.25	0.014	10.2
A2	216	0.25	1.87	0.25	0.015	13.0
Yoakum (B1)	120	0.25	0.91	0.23	0.046	22.1
B2	132	0.25	0.73	0.23	0.051	26.9
C1	58	0.25	0.57	0.19	0.129	30.1
C2	80	0.25	0.95	0.19	0.070	22.5

The difference in the estimated pavement fatigue lives (after PP2 short-term aging) for the mixtures is striking. The C and the B mixtures have longer estimated service life than the A mixture even though the A mixture has higher fatigue life than the other mixtures at PP2 level aging. It should be noted again that PP2 short-term aging produces a binder in the mixture that is significantly more aged than the SAFT (rolling thin film oven test equivalent) aged binder. How PP2 aging compares to the aging of an in-service HMAC pavement is yet unknown. However, based upon the work of [Glover et al. \(2005\)](#), the PP2 aging may reflect as much as 4 years of HMAC pavement in-service life. If so, the 10 years after PP2 (A1 mixture) amounts to 14 years of HMAC pavement total service life, the 20 years after PP2 (Yoakum mixture) amounts to 24 years, and the 30 years after PP2 for the C1 mixture would correspond to 34 years of HMAC pavement total service life.

The differences in pavement fatigue lives for the two mixtures are the results of K_1 , the rate at which the fatigue life declines with oxidative hardening of the binder, and K_2 , the binder's hardening rate in the pavement. All of these parameters favor the C1 mixtures in this instance and their combination results in the significant difference in expected pavement life. This result is shown in [Figure 4-7](#), where the curved lines represent the remaining service life change with aging and the straight lines represent remaining service life change without aging impact. The remaining fraction of estimated service life drastically decreases with aging time in all cases, when aging impact was considered.

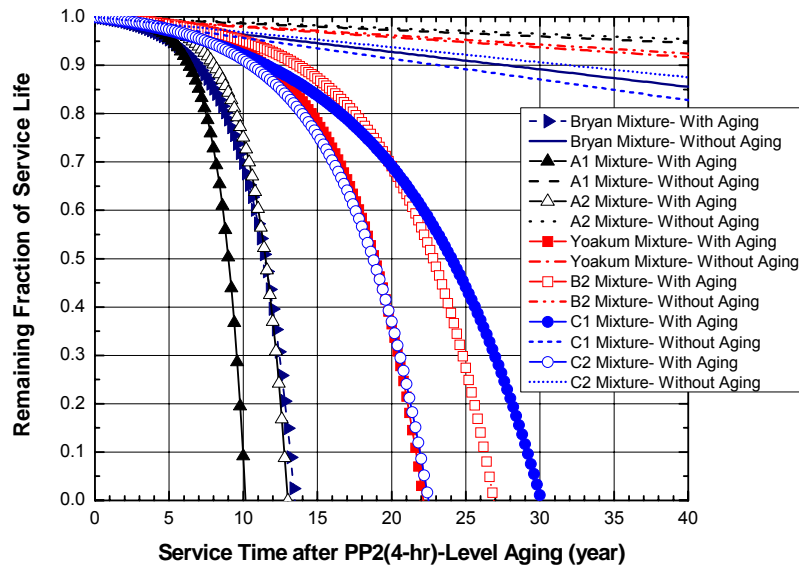


Figure 4-7. The Effect of Oxidative Aging on Estimated Pavement Service Life.

For comparison, the global aging model (GAM) of [Mirza and Witeczak \(1995\)](#) was used to calculate viscosity at 60 °C (140 °F) versus time for the Bryan binder (the unmodified binder) for use in lieu of the experimental hardening rate data. For each viscosity over time, a value of the DSR function was determined from the known viscosity versus DSR function relationship for this specific binder. Thus DSR hardening over time was determined from the GAM. Then, using the decline in fatigue life that results from increases in the DSR function, Field N_f as a function of time was determined. Finally, the integral in [Equation 4-5](#) was evaluated numerically to give t_{end} . The value thus obtained from the GAM (using a mean average annual temperature of 70 °C [158 °F] and a mix/lay down viscosity of 6,500 poise) was 73 years versus 12.9 years from the laboratory and field experimental data.

Additional comments about pavement aging are appropriate. The above data suggest that when binder aging occurs in the pavement, it can have a significant impact on pavement service life in terms of fatigue performance. However, it does not address whether or not binders in pavements actually age. At least one report in the literature is used to support the idea that pavements age primarily near the surface and little more than an inch below the surface, and the GAM appears to follow this assumption ([Coons and Wright, 1968](#)).

A separate but related issue is the extent to which binders in pavements harden in service and how quickly they harden. This issue is discussed by [Al-Azri et al. \(2006\)](#).

SUMMARY

Binder oxidative aging in mixtures significantly decreases controlled-strain fatigue performance. Fatigue life decline with binder oxidation is characteristic of each mixture type. The cumulative damage approach provides a rational method for quantitatively estimating pavement service life by simultaneously considering both the pavement loading rate and the fatigue life decline due to binder oxidative aging. The differences in expected pavement life arise from differences in their initial fatigue lives and much more significantly from different declines in fatigue life with binder stiffening combined with different binder hardening rates in the mixtures. The cumulative damage controlled-strain calculation shows a rapidly accelerating decline in pavement life as oxidative aging progresses.

CHAPTER 5

BINDER-MIXTURE CHARACTERIZATION

Pavements deteriorate over time and eventually fail in service. Two common failure modes in Texas are permanent deformation (e.g., rutting) and fatigue cracking. Permanent deformation occurs earlier in service due to heavy traffic at higher temperature when asphalt is softer, whereas fatigue failure happens later in service due to binder oxidative aging and repeated traffic loads.

This project found that binder oxidation has a significant impact on mixture fatigue performance, a result that is documented in [Chapter 4](#) of this report. The work reported in this chapter addresses binder-mixture relationships besides fatigue and the impact of oxidative binder hardening on these relationships. Of particular interest was the impact of binder aging on mixture stiffness, as characterized by the mixture's rheology. In addition to the aging effect, the impact on mixture stiffness and fatigue life due to binder hardening that results from temperature decreases was studied as a possible rapid surrogate for the effects of oxidative aging.

MATERIALS AND METHODS

Loose mix, aged according to AASHTO PP2 4-hr short-term aging, was compacted, tested in the nondestructive relaxation modulus procedure, and aged further in a 60 °C (140 °F) environmental room ([AASHTO, 1994](#)). Two types of mixtures were aged at intervals of 3 months (from 0 to 9 months) and tested after each of these aging intervals. In this way, the same physical specimen was tested at each aging level so that the effect of binder aging could be determined independent of other mixture variables. Replicate compacted mixture specimens were aged for the specified intervals, and the binder was recovered and tested for DSR properties that could be compared to the mixture properties.

Note that materials from Report [0-4468-2](#) ([Walubita et al., 2005b](#)) and [Chapters 2](#) and [3](#) of this report are also discussed in this chapter.

Binders and Tests

To associate oxidative binder hardening with mixture stiffening, two different binders were used in this part of the project: a PG 64-22 from a basic mixture design and a PG 76-22 SBS from a rut resistance mixture design. The mixtures were conditioned, and the binders were recovered and tested as shown in [Figure 5-1](#).

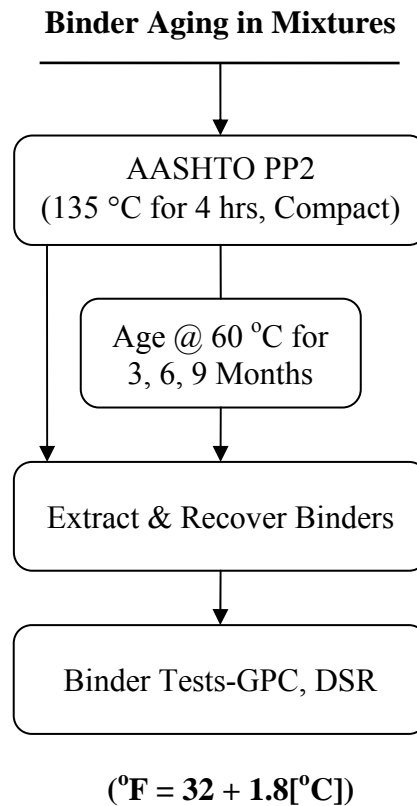


Figure 5-1. Binder Oxidative Aging and Testing.

Binders were recovered from laboratory mixtures through the extraction and recovery process. Then, size exclusion chromatography was used to ensure complete solvent removal in the recovered binders, and dynamic shear rheometer tests were used to measure rheological properties of recovered binders; details were described in [Chapter 4](#).

From DSR measurements, dynamic storage (G') and loss moduli (G'') were measured at three different temperatures (20, 40, 60 °C [68, 104, 140 °F]), with a 2.5 cm (0.98 inch) composite parallel plate used for 60 °C measurement and a 1.5 cm (0.59 inch) metal parallel plate used for 20 (68) and 40 °C (104 °F) in order to prevent upper assembly compliance problems with the stiffest binder.

Master curves for the dynamic complex modulus (G^*) were constructed using time-temperature superposition (TTSP) at 20 °C and compared with Mixture G^* (Ferry, 1980, Williams, 1971). In addition to master-curves, the DSR function ($G'/(η'/G')$), measured at 44.7 °C (112.5 °F), 10 rad/s but shifted to 15 °C (59 °F), 0.005 rad/s by TTSP, was used to track changes in binders with oxidative aging (Ruan et al., 2003).

HMAC Mixtures and Tests

Two different HMAC mixtures were used to assess the binder-mixture (BM) relationships. One was a dense graded TxDOT Type C mixture with a PG 64-22 binder and limestone aggregate (defined as the Bryan mixture), and the other was a 12.5 mm Superpave HMAC mixture with a PG 76-22 SBS modified binder and river gravel aggregate (defined as the Yoakum mixture). The mixture BM test was the same CMSE relaxation modulus tensile test described in Chapter 4. Because the RM test was assumed to be nondestructive, the same HMAC specimen was repeatedly tested at different aging conditions. Thus data were obtained at each test temperature and at each aging level for which the only variable mixture parameter was binder stiffening; other mixture parameters (void in mineral aggregates [VMA], void filled with asphalt [VFA], binder content, aggregate size distribution and configuration, etc.) were identical within the same specimen. The test was performed with both mixtures (Bryan and Yoakum) at 0, 3, 6, and 9 months beyond PP2, 4-hr aging conditions (60 °C [140 °F], 1 atm [14.7 psi] air) with at least two replicate specimens for each mixture. Figure 5-2 is a schematic illustration of the BM characterization test plan with RM testing.

The data obtained from the tensile RM test include the time-dependent elastic relaxation modulus ($E(t)$), loading time (t), and test temperature (T). From these data, a master curve for $E(t)$ was constructed at a reference temperature of 20 °C (68 °F) by using TTSP. Then, dynamic mixture storage and loss moduli were calculated as described previously (Walubita et al., 2005b).

A visco-elastic (VE) function for mixtures was calculated to be compared with binder DSR function in the frequency range where neither viscous nor elastic properties are dominant (Walubita et al., 2005b).

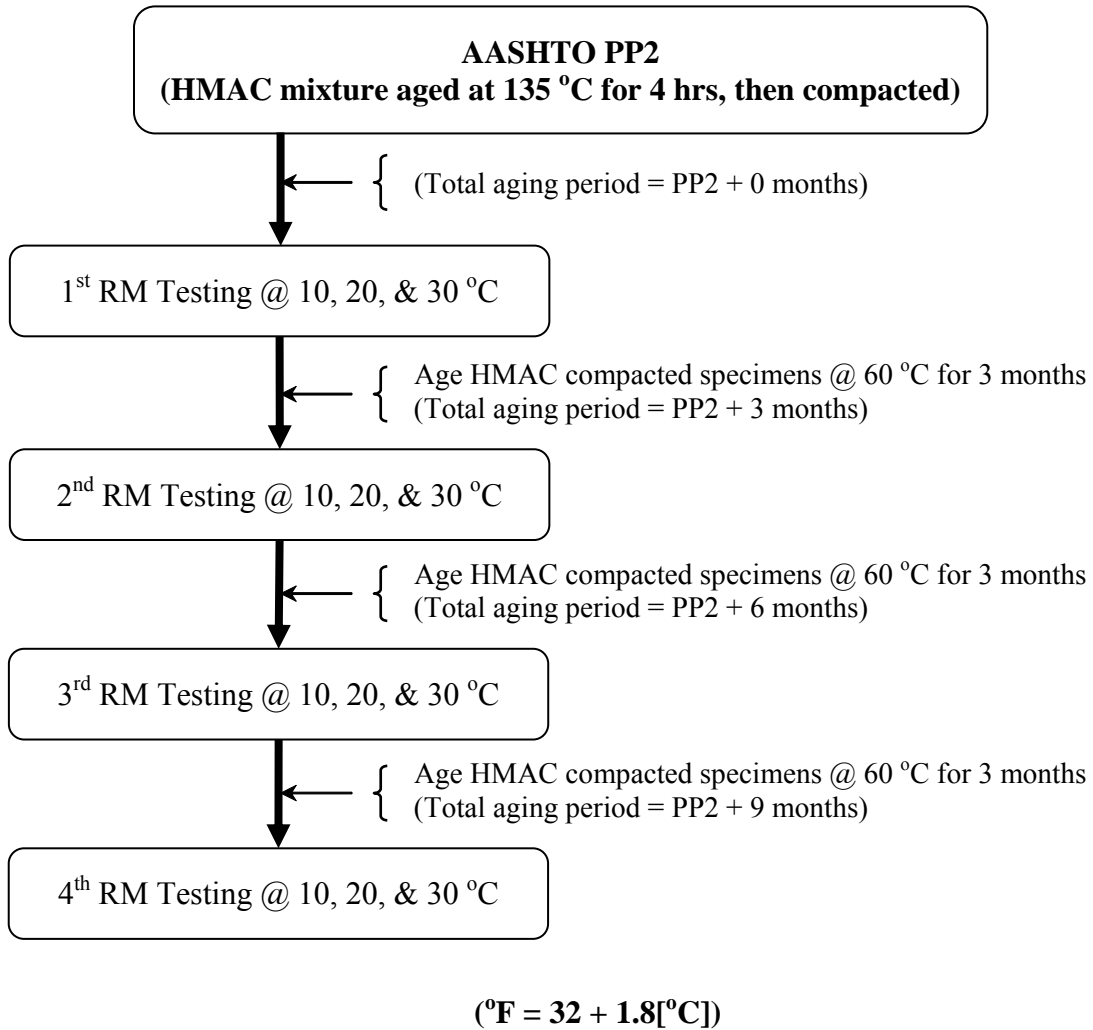


Figure 5-2. Binder-Mixture Characterization Test Procedure.

RESULTS

The test results are presented in five sections that address (1) binder rheology, (2) mixture rheology, (3) binder-mixture relationships (including the impact of temperature compared to that of oxidation), (4) the impact of temperature versus oxidation on DSR map, and (5) the impact of temperature on mixture fatigue resistance.

As discussed at the beginning of this chapter, aged mixture samples were prepared using the PP2 4-hr short-term procedure. This aged mixture was then used to make replicate compacted mixtures. One of these replicates was tested as is (PP2 plus 0 months), and then aged and tested for three more cycles, according to [Figure 5-2](#). Note that the RM data from 9-month aged mixtures are not presented due to its possible damage from the RM tests for 6-month aged mixtures.

Binder was recovered from other replicate compacted and aged mixture samples and tested to provide binder properties to compare to the tested mixtures. From the binder properties and their corresponding mixture properties, the effect of binder hardening on mixtures was evaluated directly and without the variability created by mixture parameters other than binder rheology.

Effect of Mixture Oxidation on Binder Rheology

Binder master curves at 20 °C (68 °F) for the complex dynamic shear modulus $G^*(\omega)$ were used to track changes in binder properties with aging. [Figures 5-3](#) and [5-4](#) show the results for binders recovered from Bryan and Yoakum mixtures, respectively. The Yoakum mixture includes all four levels of aging.

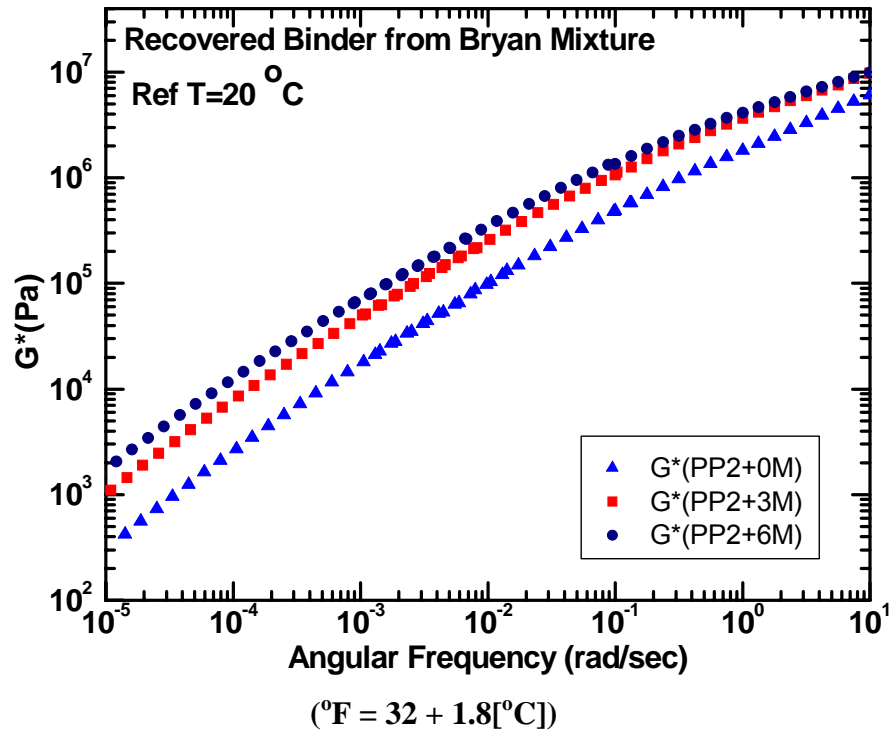


Figure 5-3. Recovered Binder Master Curves for $G^*(\omega)$ (Bryan Mixture).

The figures show that $G^*(\omega)$ increases with aging for both unmodified (Bryan) and modified (Yoakum) binders. Continued binder hardening is evident through the 9-month aging level. These increases at low frequency reflect the well-documented, and seemingly without-limit, increases in the low shear rate viscosity (η_0^*) that accompany binder aging because $\eta^* = G^*/\omega$.

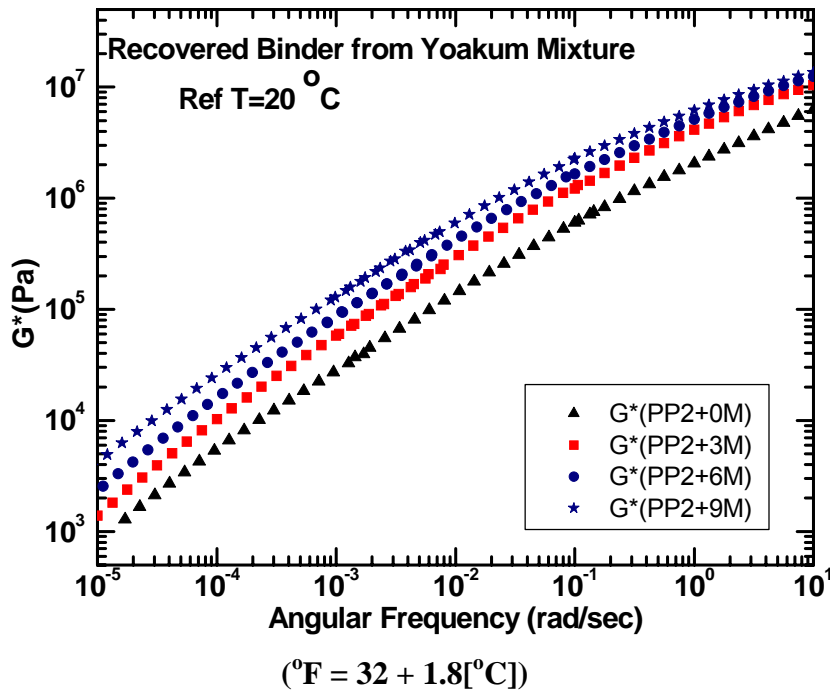


Figure 5-4. Recovered Binder Master Curves for $G^*(\omega)$ (Yoakum Mixture).

DSR map aging paths for the binder recovered from aged Bryan and Yoakum mixtures, and for neat-aged binders, are shown in Figures 5-5 and 5-6. In each case, both recovered and neat-aged binders move upward and to the left with aging, as has been observed previously (Glover et al., 2005, Ruan et al., 2003). Coincidentally, these two binder paths very nearly overlay each other even though they are different base binders and the Yoakum binder is polymer modified. Additionally, the Yoakum binder is stiffer (located more towards the top left corner) than the Bryan binder at each level of aging. DSR function values beyond SAFT+6M (neat) or PP2+6M (mixture) are far more aged than standard PAV-aged (2.1 MPa [304.6 psi], 100 °C [212 °F] for 20 hrs, 3 mm [0.12 inch] thickness) binders. The PAV* 16-hr and PAV*32 hr procedures also are shown for comparison; these are aging procedures that are being considered in lieu of the standard PAV test (Juristyarini, 2003).

The curved, dashed lines shown in Figures 5-5 and 5-6 are lines of constant ductility (cm at 15 °C, 1 cm/min) (59 °F, 0.39 inch/min) that were determined for unmodified binders by Ruan et al. (2003); as a binder ages, its ductility decreases. Kandhal (1977) concluded that a ductility of 3 cm (1.2 inch) at 15 °C is a value that corresponds well to age-related cracking failure in HMA pavements.

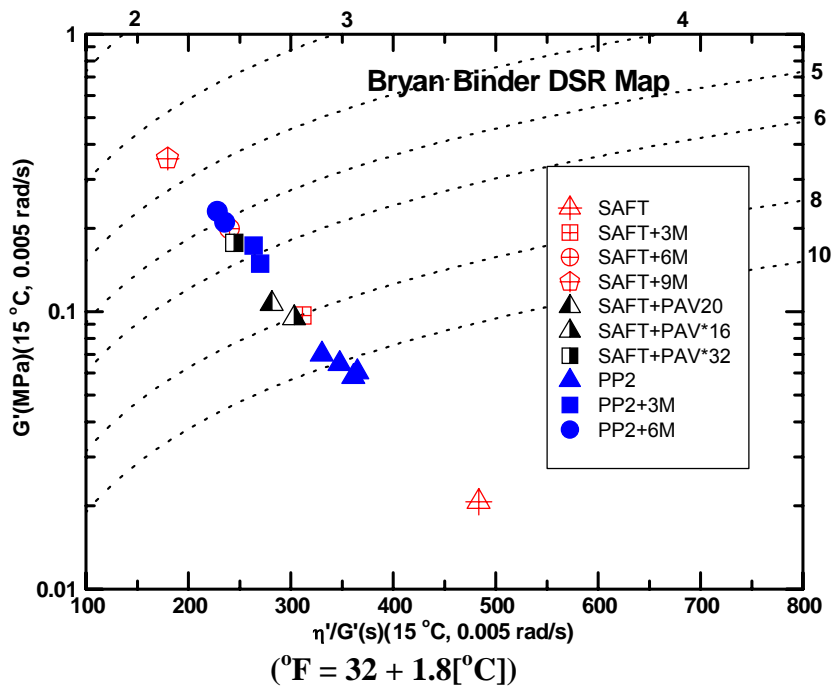


Figure 5-5. DSR Function of Binders for Bryan Mixture.

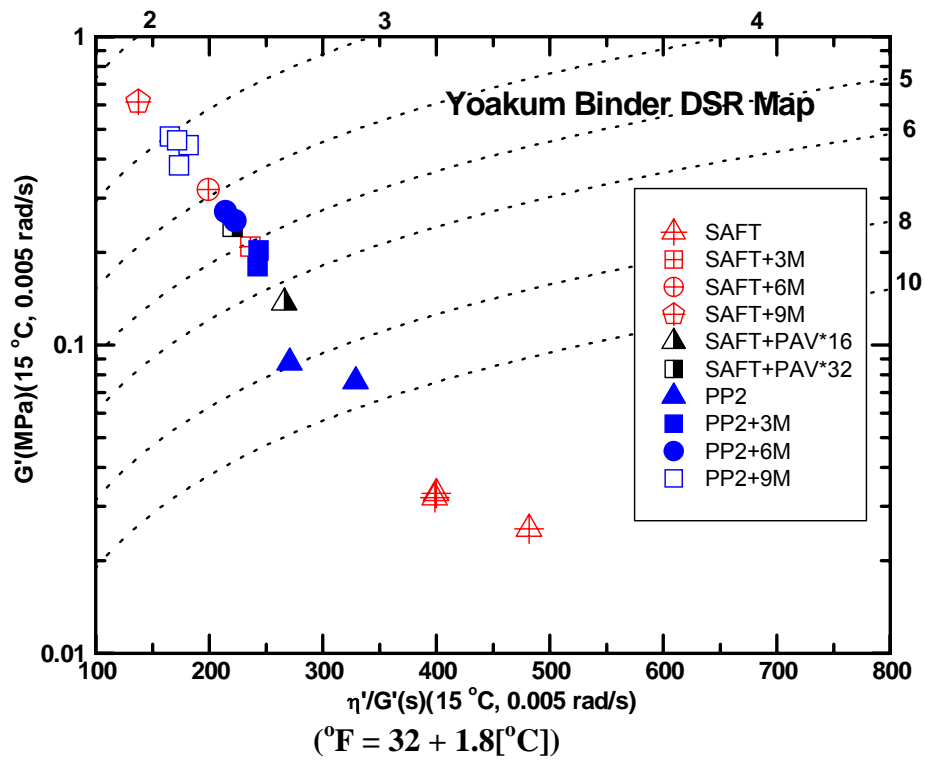


Figure 5-6. DSR Function of Binders for Yoakum Mixture.

Effect of Mixture Oxidation on Mixture Rheology

Binder oxidation affects mixture properties as well as binder. Figures 5-7 and 5-8 show mixture stiffness increases due to binder oxidation. Elastic modulus ($E(t)$) in a controlled tensile strain mode was measured at each aging level (PP2 + 0, 3, and 6 months). Tensile RM master curves were determined for both the Bryan and Yoakum mixtures at a reference temperature of 20 °C (68 °F). Details of the procedure were reported previously (Walubita et al., 2005b).

Clearly, there are inconsistencies in the data, most notably toward the end of each relaxation test, that make the master curve determination somewhat problematic. The slope ($d \log E(t) / d \log t_r$) is assumed to be a function of time to allow the master curves to be non-linear on the log-log plot, but the amount of curvature built into the model by the value of a coefficient is somewhat subjective. In addition, it is necessary to place unequal weighting on different parts of each relaxation experiment when performing the time-temperature shifting, and this weighting also is somewhat subjective. The net effect is that the master curves are subject to some degree of uncertainty.

Additional experience with this method and independent verification with other experiments (dynamic modulus, for example) is necessary in order to achieve more confidence in the mixture visco-elastic properties. The objective of obtaining a set of data at different aging levels from the same mixture specimen is to study the effect of binder aging alone on mixture stiffness and visco-elastic behavior. If different specimens are studied, then the whole host of mixture variables (aggregate gradation, VMA, VFA, binder content, and aggregate alignment configuration) is brought to play, and greater variability in the aging data will result.

From these figures, it is clear that oxidative aging stiffens the tensile RM of the mixture significantly, consistent with stiffening of the neat binder with aging. Also noted is that the Bryan mixture is stiffer than the Yoakum mixture at comparable levels of aging and test conditions even though, as noted above, the Bryan binder is less stiff than the Yoakum binder at comparable aging conditions.

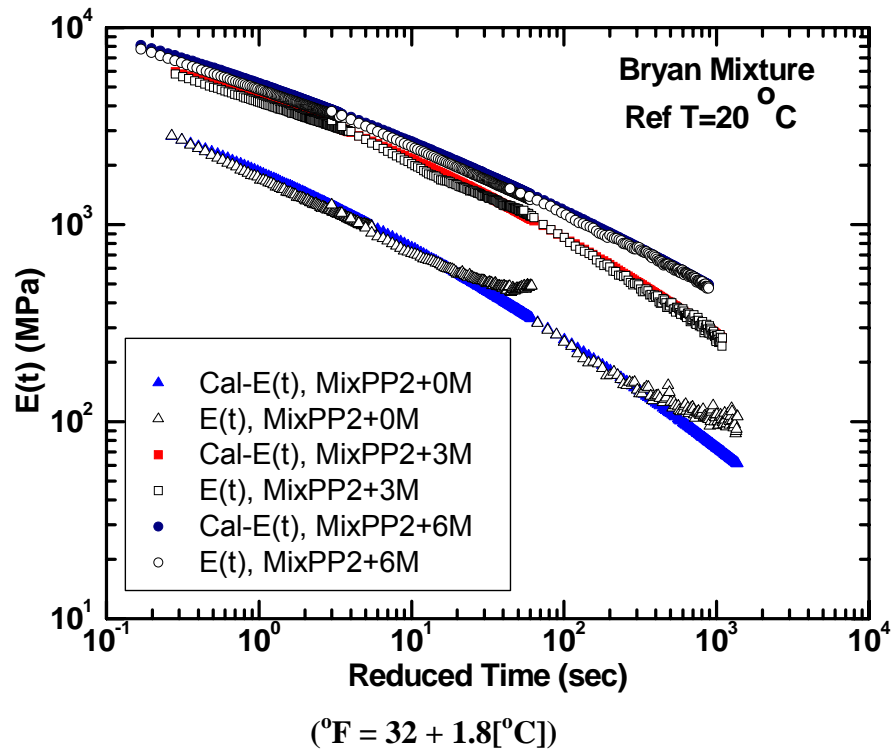


Figure 5-7. Master Curves of Bryan Mixture for E(t).

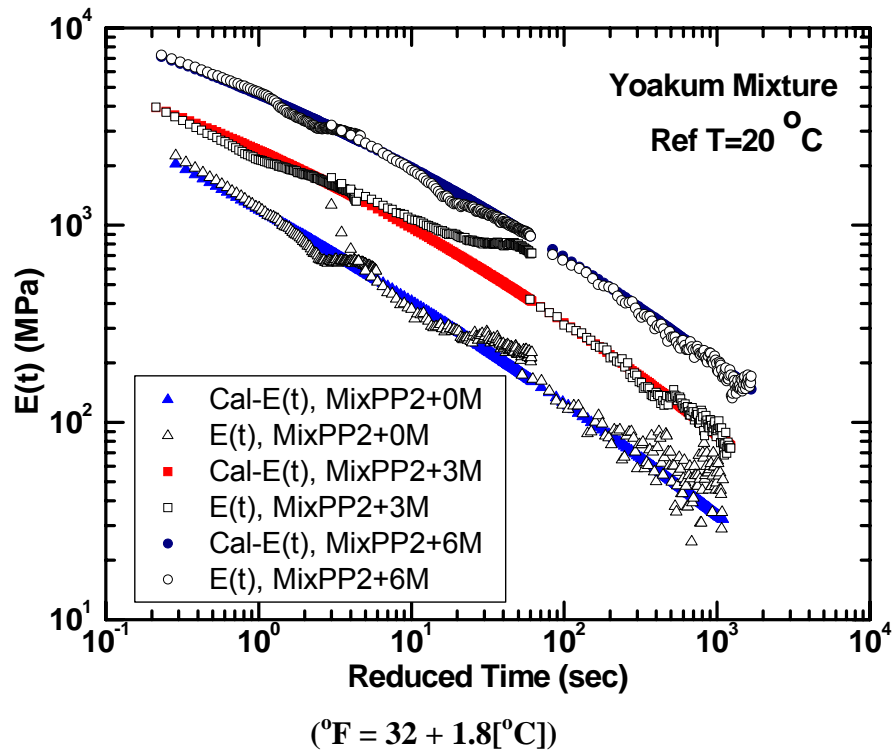


Figure 5-8. Master Curves of Yoakum Mixture for E(t).

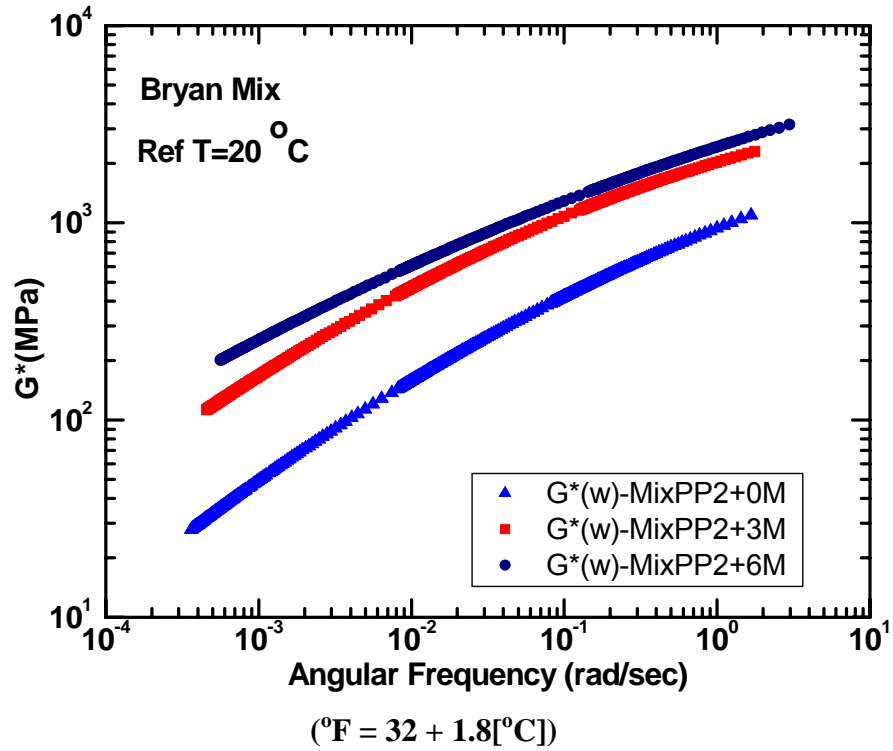


Figure 5-9. Master Curves of Bryan Mixture for $G^*(\omega)$.

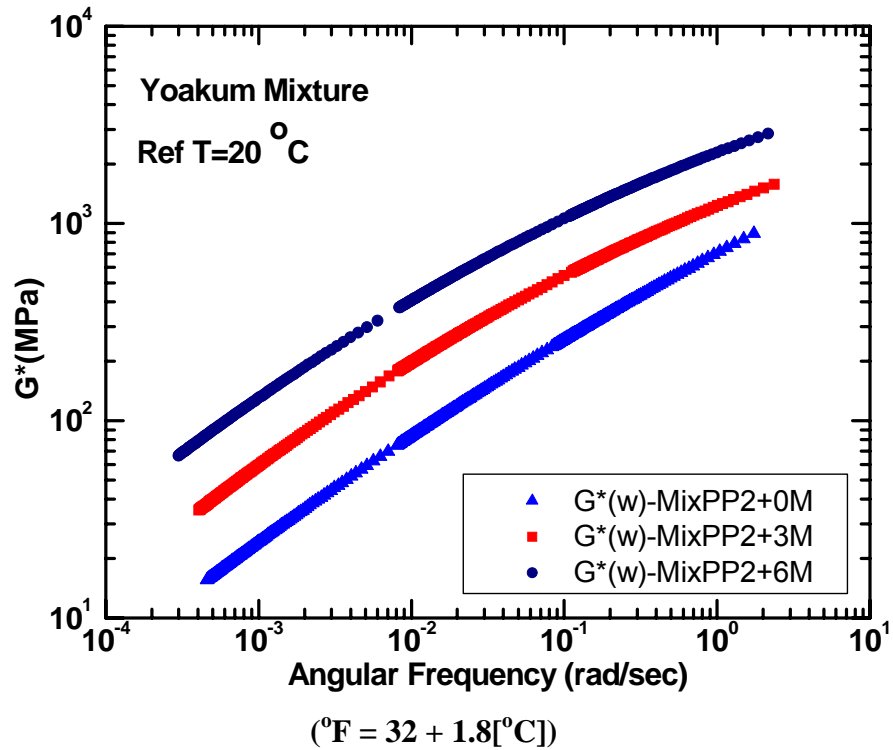


Figure 5-10. Master Curves of Yoakum Mixture for $G^*(\omega)$.

From these tensile RM master curves, dynamic shear moduli master curves were calculated for the mixture, at a reference temperature of 20 °C (68 °F). The results are shown in Figures 5-9 and 5-10 (Walubita et al., 2005b). Note that G^* increases with aging for both mixtures and that the Bryan mixture is stiffer than the Yoakum mixture, most evident at the lower frequencies.

Similar to the DSR map for the recovered binders, a visco-elastic property aging map can be constructed from the mixture visco-elastic master curves. As described previously (Walubita et al., 2005b), values from the 20 °C reference master curves at 0.002 rad/s were used to plot G' versus η'/G' , and the results are shown in Figure 5-11 (Bryan) and 5-12 (Yoakum). In both figures, one 6-month aged mixture (star symbol) is a different compacted mixture specimen than the others; nevertheless, the VE values for the two 6-month aged mixtures are quite close.

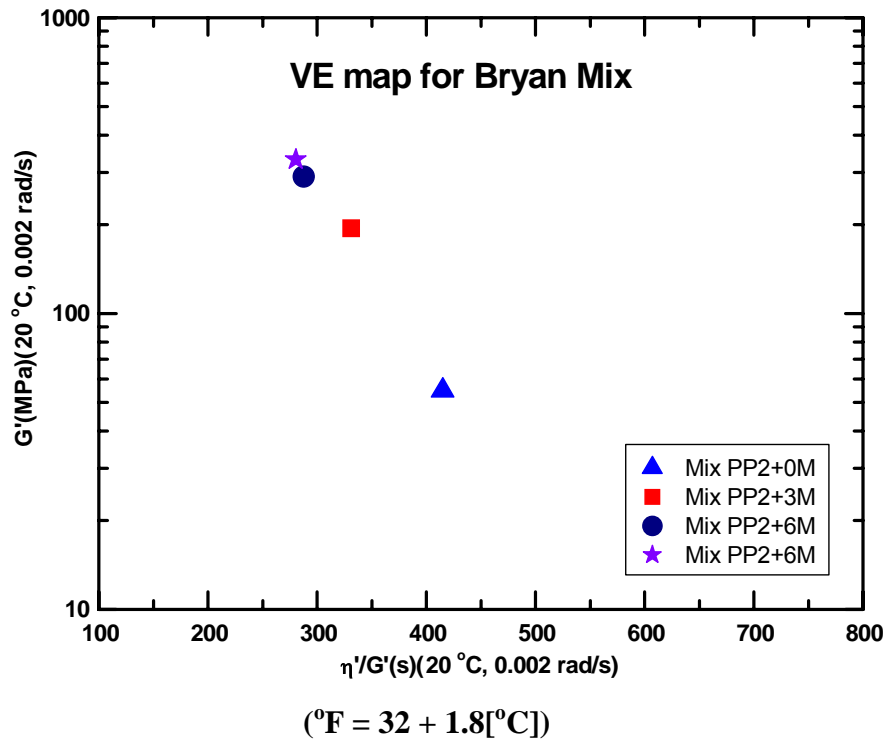


Figure 5-11. VE Function of Bryan Mixture.

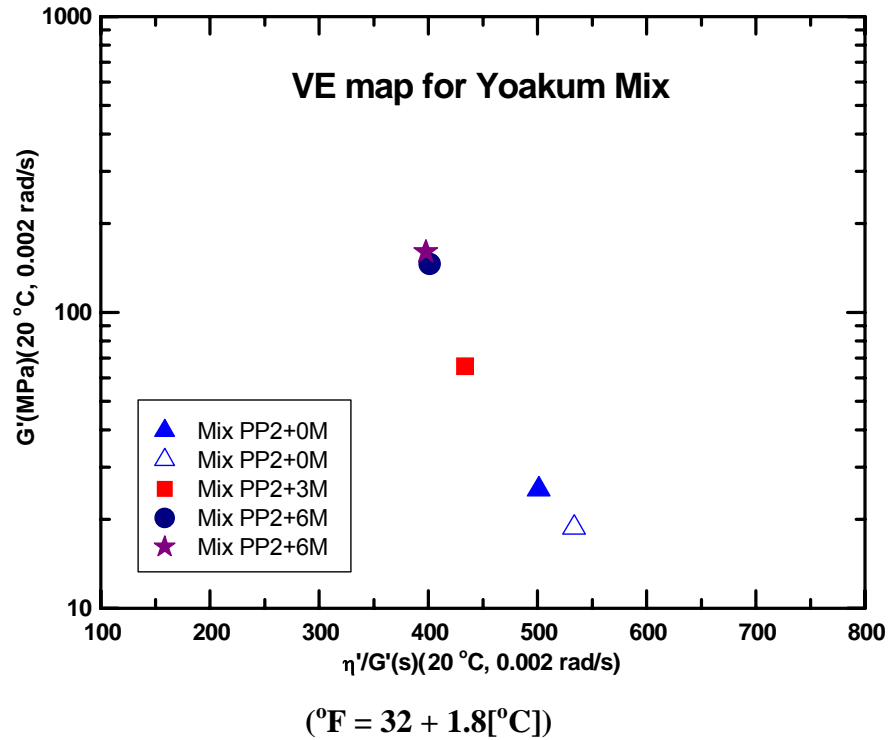


Figure 5-12. VE Function of Yoakum Mixture.

Binder-Mixture Relationships

The previous sections considered binder and mixture rheology, as affected by mixture oxidation, separately. Binder master curves, binder movement across the DSR map with aging, mixture master curves, and the mixture movement across a mixture VE function map were presented.

In this section, the mixture properties are related to their corresponding analogous binder properties. For example, a mixture G^* is related to binder G^* (at the same reference temperature and frequency), or a mixture VE function is related to its binder DSR function. Working from the mixture and binder master curves, these relationships were obtained over a range of mixture and binder properties.

Determining the impact of binder oxidation on mixture rheology, separate from other mixture variables and parameters, was of particular interest in this effort. Key to achieving this objective was observing changes in mixture rheology that occur due to oxidative aging of the same mixture specimen, as was outlined in [Figure 5-2](#).

As noted previously, the DSR function relates well to the binder ductility at 15 °C, 1 cm/min. This ductility has been reported to relate to road failure, with 3 cm being a performance limit. The objective in developing a mixture VE function is to assess whether a mixture property might be used in lieu of a binder property as an indicator of durability as well as to better understand the relation between mixture and binder properties.

Relating mixture G^* to binder G^* is of interest because of correlations previously reported in the literature, correlations that were developed through model parameter estimates using a large number of different mixtures ([Christensen et al., 2003](#)). The work reported in this section provides a detailed experimental analysis of one such correlation through measurements of changes in mixture G^* caused by binder oxidation and by changes in temperatures, while mixture parameters and variables remain constant.

VE Function Related to the Binder DSR Function

The VE function mixture trends of the previous section are obvious and very similar to those of the recovered binder DSR map. With aging, the VE function moves to the left and upward due to binder stiffening. The correlation between the mixture VE function and binder DSR function is shown in [Figure 5-13](#). Interestingly, the slopes of the Bryan and Yoakum plots are very close and differences are manifested primarily in an offset (magnitude) of the two sets of data. For each aging level, the Yoakum binder is stiffer than Bryan binder whereas the Bryan mixture is stiffer than the Yoakum mixture.

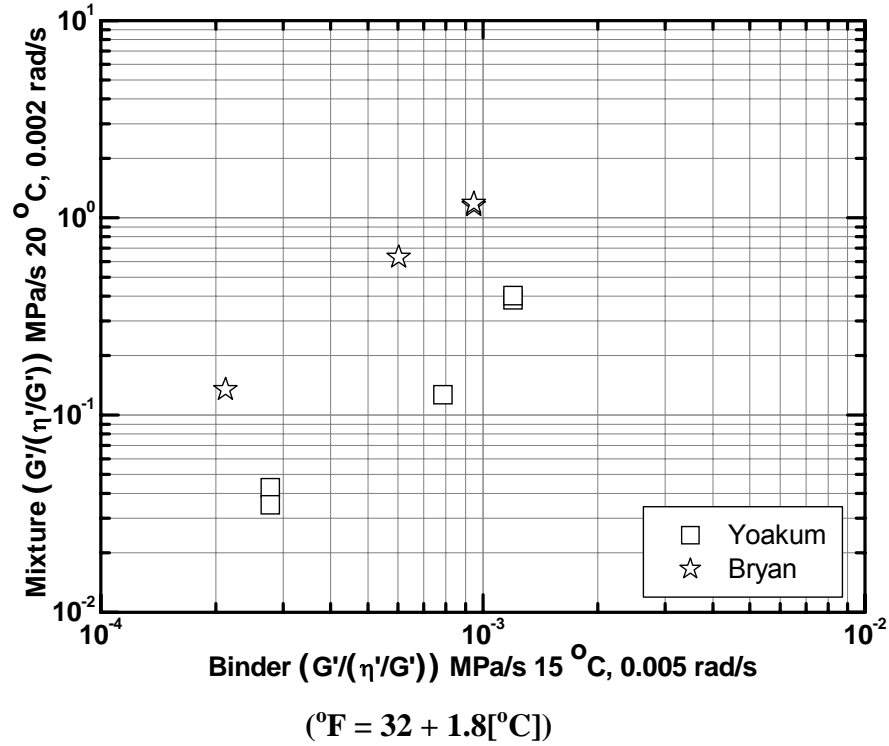


Figure 5-13. VE Function versus DSR Function.

Mixture G^* versus Binder G^*

Hirsch Model. According to Christensen et al.(2003), G^* for a mixture is a function of aggregate contact volume, voids in mineral aggregate, voids filled with asphalt, and G^* of the binder according to the Hirsch model, which is expressed in Equations 5-1 and 5-2.

$$\begin{aligned}
 |G^*|_{\text{mix}} = & Pc \left[601,000(1 - \text{VMA}/100) + |G^*|_{\text{binder}} \left(\frac{\text{VFA} \times \text{VMA}}{10,000} \right) \right] \\
 & + (1 - Pc) \left[\frac{1 - \text{VMA}/100}{601,000} + \frac{\text{VMA}}{\text{VFA} |G^*|_{\text{binder}}} \right]^{-1}
 \end{aligned} \tag{5-1}$$

$$P_c = \frac{\left(3 + \frac{VFA \times |G^*|_{\text{binder}}}{VMA}\right)^{0.678}}{396 + \left(\frac{VFA \times |G^*|_{\text{binder}}}{VMA}\right)^{0.678}} \quad (5-2)$$

where:

- P_c = Aggregate contact volume
- VFA = Voids filled with asphalt
- VMA = Voids in the mineral aggregate

Figure 5-14 shows the mixture G* as a function of binder G* according to the Hirsch model for Bryan mixture design which has a VMA of 17 and a VFA of 58.8. According to this model, the mixture G* varies by less than two orders of magnitude as the binder G* varies by three orders of magnitude.

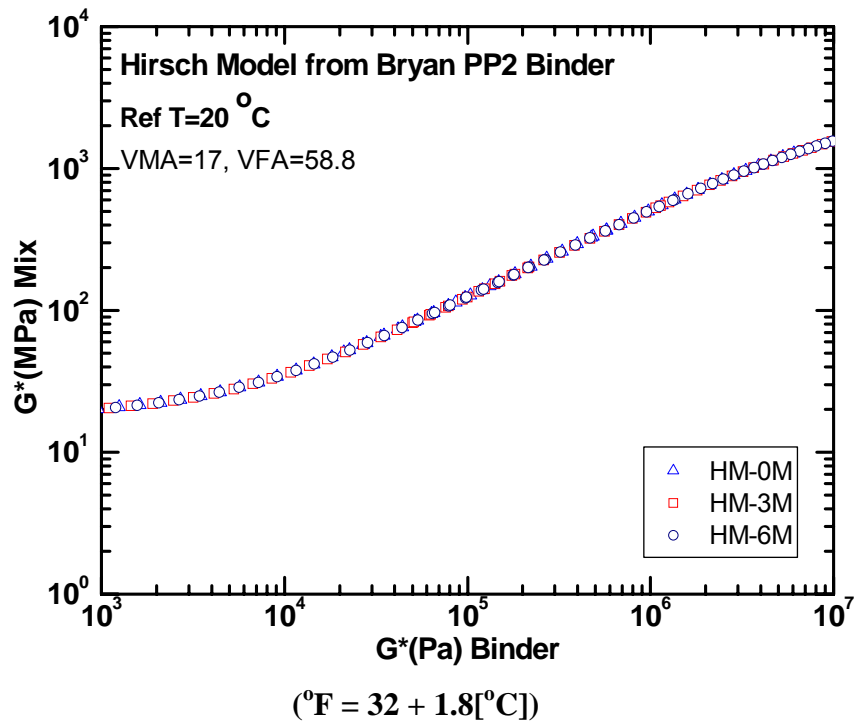


Figure 5-14. Hirsch Model from Bryan PP2 Binder.

Subsequent aging of both the Bryan and Yoakum compacted mixtures, to PP2+3M and PP2+6M levels, shifted the mixture-binder curves further away from the PP2-0M data. These shifts are contrary to the Hirsch model which assumes a shift along the same curve rather than away from it, as noted above. These shifts with aging are indicated by the lines that connect points at the same test frequency at each level of aging. These lines represent the path followed at a constant test temperature (20 °C [68 °F]) and test frequency while the binder stiffens due to oxidation. According to the Hirsch model, such lines would be tangent to the PP2-0M curve. The fact that they are not indicates that the changes in binder composition that occur with oxidation play a more fundamental role in establishing mixture G^* than just changing binder G^* .

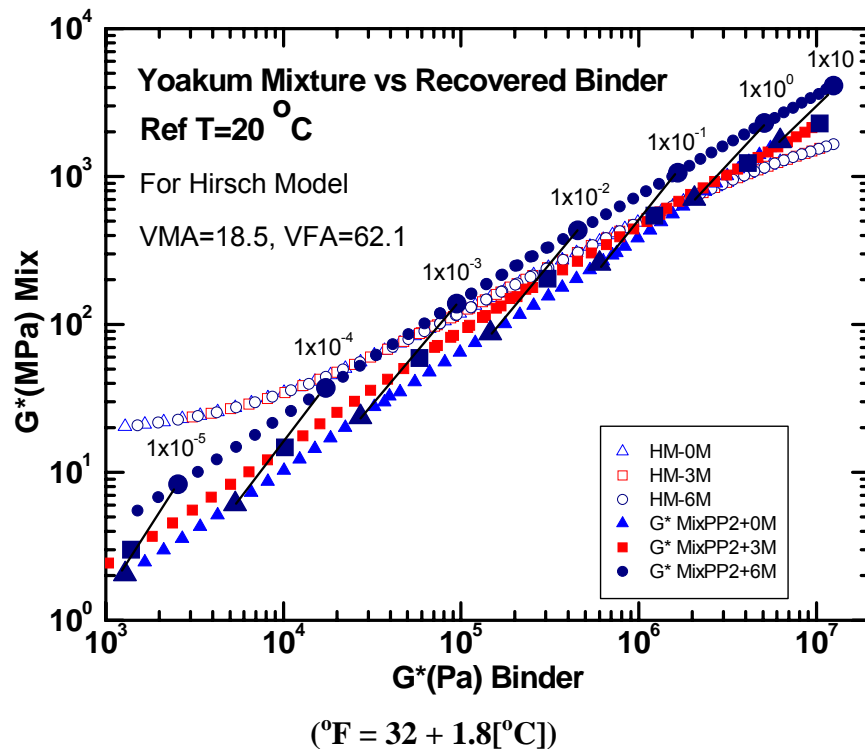


Figure 5-16. Comparison between Yoakum Mixture PP2 and Hirsch Model.

Mixture Stiffening from Binder Hardening: Oxidation versus Temperature. In the paragraphs above, the effect of oxidative aging on the mixture G^* versus binder G^* relationships was presented, with the conclusion that binder stiffening due to oxidation has a different effect than that assumed by the Hirsch model. In this section, the effect of stiffening due to a decreasing temperature is considered and compared to the oxidation results.

For the PP2 level of aging (PP2+0M), mixture and binder master curves were determined at several different reference temperatures: 10, 20, 30, and 40 °C (50, 68, 86, and 104 °F). Then the mixture and binder G^* values at 0.01 rad/s were added to Figures 5-15 and 5-16 to produce Figures 5-17 and 5-18. These new data produce a path that would be followed if the PP2-aged mixture were tested first at 40 °C (104 °F), then 30 °C (86 °F), then 20 °C (68 °F), and finally 10 °C (50 °F), all at 0.01 rad/s.

Interestingly, this temperature-stiffening path much more nearly follows the PP2+0M aging state curve than the oxidative aging path. For example, starting at the 20 °C (68 °F) point and moving toward the 10 °C (50 °F) point (while holding the frequency at 0.01 rad/s), the path is nearly tangent to the PP2+0M curve and much more in agreement with the Hirsch model calculations. Starting at that same point and increasing aging (while holding the temperature at 20 °C [68 °F] and the test frequency at 0.01 rad/s), the path (shown by the solid line) is much steeper and moves away from the PP2+0M curve. These results again suggest a fundamental difference between changes in mixture-binder relations brought on by decreasing temperature versus those caused by oxidation. This is an important observation and bears further study.

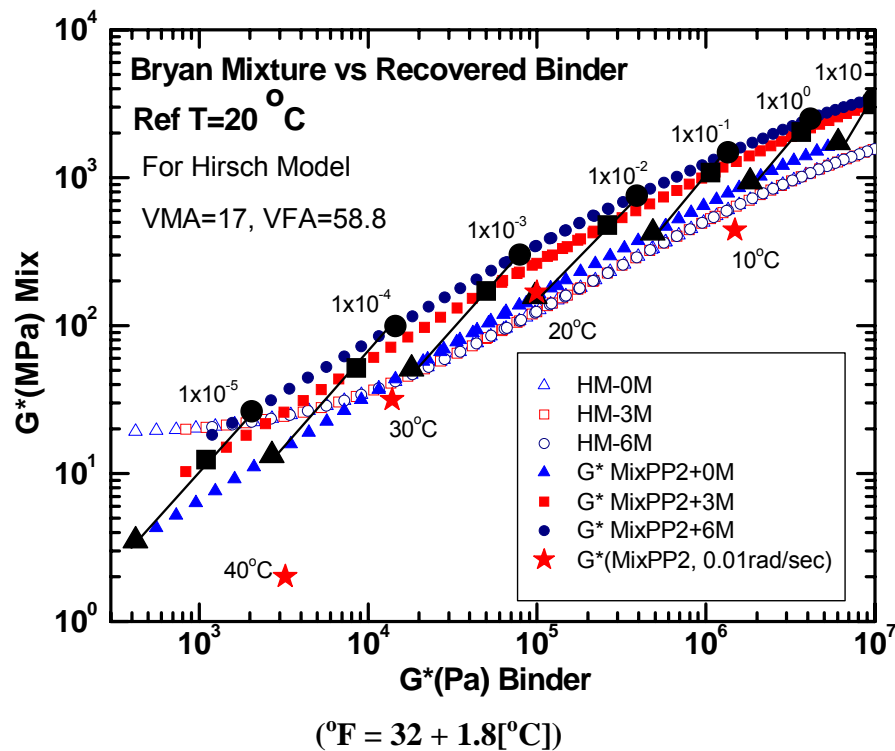


Figure 5-17. Mixture Stiffening for Bryan Mixture: Oxidation versus Temperature.

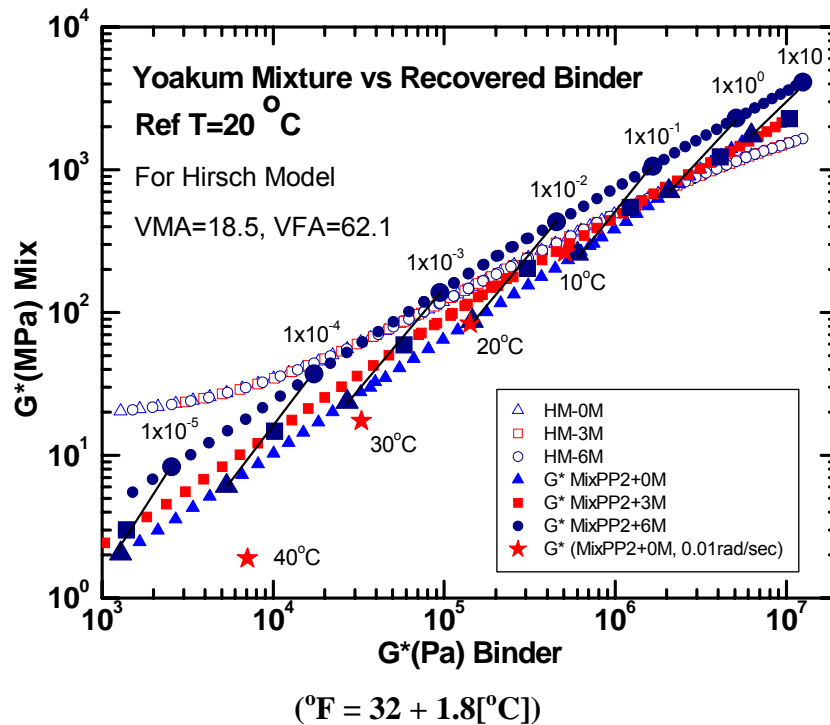


Figure 5-18. Mixture Stiffening for Yoakum Mixture: Oxidation versus Temperature.

Binder Stiffening: Oxidation versus Temperature. The impact of temperature change on binder movement across the DSR map was evaluated to further explain binder characteristics. Of interest is how the impact of binder stiffening due to decreases in temperature compared to stiffening due to oxidation (both oxidation as neat binders and in compacted mixtures).

Recovered binders at PP2 level aging (PP2+0M) were used to understand temperature hardening effects. G' and G'' at 10 rad/s were measured at several temperatures and converted by TTSP to DSR function values at a frequency of 0.005 rad/s. The measurement temperatures were 50, 45, 40, 35, and 30 °C (122, 113, 104, 95, and 86 °F) and the corresponding reference temperatures were 20, 15, 10, 5, and 0 °C (68, 59, 50, 41, and 32 °F).

The results are shown in Figures 5-19 and 5-20, together with the data in Figures 5-5 and 5-6 for comparison. Both the measurement and reference temperatures are shown for convenience. The path across the DSR map followed by these measurements at different temperatures tracks the aged-binder path for the Bryan binder well. The agreement is somewhat less for the Yoakum binder, especially for the measurements at higher temperatures (softer binder).

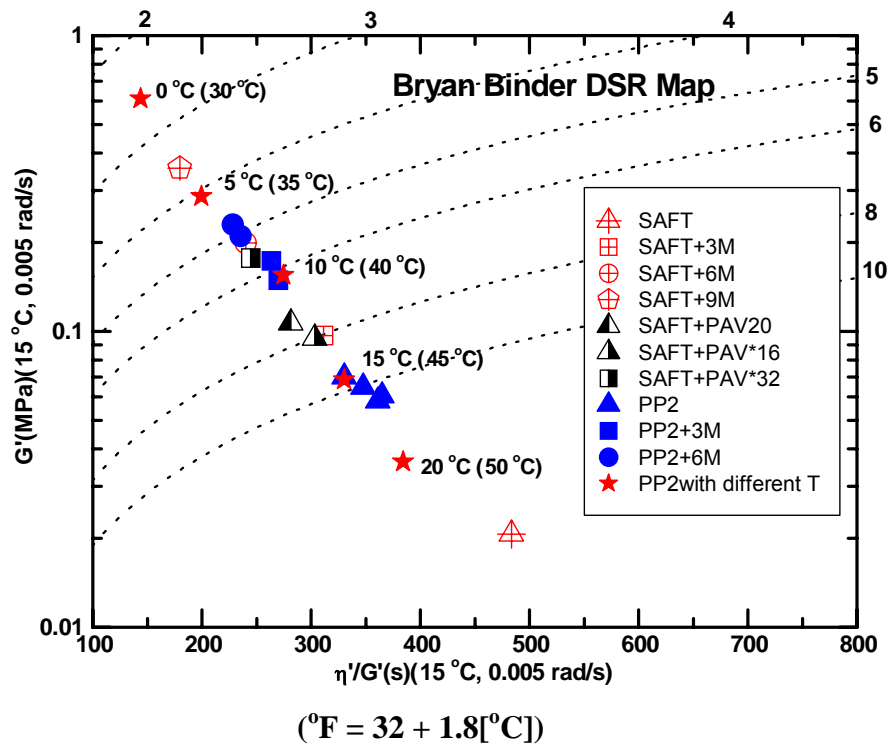


Figure 5-19. Binder Stiffening for Bryan Mixture: Oxidation versus Temperature.

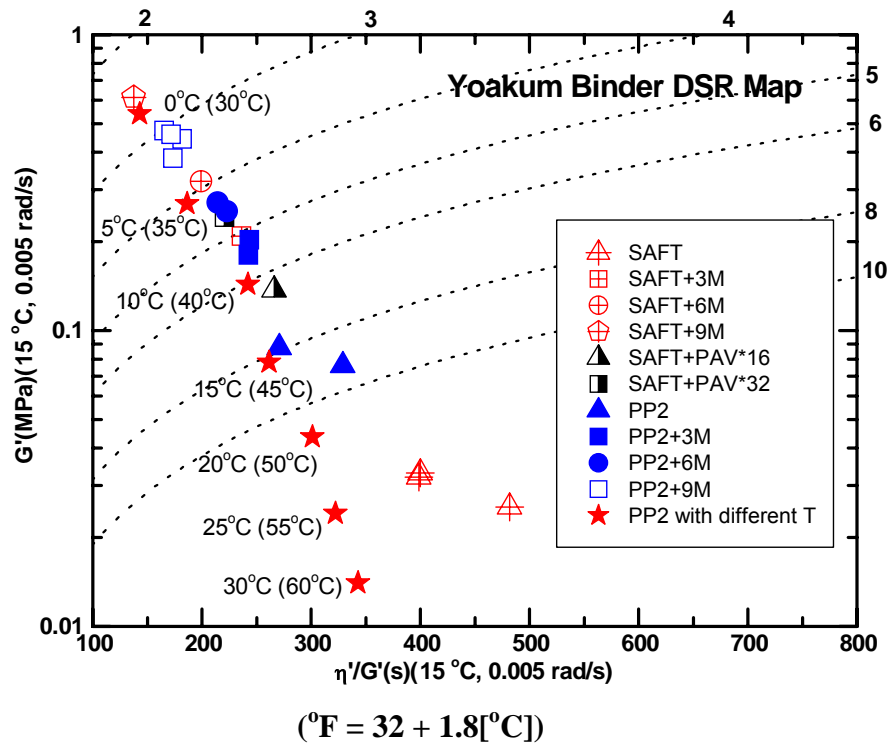
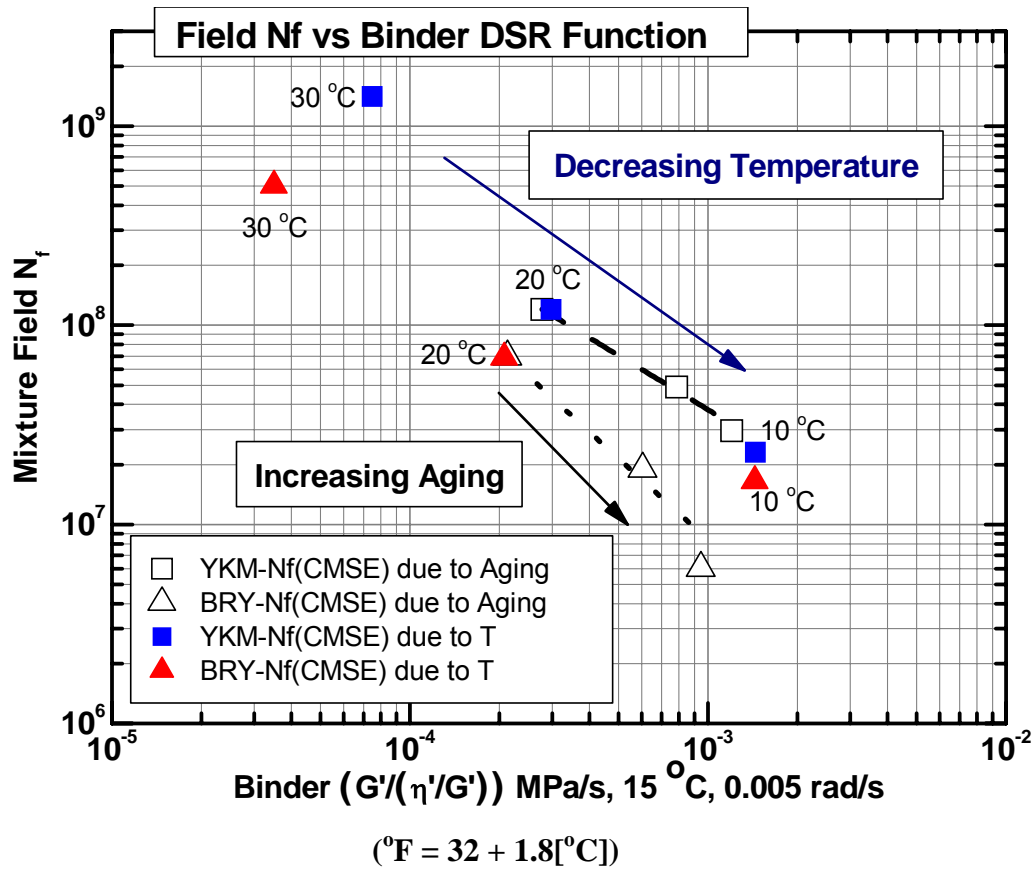


Figure 5-20. Binder Stiffening for Yoakum Mixture: Oxidation versus Temperature.

The stiffer binder regions are particularly relevant to pavement failure, and in this region the agreement provides significant hope that temperature may be used to establish an aging path as a more rapid surrogate method for aging tests. Data on more binders are needed to assess the universality of this approach. Also, it should be noted that even though the aging path across the DSR map might be determined by measurements at different temperatures, the *rate* across the map due to oxidation cannot be determined by a surrogate temperature test protocol.

Impact of Temperature on Mixture Fatigue. Previous sections have addressed the question of whether binder stiffening due to decreasing temperature might be used as a surrogate to predict the impact of oxidation. The results were inconclusive because the mixture G^* versus binder G^* relations were shifted differently by temperature than by oxidation; yet the binder path across the DSR map (after a certain level of stiffness was reached) was essentially the same, whether determined by decreasing temperature or by oxidation. This section addresses a third comparison of temperature versus oxidation, i.e., their impact on mixture fatigue life.

In [Figure 4-1](#), the mixture Field N_f (CMSE calculation at 20 °C [68 °F]) decline with oxidation was presented as a function of the binder DSR function (at 15 °C [59 °F], 0.005 rad/s) for both the Bryan and Yoakum mixtures. Using mixture and binder PP2+0M master curves, calculations were also done for the mixture N_f at 30 (86) and 10 °C (50 °F) and for the binder DSR function at 25 (77) and 5 °C (41 °F). These calculations shift both the mixture and binder PP2+0M data to 10 degrees higher and 10 degrees lower than the data reported previously. These additional data are compared to the oxidative aging results in [Figure 5-21](#).



Figures 5-21. Fatigue Life Decline with Binder Hardening.

As would be expected, decreasing the temperature results in a decline in fatigue life, most certainly because of the stiffening of the binder. Furthermore, the decline in mixture N_f relates to the increase in binder DSR function quite well, in a quantitative sense. For the Bryan mixture, the agreement with the aging decline is excellent; for the Yoakum mixture, the agreement is not as good, with significantly less decline due to temperature than to aging. The differences in the comparison may be related to the fact that the Yoakum binder is SBS polymer modified whereas the Bryan binder is unmodified. More data are needed on a variety of mixtures and binders to better determine whether temperature can be used as a surrogate for the effects of oxidative aging.

SUMMARY

In this chapter, two HMAC mixtures were tested to obtain mixture visco-elastic properties at three conditions (0, 3, and 6 months) of binder aging. Nondestructive tensile RM tests were used to produce mixture dynamic shear complex moduli master curves. Binders recovered from aged mixtures were used to determine corresponding master curves for the binder. From these binder-mixture aging experiments, the following results were obtained:

- Mixtures stiffened significantly in response to binder oxidative aging. Mixture stiffening was reflected in both the tensile relaxation modulus and the dynamic shear moduli.
- A mixture visco-elastic property map of G' versus η'/G' at the three levels of mixture aging (PP2, PP2+3M, PP2+6M) provided a useful means of tracking mixture stiffening with binder oxidative aging. This mixture VE map is analogous to the binder DSR map developed in Project 0-1872 ([Glover et al., 2005](#)).
- A mixture VE function, defined as $G'/(\eta'/G')$ at 20 °C, 0.002 rad/s, correlated linearly with the binder DSR function $G'/(\eta'/G')$ at 15 °C (59 °F), 0.005 rad/s.
- The Bryan (PG 64-22) binder was softer than the Yoakum (PG 76-22) binder. Conversely, the Bryan mixture was stiffer than the Yoakum mixture at comparable angular frequency or binder stiffness.
- The Hirsch model provided a reasonable correlation between binder and mixture G^* at PP2 level aging, especially for the Bryan mixture.
- Changes in mixture stiffness with temperature at PP2 level aging followed the Hirsch model reasonably well.
- Changes in mixture stiffness with aging deviated significantly from the Hirsch model (stiffened the mixture more).
- Binder stiffening with decreasing temperature followed much the same path on the DSR map as aging.
- The effect of temperature on mixture fatigue life may provide a means of estimating the effect of aging. Data on additional mixtures are required to establish the accuracy of such estimates.

CHAPTER 6

PROPOSAL FOR A SURROGATE FATIGUE TEST PROTOCOL

The CMSE fatigue analysis approach offers a promising and rational methodology for N_f prediction based on fundamental material properties. Although a spreadsheet was developed to simplify the analysis, the N_f prediction process is lengthy and requires a number of inputs including measured material properties, environmental conditions, pavement structure, and traffic loading. For mix design and HMAC mixture screening for fatigue resistance, a simpler, faster test methodology is required. This chapter explores the possibility of establishing a surrogate fatigue test protocol based on the CMSE fatigue analysis approach, specifically the measured fundamental material properties that are considered critical to HMAC mixture fatigue resistance. The measured property and corresponding limiting threshold selected for the surrogate fatigue test distinguishes between mix designs or HMAC mixtures that exhibit adequate fatigue resistance and those that do not without predicting N_f .

To explore the possibility of establishing a surrogate fatigue test protocol, the results of three CMSE laboratory tests (TS, RM, and RDT) conducted on seven HMAC mixtures at 0 months aging condition (Table 2-5) were evaluated. In this chapter, the methodology for the analysis is discussed followed by the test results and analyses. A discussion of the results is subsequently presented followed by a summary of the findings and recommendations.

METHODOLOGY

The analysis methodology for establishing a surrogate fatigue test protocol consisted of the following steps:

- (1) laboratory testing and material property characterization,
- (2) CMSE N_f prediction,
- (3) analysis of material properties as a function of predicted CMSE N_f ,
- (4) establishment of limiting threshold values, and
- (5) proposal of a surrogate fatigue test protocol.

Step 1: Laboratory Testing and Material Property Characterization

Fundamental material properties for the HMAC mixtures were measured consistent with the CMSE laboratory test protocols discussed in [Chapter 2](#). The results are listed in [Chapter 3](#) of this report. These material properties included the HMAC mixture tensile strength (σ_t) and the tensile failure strain (ϵ_f) at break under tensile loading from the TS test ([Table 3-6](#)), the relaxation modulus (E_I) and the stress relaxation rate (m) under tensile loading from the RM test ([Figures 3-7](#) and [3-8](#)), and the rate of fracture damage accumulation (b) from the RDT test ([Figure 3-9](#)). Note that these material properties constitute input data for the CMSE N_f prediction ([Walubita et al., 2005b](#)). Although various laboratory tests such as the DSR and SE were conducted as part of the overall CMSE laboratory test protocols ([Chapter 2](#)), only the TS, RM, and RDT tests which directly measure HMAC mixture properties were evaluated as candidate surrogate fatigue tests. The laboratory test procedures for these tests (TS, RM, and RDT) are discussed in [Appendix B](#) of this report.

Step 2: CMSE N_f Prediction

Using the material properties determined from step 1 and other required input variables (such as binder and aggregate SE data, PS, traffic loading, and environment), the HMAC mixture N_f values were predicted using the CMSE fatigue analysis approach as described in [Chapter 3](#) ([Walubita et al., 2006](#)). The N_f results for the seven HMAC mixtures (A00 [Bryan], A10, A20, B10, B20, C10, and C20) are listed in [Table 3-9](#) ([Chapter 3](#)). In this project, the CMSE N_f prediction was based on a 20-year design period at a 95 percent reliability level, and aging effects were incorporated through the SF_{ag} .

Step 3: Analysis of Material Properties as a Function of Predicted CMSE N_f

In this step, the measured material properties were comparatively evaluated and correlated with adequate HMAC mixture fatigue resistance based on the predicted CMSE N_f values. According to the CMSE approach ([Equation 3-6](#)), adequate and inadequate HMAC mixture fatigue resistance is defined as follows:

- Adequate HMAC mixture fatigue resistance:

$$N_f \geq |Q \times \text{TrafficDesign}_{ESALs}| \quad (6-1)$$

- Inadequate HMAC mixture fatigue resistance:

$$N_f < |Q \times \text{TrafficDesign}_{ESALs}| \quad (6-2)$$

In Equations 6-1 and 6-2, Q is a reliability factor that accounts for HMAC mixture characterization and traffic prediction variability and the anticipated uncertainties in the HMAC mixture fatigue performance during service. A Q value of 1.0 was used in this project. *Traffic Design_{ESALs}* represents the total number of traffic design ESALs (18 kip [80 kN]) estimated over a given design period, e.g., 20 years in this project (Walubita 2005b). In this project, five hypothetical pavement structures (Table 2-7) and two Texas environmental conditions (Figure 2-3) were considered.

Step 4: Establishment of Limiting Fatigue Threshold Values

Based on the analysis in step 3, limiting fatigue threshold values were established for each material property to discriminate between mixtures with adequate and inadequate fatigue resistance. As described in step 3, this analysis was based on the CMSE N_f results matched against the predicted and anticipated traffic ESALs over a 20-year design period for selected pavement structures and environmental conditions.

Step 5: Proposal of a Surrogate Fatigue Test Protocol

The final step consisted of proposing a surrogate fatigue test protocol from the three candidate CMSE laboratory tests (TS, RM, and RDT). The evaluation of these candidate tests and the proposed surrogate protocol were based on the following two major factors:

- (1) the potential of the test protocol and its associated limiting threshold value to provide a good correlation with the CMSE N_f predictions in terms of discriminating between adequate and inadequate fatigue resistance relative to the predicted and anticipated traffic loading ESALs; and
- (2) simplicity, test time duration, practicality, and cost considerations (in terms of test and analysis time) of the test protocol in terms of implementation and practical application.

A weighted rating system was used to rank these two evaluation factors with a total attainable score of 100 percent for the test protocols. The first factor was considered more critical to fatigue performance in terms of differentiating between mixtures with adequate and inadequate fatigue resistance. Consequently, the weighted scores were arbitrarily assigned as follows:

- Good correlation and tie to CMSE N_f prediction = 65 percent
- Simplicity, test time duration, practicality, and costs = 35 percent

During the evaluation, the test protocol whose limiting threshold value provided the best correlation with CMSE N_f prediction was assigned a total score of 65 percent for the first factor. Similarly, the test protocol that was evaluated as the best in terms of simplicity, test time duration, practicality, and costs was assigned a total score of 35 percent for the second factor. Finally, the test protocol with the highest combined score was selected and recommended as the proposed surrogate fatigue test protocol.

MATERIAL PROPERTIES AND N_f PREDICTION

The TS, RM, and RDT test data were utilized to establish limiting threshold values for mix design and screening to select fatigue resistant HMAC mixtures. This was based on the CMSE N_f results (using the SF_{ag} method) matched against the predicted and anticipated traffic ESALs over a 20-year design period for given pavement structure and environmental conditions. The CMSE N_f was also predicted over a 20-year design period assuming a 20-year aging exposure period using the SF_{ag} method.

The proposed limiting threshold values that distinguished between mixtures with adequate and inadequate fatigue resistance are presented in this section. Example results are graphically presented for PS#1 and the WW environment for the 0 months HMAC mixtures in [Table 2-5 \(Chapter 2\)](#). A summary of the results for all five pavement structures and two environmental conditions discussed in [Chapter 2](#) is also presented in this section. Note that the results (N_f and SF_{ag} method) in this chapter are extracted from [Chapter 3](#) of this report, and they were analyzed at a reference temperature of 20 °C (68 °F). An analysis based on the pavement service life and the SF_{aging} method presented in [Chapter 4](#) is also discussed.

Tensile Strength Criteria

The TS results in terms of σ_t and ϵ_f plotted as a function of the CMSE predicted N_f for PS#1 and the WW environment (for 0-month HMAC mixtures) are shown in [Figures 6-1 and 6-2](#). Note that for PS#1 with design traffic ESALs of 5.00 E+06 ([Table 2-7](#)), adequate fatigue resistance was defined as $N_f \geq 5.00 \text{ E}+06$ for this pavement structure.

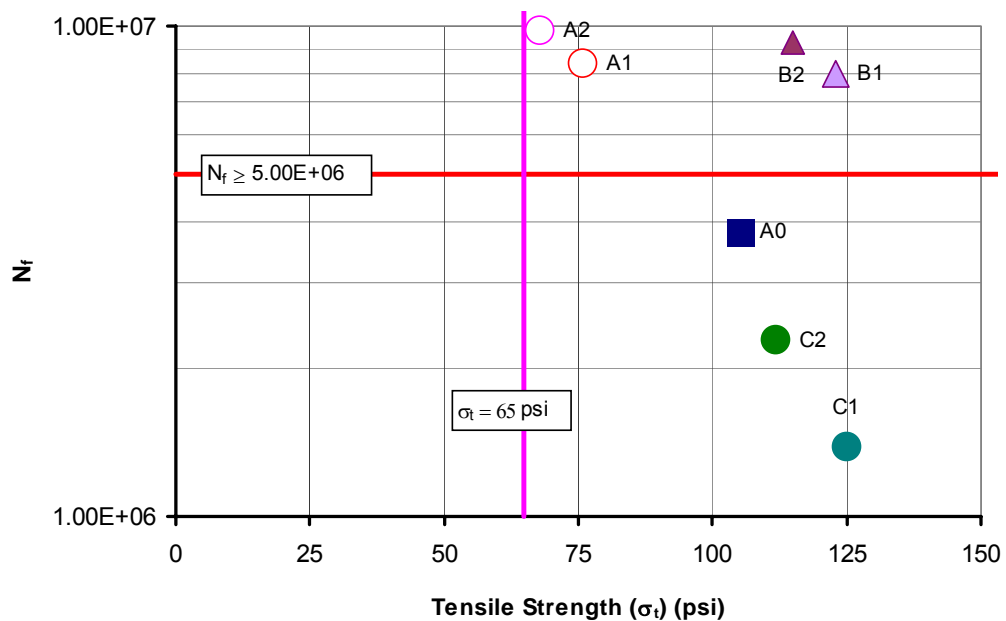


Figure 6-1. Tensile Strength (σ_t) versus N_f .

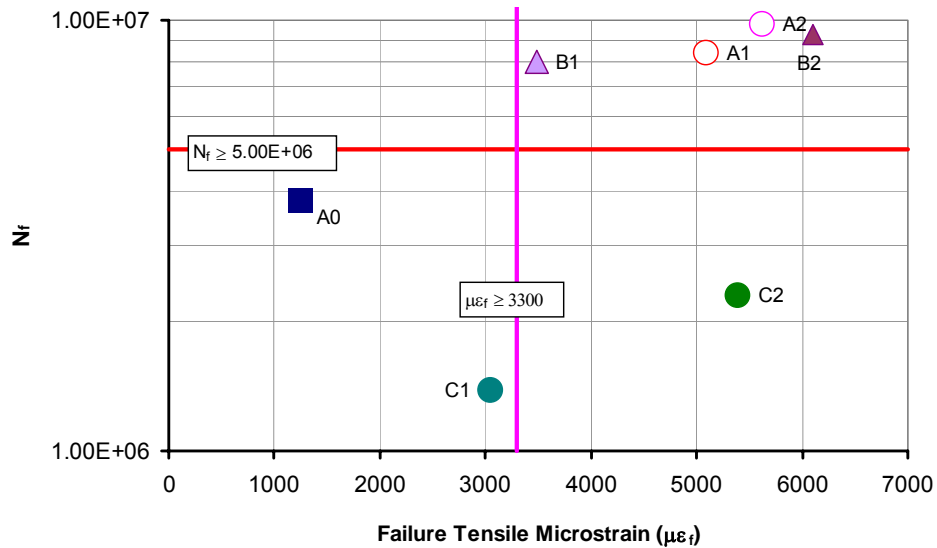


Figure 6-2. Failure Strain (ϵ_f) versus N_f .

Based on Figures 6-1 and 6-2, the proposed TS limiting threshold values are:

- Tensile strength: $\sigma_t \geq 65$ psi
- Failure strain: $\epsilon_f \geq 3300 \mu\epsilon$

Any HMAC mixture not meeting these threshold values would be considered inadequate in terms of fatigue resistance, and remedial measures to improve this mixture (e.g., increasing the binder content) would be required. With the exception of HMAC mixture C, the ϵ_f property provided a better correlation with the CMSE N_f predictions in terms of discriminating between mixtures with adequate and inadequate fatigue resistance compared to the σ_t property.

According to the σ_t property, all mixtures would exhibit adequate fatigue resistance when in fact mixtures A0, C1, and C2 are not based on the 5.00 E+06 design traffic ESALs (Table 2-7).

Consequently, if the results obtained using the σ_t and ϵ_f properties do not agree, the ϵ_f criterion should govern. Based on Table 2-3 (Chapter 2) and Figure 6-2, ϵ_f is dependent on the binder content; the higher the binder content, the higher the ϵ_f value in magnitude. This observation has also been reported by other researchers including Kandhal and Chakraborty (1996). The percentage binder contents of the HMAC mixtures in Figure 6-2 by weight of aggregate were 4.6 (A0), 5.3 (A1), 5.8 (A2), 5.6 (B1), 6.1 (B2), 5.5 (C1), and 6.0 (C2), respectively.

Relaxation Modulus Criteria

Figures 6-3 and 6-4 show the RM results (E_I and m value [tension]) plotted as a function of the CMSE N_f predictions for PS#1 and the WW environment for the 0-month HMAC mixtures listed in Table 2-5 (Chapter 2). For PS#1, adequate fatigue resistance is considered to be $N_f \geq 5.00 \text{ E}+06$ based on the traffic design ESALs in Table 2-7.

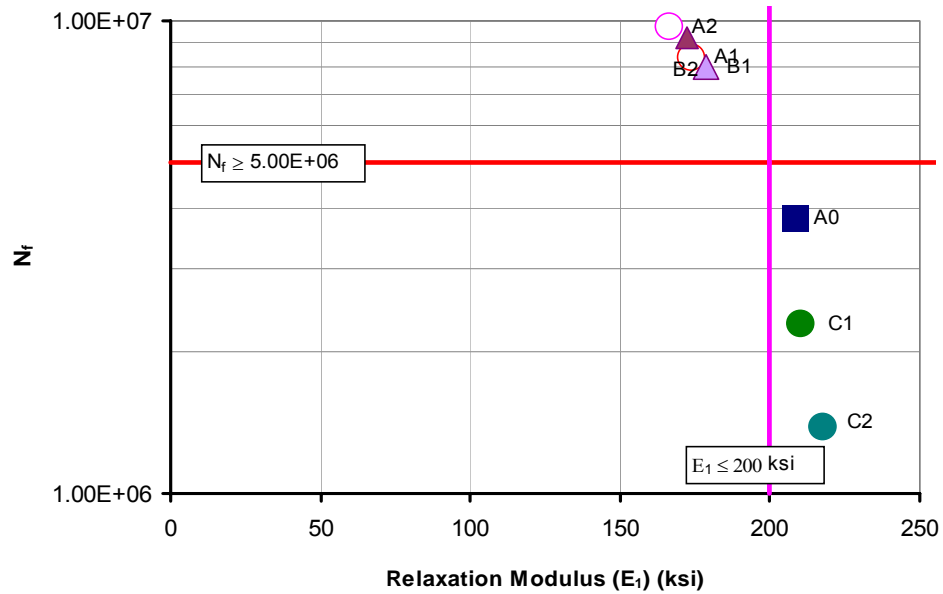


Figure 6-3. Relaxation Modulus (Tension) (E_I) versus N_f .

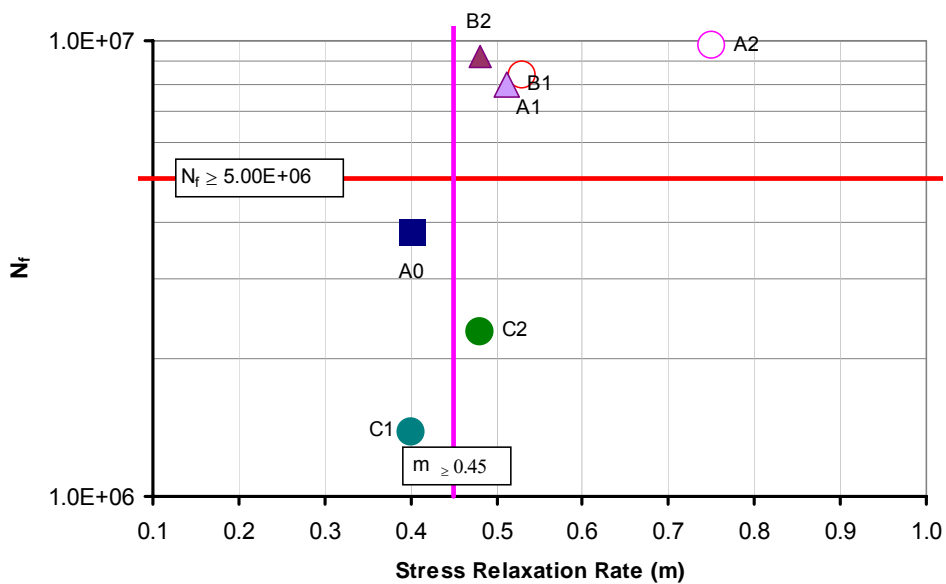


Figure 6-4. Stress Relaxation Rate (m) (Tension) versus N_f .

From Figures 6-3 and 6-4, the proposed RM limiting threshold values are:

- Relaxation modulus: $E_I \leq 200$ ksi
- Stress relaxation rate: $m \geq 0.45$

Any HMAC mixture not meeting these threshold values would be considered inadequate in terms of fatigue resistance, and remedial measures to improve this mixture (e.g., increasing the binder content) would be required. While HMAC mixture C appears to be the outlier in both cases, the E_I property provided a better correlation with the CMSE N_f predictions in terms of discriminating between mixtures with adequate and inadequate fatigue resistance compared to the m property. Although the E_I property provided a better N_f correlation for PS#1 in the WW environment, this trend was not consistent with other pavement structures considered.

Repeated Direct-Tension Criteria

The rate of fracture damage accumulation (b) for each HMAC mixture (Table 2-5, Chapter 2) for PS#1 and the WW environment plotted as a function of N_f is shown in Figure 6-5. For this pavement structure, adequate fatigue resistance is considered to be $N_f \geq 5.00 \text{ E}+06$ based on the traffic design ESALs in Table 2-7.

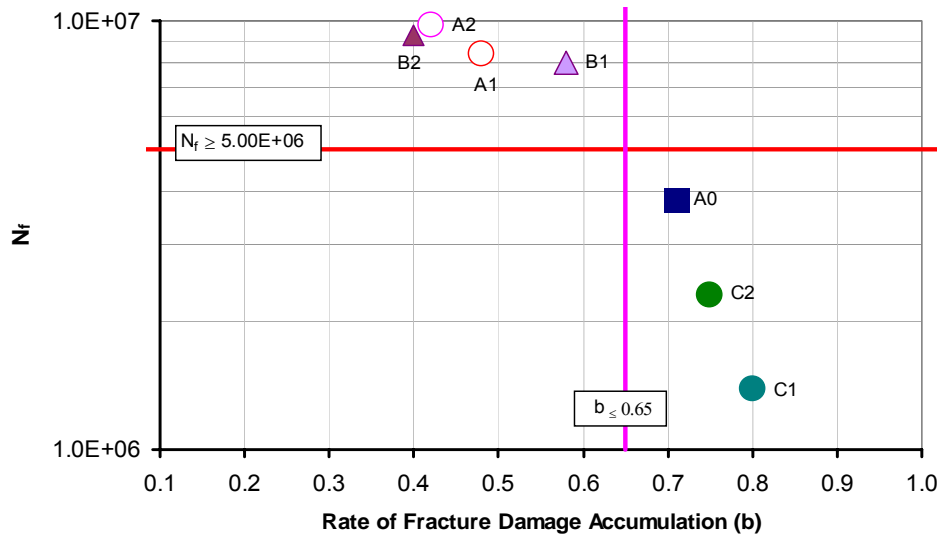


Figure 6-5. Rate of Fracture Damage Accumulation (b) versus N_f .

The proposed RDT limiting threshold value according to Figure 6-5 is:

- Rate of fracture damage accumulation: $b \leq 0.65$

Any HMAC mixture not meeting this threshold value would be considered inadequate in terms of fatigue resistance. Based on Figure 6-5, the b property provided a good correlation with N_f in terms of differentiating between mixtures with adequate and inadequate fatigue resistance compared to all other material properties evaluated in Figures 6-1 through 6-4. Excluding HMAC mixture C, the rank order of correlation with N_f for these material properties for PS# 1 and the WW environment is as follows: b (RDT), E_I (RM), ε_f (TS), m (RM), and σ_t (TS).

Limiting Fatigue Threshold Values

Table 6-1 provides a summary of the results for all five pavement structures (PS) and the two environmental conditions considered in this project. Table 6-1 shows the mean, minimum, maximum, range, standard deviation (Stdev), and coefficient of variation (COV) of the threshold values. The considerable width of the threshold ranges for some of the material properties in Table 6-1 suggests that specific threshold values may need to be established for each specific mixture type (e.g., HMAC mixture C [PG 76-22 (TR)]) and environment in the future. The values shown in Table 6-1 are limited to the materials, pavement structures, and environmental conditions considered in this project, but they nonetheless provide a baseline against which to rapidly screen HMAC mixtures for fatigue resistance or use as mix-design criteria.

In terms of statistical analysis, the material properties ε_f , E_I , and m exhibited considerably higher variability compared to the σ_t or b property. The COV values for ε_f , E_I , and m were relatively higher than the typical ± 15 percent COV for HMAC mixtures attributable to HMAC heterogeneity and experimental errors (Medani et al., 2004). For the E_I and m results, the high statistical variability is attributed to errors in the analysis methodology when generating the $E(t)$ master curves and possibly data inconsistency.

Table 6-1. Limiting Fatigue Threshold Values.

PS#	Environment	σ_t (psi)	ε_f ($\mu\varepsilon$)	E_1 (ksi)	m	b
		$[\geq]$	$[\geq]$	$[\leq]$	$[\geq]$	$[\leq]$
1	WW	65	3300	200	0.45	0.65
2	WW	90	2900	260	0.45	0.63
3	WW	85	3250	126	0.48	0.58
4	WW	70	2900	144	0.48	0.57
5	WW	95	2800	218	0.34	0.70
1	DC	104	2500	216	0.49	0.75
2	DC	100	3300	200	0.50	0.65
3	DC	80	4600	206	0.55	0.68
4	DC	93	3000	261	0.56	0.73
5	DC	86	3250	210	0.33	0.52
Minimum		65	2500	126	0.33	0.52
Mean		80	3180	204	0.46	0.65
Maximum		104	4600	261	0.56	0.75
Range		65 - 104	2500 - 4600	126 - 261	0.33 - 0.56	0.52 - 0.75
Stdev		12.44	562.83	42.76	0.08	0.07
COV		15.55%	17.70%	20.96%	16.54%	11.33%

Overall, the b parameter provided the best correlation with N_f , followed consecutively by the ε_f , E_1 , σ_t , and m values, respectively. Thus the rank order for a proposed surrogate fatigue test protocol would be RDT, TS, and RM, respectively. With the exception of HMAC mixture C, the results also showed that an HMAC mixture passing the TS (ε_f) criterion also passed the RDT (b) criterion. This observation suggests that the ε_f and b properties are interrelated. Further research is thus recommended to investigate the ε_f - b relationship.

In general, inconsistent results were obtained for HMAC mixture C. For example, while the ε_f value in Figure 6-2 was considerably higher than the proposed 3300 $\mu\varepsilon$ threshold value (particularly for C2 with 5387 $\mu\varepsilon$), the mixture nevertheless exhibited inadequate fatigue resistance.

This inadequacy in fatigue resistance for HMAC mixture C was attributed to the fact that the PG 76-22 (TR) binder and the associated mix design was probably not suitable for this particular pavement structure (PS#1) and environment (WW). Also, the PG 76-22 (TR) binder is generally more difficult to work with in the laboratory (i.e., stiff and sticky). Consequently there could have been experimental errors arising from sample fabrication and/or actual laboratory testing. However, it could also be possible that the SF_{ag} method used to incorporate aging effects may not be ideal for the PG 76-22 (TR) binder. Consequently, further research on the SF_{ag} with more HMAC mixtures and PG 76-22 (TR) binder is recommended.

Pavement Service Life and the SF_{aging} Method

A similar analysis of establishing limiting fatigue threshold values for the TS, RM, and RDT test protocols was also conducted using the pavement service life (instead of N_f) based on the SF_{aging} method. Determination of the pavement service life (X_{PSL}) using the SF_{aging} method of incorporating aging effects is discussed in [Chapter 4](#) of this report. Based on the 20-year design period for all pavement structures ([Chapter 2](#)), adequate fatigue resistance based on this method is considered to be $X_{PSL} \geq 20$ years.

From the results presented in [Appendix E](#) based on PS#1 and WW environment, a good correlation between the measured material properties and the estimated pavement service lives was obtained only for the TS test. Inconclusive results were obtained for the RM and RDT tests, and consequently no ranking of the test protocols could be accomplished with this method. More research and data are required to facilitate a comprehensive analysis.

SELECTION OF A SURROGATE FATIGUE TEST PROTOCOL

This section presents an evaluation of the CMSE test protocols. A ranking of the test protocols based on step 5 of the methodology is presented, followed by a recommendation of the proposed surrogate fatigue test protocol. An initial validation of the proposed surrogate fatigue tests based on a correlation with other laboratory tests and analysis methodologies is also discussed.

Ranking of the Test Protocols

On a comparative basis, the RDT (b) criterion provided the best correlation with the CMSE N_f predictions in terms of discriminating between mixtures with adequate and inadequate fatigue resistance relative to the predicted and anticipated traffic loading ESALs. Consequently, the RDT test protocol was assigned a score of 65 percent based on its good correlation with N_f . The TS test protocol (ϵ_f criterion) followed next with an assigned score of 55 percent for this first evaluation factor, and the RM (E_I criterion) test protocol was last with an assigned score of 40 percent. On this basis, the RDT criterion would be recommended and the TS (ϵ_f criterion) would be recommended as the second alternative. In terms of simplicity, practicality, and cost considerations; the TS test protocol was ranked first with a score of 35 percent followed consecutively by the RDT test protocol (25 percent) and the RM test protocol (20 percent), respectively. Unlike the TS and the RDT tests which are conducted at a single test temperature (ambient or 20 °C [68 °F]), the RM test is run at three temperatures (10, 20, and 30 °C [50, 68, and 86 °F]). This fact makes the RM test less desirable in terms of both practicality and cost considerations (a temperature chamber is required), and thus this test protocol was assigned the lowest score for this second evaluation factor. The ranking (and score) results are summarized in [Table 6-2](#).

Table 6-2. Ranking Results of the Test Protocols.

Test	(1) Correlation with N_f		(2) Simplicity		Total Scores	Overall Ranking	Surrogate Test Protocol
	Score	Ranking	Score	Ranking			
TS	50%	2	35%	1	85%	2	TS (ϵ_f)
RM	40%	3	20%	3	60%	3	RM (E_I & m)
RDT	65%	1	25%	2	90%	1	RDT (b)

Note that the TS test time (\cong 5 minutes) is the shortest and that this test protocol also has the simplest analysis procedure compared to the RM or RDT protocols. Additionally, both the RM and RDT test protocols are dependent on the TS test in terms of determining the input loads (strain magnitude).

The RM and RDT tests require 20 percent and 35 percent of the ε_f from the TS test as inputs, respectively. In addition, the current CMSE analysis procedure requires RM data (E_I , m , and a_T) as input loads when analyzing the RDT test data and determining the b parameter. In summary, the RDT test protocol is dependent on both the TS and RM tests in the current CMSE approach. On this basis, the TS test protocol is preferred.

According to [Table 6-2](#), the overall ranking based on the total scores is as follows: RDT (90 percent), TS (85 percent), and RM (60 percent). In consideration of the dependence of the RDT and RM tests on TS testing, this report proposes the following:

- (1) The TS test protocol with a threshold value of $\varepsilon_f \geq 3180 \mu\varepsilon$ should be used as a surrogate fatigue test protocol where a rapid mix-design check or HMAC mixture screening for fatigue is required.
- (2) The RDT test protocol with a threshold value of $b \leq 0.65$ should be used where a comprehensive mix-design check or HMAC mixture screening for fatigue is required or where the TS criterion produced inconclusive results or is considered insufficient.
- (3) A combination of both the TS and RDT protocols should be employed together as a comprehensive surrogate fatigue test protocol.

The limited results in this project showed that an HMAC mixture which passes the TS ε_f criterion will also pass the RDT b criterion. Consequently, the RDT check may be unnecessary if sufficient results can be obtained from the TS test.

RDT Testing and Data Analysis

In the current CMSE setup, the RDT test data analysis is dependent on the RM output data (E_I , m , and a_T). To eliminate this dependence, a fixed m value of 0.45 is proposed while the E_I value can easily be determined from the first RDT load cycle during the unloading phase. An m value of 0.45 is considered a reasonable and conservative number and is also comparable to the mean m value (0.47) obtained in this project ([Table 6-1](#)) or TxDOT Project 0-4688 ($m_{average(0\ months)} \cong 0.455$) ([Ofori-Abebresse 2006](#)).

The HMAC mixture is considered undamaged in the first RDT load cycle, and thus the E_I determined in the unloading phase of the RDT cycle is considered acceptable as a close simulation of the E_I that would be obtained from a nondestructive relaxation test (RM).

Figure 6-6 illustrates the loading and unloading phases of a single RDT cycle.

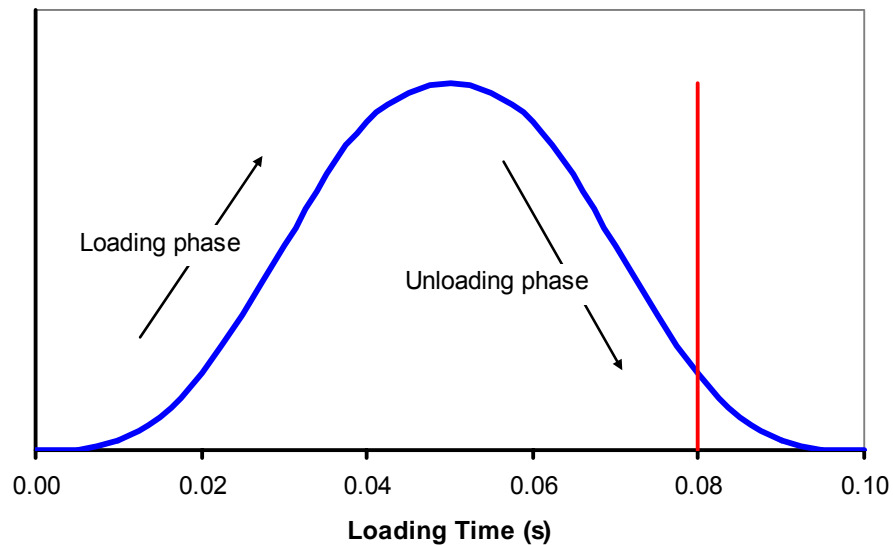


Figure 6-6. The RDT Loading Sequence.

The RDT test protocol for a surrogate test should also be conducted at ambient (room) temperature or 20 °C (68 °F), thus eliminating the need for the a_T value from the RM data. This approach utilizing E_I from the first RDT load cycle in the unloading phase, $m = 0.45$, and $a_T = 1$ was evaluated in this project and produced reasonable results. The difference in the computed b values was no more than 15 percent. The TS test is nonetheless still required to determine the RDT input of strain magnitude.

Recommendation for a Proposed Surrogate Fatigue Test Protocol

Based on the data analyzed as described in this chapter, the following recommendations are proposed:

- The TS is preferred as a surrogate fatigue test protocol (test time \cong 5 minutes) based on practicality, simplicity, and cost considerations. The preliminary proposed limiting fatigue threshold value is the failure tensile strain (ε_f) with a threshold value of $\varepsilon_f \geq 3180 \mu\varepsilon$.
- The RDT is recommended as the second possible surrogate fatigue test protocol (test time \cong 20 minutes) based on its correlation with N_f . The proposed RDT limiting fatigue threshold value is $b \leq 0.65$. The RDT (b) criterion is recommended for a comprehensive analysis or where the TS ε_f criterion produced inconclusive results or is considered insufficient. In the current CMSE approach, however, the RDT requires the TS results to determine the RDT input load in terms of the strain magnitude. So with the RDT as a surrogate test, the TS test is also required.
- Alternatively, both the TS and RDT can be used as one comprehensive TS-RDT surrogate fatigue test protocol (total test time \cong 25 minutes). In this case, both the TS (ε_f) and RDT (b) criteria can be checked. This is a logical proposal considering that in the current CMSE approach, the RDT test cannot be conducted without the TS test. If the results do not agree, the RDT (b) criterion should govern. In general, however, data in this chapter showed that an HMAC mixture which passed the TS ε_f criterion also passed the RDT b criterion.
- In terms of mix design and HMAC mixture screening based on these proposed surrogate fatigue test protocols:
 - (1) If two or more HMAC mixtures are evaluated, the mixture that *passes* the limiting fatigue threshold value with the *highest* ε_f (TS) value and/or the *lowest* b (RDT) value is selected.
 - (2) If the HMAC mixture(s) does(do) *not pass* the limiting fatigue threshold value, then the mixture requires improvement. This improvement may be accomplished by increasing the binder content, changing the aggregate gradation, introducing additives, and/or changing the material type (binder and/or aggregate).

In view of the above recommendations, more research is recommended to refine the ε_f threshold value and further investigate the correlation of ε_f with N_f . Further research is also required to explore the possibility of eliminating the dependence of the RDT test on the TS test.

TS-RDT Preliminary Validation

The initial laboratory validation of the TS-RDT surrogate fatigue test protocol was evaluated based on a correlation with the flexural bending beam (BB) fatigue test, overlay test (OT), and MEPDG results for three HMAC mixtures: A0 (Bryan), B1 (Yoakum [rut resistant]), and D (Waco [fatigue resistant]) (Ofori-Abebresse 2006, Walubita et al., 2005b, Zhou and Scullion, 2006). Table 6-3 summarizes the HMAC mixture ranking according to the TS-RDT criteria, BB testing, OT testing, and the MEPDG analysis.

Table 6-3. Comparison of HMAC Mixture Results (TS-RDT, BB, OT, and MEPDG).

HMAC Mixture	TS-RDT			BB		OT		MEPDG	
	R	ε_f ($\mu\varepsilon$)	b	R	N_{BB}	R	N_{OT}	R	N_f
A0	3	1245	0.71	3	131,000	3	3	3	4.71 E+06
B1	2	3483	0.58	2	224,000	2	325	2	6.21 E+06
D	1	3561	0.52	1	443,000	1	>750	1	8.89 E+06

Notation: R = ranking in terms of expected performance; N = number of laboratory load cycles to failure (fatigue for BB [N_{BB}] and reflective cracking for OT [N_{OT}]); N_f = HMAC mixture fatigue life predicted over a 20-year design period in terms of traffic ESALs.

In Table 6-3, the BB, OT, and MEPDG results are excerpts from Walubita (2006), Zhou et al. (2006), and Walubita et al. (2006), respectively. The TS-RDT results for HMAC mixture D (Waco) were excerpted from Ofori-Abebresse (2006). Also, with the OT results, N refers to the number of load cycles to failure with respect to reflective cracking. The OT test is typically used to characterize HMAC mixtures for reflective cracking resistance (Zhou and Scullion 2006). The results nonetheless provide an initial means to evaluate the validity of the TS-RDT test protocols.

According to [Table 6-3](#), the following HMAC mixture ranking in terms of performance prediction is the same for all the analysis methodologies: 1 (D), 2 (B1), and 3 (A0). This correlation is noteworthy considering that the four approaches were formulated on different principles and concepts and utilize different laboratory test protocols and analysis procedures. This finding reflects the potential of the CMSE TS-RDT tests as surrogate fatigue test protocols.

As expected, HMAC mixture D that was designed to be fatigue resistant ranked number 1 in terms of the theoretically expected fatigue performance, followed consecutively by HMAC mixture B1 (2) and A0 (3). The higher ranking of HMAC mixture B1 (rut resistant) compared to HMAC mixture A0 was attributed to its improved mix design in terms of the binder content and material type/characteristics. Note that HMAC mixture B1's design binder content was 5.6 percent versus 4.6 percent (by weight of aggregate) for HMAC mixture A0.

In terms of mix-design and HMAC mixture screening, [Table 6-3](#) shows that if these three HMAC mixtures (A0, B1, and D) were evaluated based on the TS-RDT criteria ($\epsilon_f \geq 3180 \mu\epsilon$ and $b \leq 0.65$), HMAC mixture D would be recommended, followed by HMAC mixture B1. HMAC mixture A0 would be considered inadequate or otherwise require improvement. According to [Table 6-3](#), HMAC mixture A0 failed both the TS and RDT criteria. Clearly, these TS-RDT results corroborate the ϵ_f - b interrelationship reported previously and suggest that ϵ_f and b are inversely related.

Overall, these results showed that the TS and RDT tests are potentially promising as surrogate fatigue test protocols for mix design and HMAC mixture screening. The tests are practical and take approximately 25 minutes to run. However, more research with additional HMAC mixtures and validation (laboratory and field) is strongly recommended.

SUMMARY

The findings of this chapter are summarized as follows:

- For simplicity and practicality, the TS test (test time: \cong 5 minutes [test temperature \cong ambient or 20 °C (68 °F)]) is proposed as a surrogate fatigue test protocol with the following limiting fatigue threshold value: $\epsilon_f \geq 3180 \mu\epsilon$.

- In terms of providing a good correlation with the HMAC mixture fatigue resistance, the RDT test (test time: $\cong 20$ minutes, test temperature \cong ambient or 20 °C [68 °F]) is proposed as the second choice for a surrogate fatigue test protocol with the following limiting fatigue threshold value: $b \leq 0.65$. The RDT b criterion is recommended for comprehensive analysis or when the TS ε_f criterion produces inconclusive results or is considered insufficient. However, the RDT dependence on TS needs to be further investigated.
- Alternatively, both the TS and RDT can be used as one comprehensive TS-RDT surrogate fatigue test protocol. If inconsistent results are obtained, the RDT (b) criterion should govern. In general, however, an HMAC mixture which passes the TS ε_f criterion will also pass the RDT b criterion.
- Any HMAC mixture not meeting the recommended limiting fatigue threshold values would be considered inadequate in terms of fatigue resistance, and the mixture would require improvement (i.e., increasing the binder content, changing the aggregate gradation, introducing additives, and/or changing the material type [binder and/or aggregate]).
- Initial laboratory validation of the TS-RDT test protocols was accomplished based on a correlation with BB, OT, and MEPDG results for three HMAC mixtures. The results obtained were reasonable and reflected the potential of the TS-RDT tests as surrogate fatigue test protocols.

Although both the CMSE approach and the laboratory tests discussed in this report are still subject to review and validation (both laboratory and field), the preliminary findings of this project provide a potentially promising framework within which a surrogate fatigue test protocol based on fundamental material properties can be established. The CMSE approach provides a rational fatigue analysis methodology for characterizing HMAC mixture fatigue resistance based on fundamental material properties and is ideal for structural design analysis and N_f performance prediction. A surrogate fatigue test protocol, in contrast, can be used for a mix-design check and HMAC mixture screening for fatigue resistance. However, considering the limited data evaluated in this chapter, more research with additional HMAC mixtures and correlation with field data are strongly recommended.

CHAPTER 7

DISCUSSION AND SYNTHESIS OF RESULTS

This chapter provides an overall discussion and synthesis of the data and results presented in this report (Chapters 1 through 6) and TTI Reports 0-4468-1 and 0-4468-2 (Walubita et al. 2005a, b). In Reports 0-4468-1 and 0-4468-2, four fatigue analysis approaches (ME, CMSE, CM, and MEPDG) were comparatively evaluated as potential methodologies for characterizing HMAC mixture fatigue resistance. The CMSE was selected and recommended as the best approach based on incorporation of fundamental mixture properties among other factors (Walubita et al. 2005a, b). The CM was recommended as the second alternative. Consequently, this chapter's discussion is predominantly focused on the CMSE approach. Statistical analyses, aging effects, and the surrogate fatigue test protocols are discussed followed by the N_f results and field performance. Further validation of the CMSE fatigue analysis approach and possible modifications to incorporate multiple distresses are then discussed, followed by a summary of the chapter.

STATISTICAL ANALYSES

The results presented in Chapters 3 to 5 demonstrated that the CMSE and CM fatigue analysis approaches constitute rational, promising methodologies for fundamentally characterizing the fatigue resistance of HMAC mixtures. Compared to other approaches examined in TxDOT Project 0-4468, the CMSE and CM approaches exhibited greater potential and flexibility to interactively incorporate fundamental material properties including binder aging that are critical to HMAC mixture fatigue performance (Walubita et al., 2005a, b). This section discusses the statistical analysis aspects of the CMSE and CM approaches.

Comparison of the CMSE and CM Approaches

A spreadsheet descriptive statistics analysis tool was utilized for the statistical prediction of N_f by both the CMSE and CM approaches. This analysis was supplemented by a one-sample *t*-test (with an assumed *t-value* of zero) utilizing the Statistical Package for Social Sciences (SPSS) analysis software (Montgomery et al., 2001). The HMAC mixture N_f statistical variability was measured in terms of the coefficient of variation of $\ln N_f$ and the 95 percent confidence interval (CI). In these analyses, the N_f logarithmic response was used to meet the assumption of normal distribution necessary for the statistical analyses.

Statistical variability in terms of the COV of $\ln N_f$ did not differ significantly between the two fatigue analysis approaches and was within the ± 15 percent error tolerance typically acceptable for HMAC mixtures and attributable to test variability and HMAC mixture inhomogeneity (Medani et al., 2004). Additionally, the 95 percent CI margin between the two approaches did not deviate by more than 15 percent. Despite this agreement, formulation of more comprehensive reliability and statistical analysis models for these approaches is recommended. For example, a mathematical model for the reliability factor Q in Equation 3-6 (Chapter 3) is needed to replace the currently assumed numerical value of 1.

Comparison of HMAC Mixtures

Generally, higher statistical variability in terms of both the COV of $\ln N_f$ and the 95 percent CI was associated with the HMAC mixtures designed with modified binders. The same trend was also observed for the HMAC mixture properties both in terms of the standard deviation and the COV. The rank order of increasing statistical variability for the HMAC mixtures in terms of binder type was: PG 64-22, PG 76-22 (SBS), and PG 76-22 (TR). Nonetheless, the variability was within the ± 15 percent error tolerance.

From laboratory experience, HMAC mixtures designed with modified binders are generally more difficult to work with in the laboratory because they are stiff and sticky. Consequently, it is more difficult to control the AV content, which probably contributed to the higher variability in the final N_f results.

Comparing the HMAC mixtures, the COV values for the AV were 3.01, 7.96, and 9.62 percent for the HMAC mixtures designed with PG 64-22, PG 76-22 (SBS), and PG 76-22 (TR) binders, respectively. This COV analysis was based on the average AV content of 20 randomized HMAC specimens per HMAC mixture type, and the analysis indicates that results associated with modified binders need to be analyzed and interpreted cautiously.

AGING EFFECTS

As demonstrated in Chapters 3 through 5 and Reports 0-4468-1 and 0-4468-2, the CMSE approach provides a rational platform for modeling the binder-HMAC mixture relationships and investigating the effects of binder oxidative aging and temperature on both HMAC mixture properties and fatigue resistance. Two different methods were utilized to incorporate the effects of binder oxidative aging in CMSE analyses. This section provides a comparative review of these binder aging methods that were employed (Walubita et al., 2005b). The binder-HMAC mixture relationships with respect to aging are also discussed.

The SF_{ag} Method – DSR_f Concept

The SF_{ag} method was formulated on the fundamental hypothesis that it is only the binder that ages in any given HMAC mixture, and therefore it is not unreasonable to determine SF_{ag} from the binder rheological properties. The rationale with the SF_{ag} method and DSR_f concept is that determination of the SF_{ag} should be based on properties of unaged and aged neat binders and allow for prediction of N_f at any desired aging exposure period using the SF_{ag} and unaged HMAC mixture properties. This method was viewed as a first step toward incorporating the effects of aging on predicted N_f using a single shift without consideration of the simultaneous and continuous process of trafficking and aging throughout the HMAC mixture design life.

In this method, SF_{ag} is considered a multiplicative factor that reduces N_f and therefore its magnitude was postulated to range between 0 and 1 ($0 < SF_{ag} \leq 1$). A numerical SF_{ag} value of 1 represents unaged conditions or no consideration of aging effects. Equation 7-1 illustrates this method:

$$N_{f(t_i)} = SF_{ag(t_i)} \times [N_{f(t_0)}] \quad (7-1)$$

where:

- $N_{f(t_i)}$ = HMAC mixture fatigue resistance predicted over an X_1 -year design period at time t_i aging exposure period (X_2 years)
- $N_{f(t_0)}$ = Initial HMAC mixture fatigue resistance at zero pavement age just after construction predicted over an X_1 -year design period
- $SF_{ag(t_i)}$ = Shift factor due to binder oxidative aging at time t_i in terms of aging exposure period (years)

Note that in [Equation 7-1](#), the HMAC mixture fatigue resistance denoted $N_{f(t_i)}$ or fatigue life is determined and defined in terms of the number of allowable traffic ESALs a pavement structure can carry over an X_1 -year design period when exposed to X_2 -years period of aging (t_i). In practical HMAC pavement designs and analyses, both X_1 and X_2 are often considered to be 20 years. That is $X_1 = X_2 = t_i = 20$.

With this SF_{ag} method, the initial $N_{f(t_0)}$ without aging effects (e.g., $N_{f(t_0)}$ in [Equation 6-1](#)) together with the design period (e.g., 20 years) are presumably known (predicted according to the CMSE approach). The question then is what is the value of $N_{f(t_i)}$ predicted over an X_1 -year design period (e.g., 20 years) with the HMAC pavement structure subjected to X_2 years (e.g., 20) of aging exposure? The answer to this question and application of the SF_{ag} method is illustrated in [Figure 7-1](#).

[Figure 7-1](#) clearly illustrates that with $SF_{ag(t_i)}$ (as a function of aging exposure period) and $N_{f(t_0)}$ known, the $N_{f(t_i)}$ predicted over a 20-year design period can be estimated for any aging exposure period desired, e.g., 0 ($SF_{ag(t_0)} = 1$), 10, 15, or 20 (as in this project). In this SF_{ag} approach, the pavement service life can simply be considered to be the number of years the HMAC pavement structure can sustain the traffic loading prior to fatigue failure, where fatigue failure is defined as the instance when the predicted HMAC fatigue resistance or $N_{f(t_i)}$ is equal to the design traffic ESALs (i.e., $N_{f(t_i)} = \text{design traffic ESALs}$). The pavement service life is illustrated in [Figure 7-1](#) and designated as X_{PSL} .

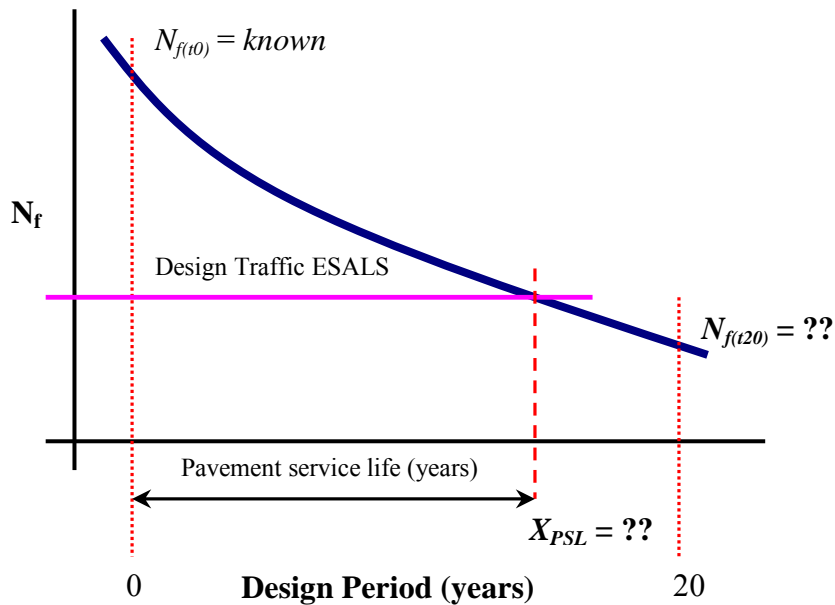


Figure 7-1. The SF_{ag} Method.

In this project, the SF_{ag} was computed as a function of the binder DSR_f and m value (slope of a plot of DSR_f versus angular frequency) at multiple laboratory aging exposure conditions for the binders. The SF_{ag} computation process is documented in Report 0-4468-2 (Walubita et al., 2005b). The DSR_f was utilized on the hypothesis that this function provides a better representation of the binder properties in terms of visco-elasticity and ductility or durability, properties that are considered critical to fatigue performance for field aged HMAC pavements (Glover et al., 2005). The DSR_f is determined as a function of the binder elastic dynamic shear modulus and dynamic viscosity measured from the DSR test (Walubita et al., 2005b).

The simplicity and potential to be used for different HMAC mix designs utilizing the same binder type are the main advantages of using the SF_{ag} for incorporating aging effects in the CMSE N_f analysis. As illustrated in Figure 7-1, the SF_{ag} method is relatively easy to understand and apply. Furthermore, the SF_{ag} allows determination of the $N_{f(t_i)}$ for any desired aging exposure period. Recommended improvements to the SF_{ag} method in the current CMSE approach include capturing and incorporating additional influencing variables that are critical to binder aging and HMAC mixture fatigue performance. These variables include binder content, AV, temperature variations, aggregate type and gradation, and traffic loading.

The SF_{aging} Method – Miners’ Cumulative Damage Hypothesis

The SF_{aging} method utilizes Miners’ cumulative damage hypothesis to characterize HMAC pavement cumulative damage as a function of both traffic loading and aging effects. It is a fundamental approach based on binder properties (aged and unaged) and HMAC mixture N_f predictions (both aged and unaged). The approach utilizes the remaining fraction of pavement service life (RFSL) concept which, when summed over the HMAC pavement’s entire life based on Miners’ cumulative damage hypothesis, must be equal to a unit (Miner, 1945).

This approach asserts that the initial (RSFL = 1) and final (RSFL = 0) RFSL values are known. In this case, the question then is how many years, defined herein as the pavement service life, it will take the HMAC pavement to reach an RSFL value of zero? Figure 7-2 illustrates the SF_{aging} method based on Miner’s cumulative damage hypothesis (Miner, 1945).

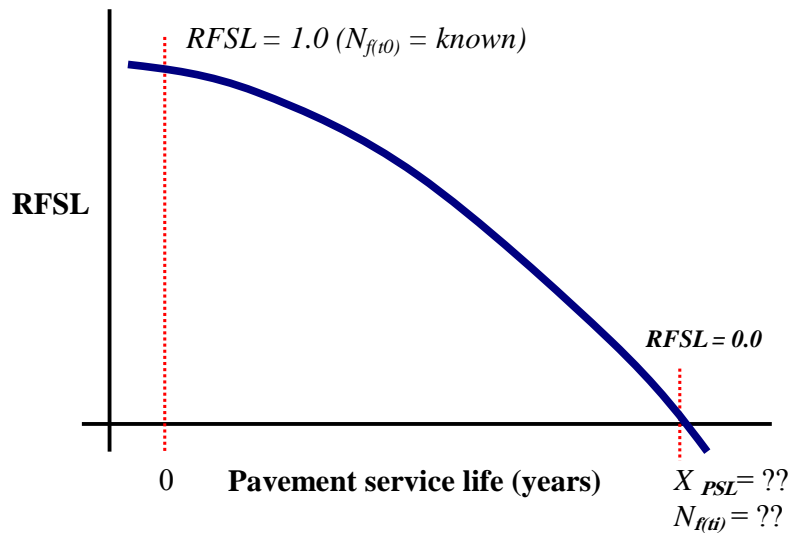


Figure 7-2. The SF_{aging} Method.

In this SF_{aging} method, both the HMAC mixture fatigue resistance ($N_{f(ti)}$) predicted over an X_I -year design period (e.g., 20 years) and the pavement service life (X_{PSL}) are determined at the instance when the RFSL value reduces to zero as illustrated in Figure 7-2. An RFSL value of zero defines fatigue failure in this approach. Like for the SF_{ag} approach, the $N_{f(ti)}$ is determined as expressed by Equation 7-3:

$$N_{f(t_i)} = SF_{aging(t_i)} \times [N_{f(t_0)}] \quad (7-3)$$

In the analysis, the cumulative damage effects of traffic loading (accounted for through a parameter R_L) and aging effects are considered simultaneously. In this SF_{aging} method, aging effects are simultaneously incorporated through the use of both unaged and aged binder properties (the DSR_f through a parameter K_2) and unaged and aged $N_{f(t_i)}$ results (through a parameter K_1), respectively. Parameters R_L , K_1 , and K_2 are defined in Chapters 4 and 5 of this report. Note that parameter K_1 is a function of both unaged and aged $N_{f(t_i)}$ predicted over an X_I -year design period, e.g., 20 years using the CMSE approach.

While the SF_{aging} method is not practical for routine mix design because it requires extensive time to age and then test the HMAC mixtures, it does provide a more fundamental and reliable understanding of the effects of changes in binder properties and the influence of other mix-design parameters and traffic loading on mixture fatigue resistance. Computation of the K_1 parameter (Chapter 4) is dependent on laboratory-aged HMAC mixture N_f . Consequently, a different methodology for computing K_1 that is independent of aged HMAC mixtures needs to be formulated.

Note that through the use of HMAC mixture N_f in the analysis, the SF_{aging} indirectly incorporates critical factors such as binder content, AV, aggregate type, and gradation. Like the SF_{ag} , the effects of temperature variations still need to be incorporated. In both cases, field validation (i.e., correlation with field aging exposure for the HMAC pavement) is still required.

Comparison and Integration of the SF_{ag} and SF_{aging} Methods

Both the SF_{ag} and SF_{aging} methods attempt to model and incorporate binder oxidative aging effects in the CMSE fatigue analysis using different approaches. With both methods, however, the final output is the expected HMAC mixture fatigue performance expressed either in terms of N_f or X_{PSL} . The SF_{ag} method is based on the binder DSR_f and assumes that N_f decline due to aging is predominantly due to binder oxidative aging.

Although this approach provides a rapid and simple approach for incorporating aging effects in N_f analysis, it does not account for mix design and other mixture effects. However, with further improvements to incorporate AV, binder content, aggregate type and gradation, and traffic loading; the SF_{ag} can be used for multiple mix designs using the same binder type.

The SF_{aging} method utilizes Miners' cumulative damage hypothesis and incorporates traffic loading, the binder DSR_f function, and HMAC mixture N_f (unaged and aged). It is a more fundamental approach but requires aged HMAC mixture data as an input. Eliminating the dependence of K_I on aged HMAC mixtures will render the SF_{ag} method feasibly applicable. [Table 7-1](#) illustrates the SF_{ag} and SF_{aging} ranking results for PS#1 and the WW environment.

Table 7-1. Ranking of the HMAC Mixtures Using the SF_{ag} and SF_{aging} Methods.

HMAC Mixture	Mix Design Characteristics	Ranking	
		SF_{ag} based on Field N_f	SF_{aging} based on Service Life
A0 (Bryan)	PG 64-22 + Limestone (4.6% binder*)	5	5
A1	PG 64-22 + Gravel (5.3% binder)	3	7
A2	PG 64-22 + Gravel (5.8% binder)	1	6
B1 (Yoakum)	PG 76-22 (SBS) + Gravel (5.6% binder)	4	4
B2	PG 76-22 (SBS) + Gravel (6.1% binder)	2	2
C1	PG 76-22 (TR/SBS) + Gravel (5.5% binder)	6	1
C2	PG 76-22 (TR/SBS) + Gravel (6.0% binder)	7	3
*All binder contents are by weight of aggregate			

From [Table 7-1](#), the ranking results for HMAC mixtures A0, B1, and B2 are similar and the results for mixtures A1, A2, C1, and C2 are not. With an increase in binder content, HMAC mixtures A1 and A2 would theoretically be expected to have a better fatigue resistance than A0 as indicated by the SF_{ag} method. However, the SF_{aging} method suggests otherwise, indicating that binder content may not be the only factor critical to HMAC fatigue resistance in terms of response to aging and cumulative fatigue damage. Other factors such as aggregate type and gradation need to be considered.

With the limited data available, a conclusive analysis can not be made for HMAC mixture C (C1 and C2). In general, however, this HMAC mixture (C) was more problematic to work with in the laboratory and exhibited greater variability in the results due to the stiff and sticky PG 76-22 (TR) binder compared to other HMAC mixtures. Consequently, it is not surprising that inconsistent results were obtained for this HMAC mixture (C) as indicated by [Table 7-1](#). More data are needed to study HMAC mixtures fabricated from this binder type. Possible sources of errors leading to inconsistent results in [Table 7-1](#) include the following:

- The current SF_{ag} approach is solely based on the binder DSR properties and does not capture the significant aspects of binder content, AV, aggregate type and gradation, and traffic loading. These factors are considered critical to the HMAC mixture response to aging and the rate of fatigue damage accumulation and significantly impact the SF_{ag} .
- Because of the limited data in this project, computation of the K_I parameter ([Equation 4-6, Chapter 4](#)) for HMAC mixtures A1, A2, B2, C1, and C2 was based only on two data points (0 and 6 months aging conditions). Two data points may not be sufficient enough to accurately represent the HMAC response to binder oxidative aging, and this could significantly impact the computed SF_{aging} .

In view of the limitations of the SF_{ag} and SF_{aging} methods, the following recommendations are proposed for future research:

- (1) Explore incorporation of mix-design characteristics, temperature variations, and traffic loading into the SF_{ag} to make it more universally applicable.
- (2) Explore computation of the K_I parameter independent of the laboratory-aged HMAC mixture N_f . In addition, the effects of temperature variations should be incorporated.
- (3) Explore integration of SF_{ag} and SF_{aging} into one single-shift factor by combining the positive aspects of each method.

Additionally, the laboratory aging exposure conditions considered in this project were purely oxidative at an AV content of 7 ± 0.5 percent for all the compacted HMAC specimens and a constant temperature of $60\text{ }^{\circ}\text{C}$ ($140\text{ }^{\circ}\text{F}$) under dry conditions. Furthermore, the oxidative aging process was assumed to occur uniformly throughout the HMAC specimens. More data with additional binders, HMAC mixtures, and laboratory aging exposure conditions are therefore needed to validate and quantify these oxidative aging effects.

The effects of AV (content and distribution) and temperature variations on aging should also be investigated. Other factors such as HMAC thickness and the effects of moisture should be considered as well. Correlations and validation with field conditions are strongly recommended.

Binder-HMAC Relationships

As an alternative to using aging shift factors, binder-HMAC mixture relationships can be used to estimate aged HMAC mixture properties from aged binders and then directly predict $N_{f(ti)}$ without using SF_{ag} or SF_{aging} . Data presented in [Chapter 5](#) of this report and Report [0-4468-2](#) on binder-HMAC mixture relationships showed a good correlation between the binder and HMAC mixture properties in response to binder oxidative aging. A HMAC mixture visco-elastic function defined as $G' / (\eta' / G')$ correlated linearly with the binder DSR function. Consequently, these binder-HMAC mixture relationships constitute a possible alternative to aging shift factors in the CMSE N_f analysis and need to be further investigated.

SURROGATE FATIGUE TEST PROTOCOLS

While the CMSE fatigue analysis approach can be rationally utilized for characterizing HMAC mixture fatigue resistance based on fundamental material properties and is ideal for structural design analysis and N_f performance prediction, a surrogate fatigue test protocol is required for rapid mix-design checks and HMAC mixture screening for fatigue resistance. Consequently, [Chapter 6](#) of this report explored the possibility of establishing a surrogate fatigue test protocol based on the CMSE approach. The following recommendations were made:

The TS Test Protocol

For simplicity and practicality, the TS test was proposed as a surrogate fatigue test protocol with a limiting fatigue threshold value of $\varepsilon_f \geq 3180 \mu\varepsilon$. The test time is at most 5 minutes at an ambient test temperature or 20 °C (68 °F). This test protocol did not, however, give the best correlation with CMSE N_f predictions.

The RDT Test Protocol

In terms of providing a good correlation with the HMAC mixture fatigue resistance, the RDT test (test time: $\cong 20$ minutes [test temperature \cong ambient or 20 °C (68 °F)]) was proposed as the second choice with a limiting fatigue threshold value of $b \leq 0.65$. The RDT b criterion is recommended for a comprehensive analysis or when the TS ε_f criterion produces inconclusive results or is considered insufficient. The RDT's major limitation is its dependence on the TS test, which needs to be further investigated.

The TS-RDT Test Protocol

In consideration of the RDT dependence on the TS test in the current CMSE approach, [Chapter 6](#) also proposed using both the TS and RDT as one comprehensive TS-RDT surrogate fatigue test protocol (total test time $\cong 25$ minutes, test temperature \cong ambient or 20 °C [68 °F]). The TS-RDT surrogate fatigue test protocols were initially validated and correlated well with BB, OT, and MEPDG results for three HMAC mixtures (see [Chapter 6](#)).

The establishment of a CMSE surrogate fatigue test protocol means that mix designs and HMAC mixtures can be rapidly screened for fatigue resistance. The full CMSE fatigue analysis approach on the other hand can be employed for structural design analysis and N_f performance prediction when characterizing HMAC mixture fatigue resistance. With the limited data evaluated in this project, more research is strongly recommended to further refine both the CMSE approach and the surrogate fatigue test protocols.

N_f RESULTS AND FIELD PERFORMANCE

The validity of the CMSE/CM N_f predictions is based on the SHRP A-357 report by [Lytton et al. \(1993\)](#) and a comparison with the ME approach and the MEPDG in Report [0-4468-2](#) ([Walubita 2006](#); [Walubita et al., 2005b](#)). Consequently, further validation of the practical application of the CMSE/CM fatigue analysis models and the computed N_f results as a function of actual field fatigue performance remains. On this basis, field validation of the CMSE/CM approaches is strongly recommended with trial HMAC pavement sections based on accelerated pavement testing and/or long-term implementation pilot projects.

Software development and subsequent integration with HMAC pavement structural design analysis to ensure adequate fatigue performance is recommended. Software development ensures a faster and reliable computing methodology for both N_f prediction and sensitivity analysis of the CMSE/CM models. Additionally, software also provides a rapid methodology for numerical validation of the CMSE concepts and analysis models.

CMSE VALIDATION AND MODIFICATION

While validation (laboratory and field) and sensitivity analysis is still required, concurrent modification is essential to improve the versatility and applicability of the CMSE approach. The flexibility and interactive nature of the numerous CMSE models offers great potential to incorporate various factors that are critical to HMAC performance. Equally, the CMSE approach can be expanded to incorporate multiple distress analyses. This section provides an insight into the variables and multiple distresses that can be incorporated in the CMSE approach.

Incorporation of Other Influencing Variables

Unlike other distresses such as rutting, fatigue cracking is a complex function of many influencing variables that need to be interactively taken into account when characterizing HMAC mixture fatigue resistance. No one factor acts independently to control fatigue cracking; all factors act interactively to prevent or cause fatigue cracking.

Additionally, the complex nature of HMAC with its non-linearity, elasto-visco-plasticity, anisotropy, aging propensity, and healing effects need to be accounted for to ensure adequate fatigue performance. The influencing factors for fatigue resistance include material properties and field conditions. Material properties are primarily a function of HMAC mix-design, and field conditions incorporate pavement structure, traffic loading, and environment. As a means to improve the CMSE fatigue analysis approach, direct incorporation of the following parameters in the analysis models is suggested:

- aggregate binder and moisture absorption capacity;
- binder content, VMA, and VFA;
- AV content and distribution; and
- shift factor due to traffic wander.

Also with further sensitivity analysis, parameters such as σ_f need to be evaluated for possible replacement with ε_f because this parameter was shown in this project to be a better indicator of HMAC mixture fatigue resistance.

Incorporation of Multiple Distress Analyses

The CMSE approach exhibits greater potential to be modified to incorporate other distress analyses such as moisture sensitivity and HMAC permanent deformation or rutting. Through the use of SE data under wet conditions, moisture sensitivity analysis can be incorporated in the CMSE analysis to simultaneously characterize the stripping potential and moisture damage susceptibility of the HMAC.

On the same basis, HMAC permanent deformation analysis can be incorporated through the VESYS model based on axial deformation measurements from the CMSE laboratory tests (Huang 1993). The CMSE laboratory tests can be modified to measure compressive axial deformations. Incorporation of multiple distress analyses will make the CMSE approach more versatile. Further research should thus consider the possibility of incorporating multiple distress analyses in the CMSE approach.

SUMMARY

The following summarizes the discussion in this chapter:

- The CMSE and CM statistical variability in terms of the N_f results were comparable and within a ± 15 percent error tolerance. However, more comprehensive reliability and statistical analysis models need to be formulated for these approaches.
- Higher statistical variability was observed for the HMAC mixtures designed with modified binders, particularly the PG 76-22 (TR) binder. This finding suggests that N_f results associated with modified binders need to be analyzed and interpreted cautiously.
- Based on the limited data in this project, SF_{ag} and SF_{aging} provided an initial means to incorporate aging effects in the CMSE analysis. However, both approaches need further validation and modification to make them universally applicable. Integration into one single aging shift factor was suggested as a possible means to address their limitations. Another alternative is to use binder-HMAC mixture relationships to address aging effects in the CMSE analysis, but this approach needs further investigation.
- The TS-RDT surrogate fatigue test protocols (total test time \cong 25 minutes, test temperature \cong ambient or 20 °C [68 °F]) provided a promising means for a rapid mix-design check and HMAC mixture screening for fatigue resistance. Further research is recommended to validate the test protocols and investigate their general applicability.
- Although reasonable results were obtained and correlated well with other fatigue analysis approaches evaluated in TxDOT Project 0-4468, further research is strongly recommended to validate the CMSE approach both in the laboratory and field. Software development including modifications to incorporate multiple distress analyses is also recommended.

Overall, this project provided a potentially promising analysis methodology (CMSE) for characterizing HMAC mixture fatigue resistance based on fundamental material properties in an interactive manner that accounts for the complex behavior of HMAC including aging effects. The research results offer an excellent framework for establishing surrogate fatigue test protocols and exploring multiple distress prediction.

CHAPTER 8

CONCLUSIONS AND RECOMMENDATIONS

This chapter provides a summary of the findings of this research project. Conclusions and recommendations are provided, followed by a closure and product deliverables.

CONCLUSIONS

Based on the materials and data presented in this report, the following conclusions were drawn:

The CMSE and CM Fatigue Analysis Approaches

- The CMSE approach provides a promising and rational methodology for fundamentally characterizing the fatigue resistance of HMAC mixtures. The approach:
 - interactively utilizes fundamental material properties to estimate N_f and discretely accounts for HMAC non-linearity, visco-elasticity, anisotropic, healing, and binder oxidative aging effects;
 - utilizes relatively simple laboratory tests and a realistic fatigue failure criterion; and
 - provides a rational basis for comparatively evaluating the effects of mix-design parameters, volumetric properties, and material type on N_f .

- Although the CM approach is relatively cheaper in terms of both laboratory testing and data analysis and predicted comparable N_f results, it is only recommended over the CMSE approach if fatigue is the only primary distress of concern or if there is limited data. Otherwise the CMSE approach is preferred because, unlike the CM, the CMSE approach has the potential to simultaneously model other distresses such as moisture damage and permanent deformation. Practical HMAC pavement structural designs are often based on a compromise among various distresses. Therefore, an approach that has the potential or whose

input data can also be utilized to simultaneously characterize other HMAC pavement distresses is preferred.

HMAC Mixture Fatigue Resistance

- HMAC mixture fatigue resistance is a complex function of:
 - mix-design parameters (air voids [AV], VMA, binder content);
 - material properties (binder, aggregate, and HMAC); and
 - traffic, pavement structure, and environment.

These factors interact differently to produce varying effects on different HMAC mixtures and should be discretely taken into account when modeling mixture fatigue resistance. Generally, an increase in binder content improved both the HMAC mixture fracture properties and fatigue resistance measured in terms of N_f magnitude. The dependence of N_f on pavement structure and the environment implies that mix design and HMAC fatigue characterization must be sufficiently integrated with HMAC pavement structural design and analysis to ensure adequate field fatigue performance.

- In terms of N_f comparison for the HMAC mixtures (based on the SF_{ag} method), the following was evident:
 - For the same gravel aggregate and gradation, the HMAC mixture designed with PG 76-22 (SBS) binder exhibited superior N_f compared to the second modified HMAC mixture with PG 76-22 (TR) binder. In fact, the HMAC mixture with PG 76-22 (TR) binder exhibited the worst N_f compared to all other HMAC mixtures considered in this project. However, the PG 76-22 (TR) binder was also found to be much stiffer than all the other binders based on the DSR $G^*/\sin \delta$ property.
 - For the same PG 64-22 binder, the HMAC mixture with gravel aggregates exhibited a significantly higher N_f than the corresponding mixture with limestone aggregates.

These results highlight the dependence of N_f on material type and HMAC mixture compatibility.

Binder-HMAC Mixture Relationships and Effects of Aging

- In consideration of the binder-HMAC mixture relationships and effects of binder oxidative aging, the following were concluded:
 - Binders and HMAC mixtures stiffen due to oxidative aging.
 - Fatigue life under laboratory controlled-strain testing declines with binder oxidative aging.
 - Fatigue life decline is characteristic of each HMAC mixture type.
 - The CMSE/CM approach provides a rational method for incorporating the effects of binder oxidation on mixture fatigue resistance.
 - Miner's cumulative damage approach can be used to quantify fatigue life decline with aging in the CMSE/CM approaches.
 - The Hirsch model provides a reasonable correlation between binder and HMAC mixture G^* values for AASHTO PP2 aging.
 - Changes in HMAC mixture stiffness with temperature follow the Hirsch model reasonably well.
 - Binder oxidation stiffens the HMAC mixture significantly more than would be indicated by the Hirsch model.
 - The effect of temperature on HMAC mixture fatigue resistance and other HMAC mixture properties may provide a means of estimating the effects of aging.

Exploration of Methods to Quantitatively Incorporate Aging in N_f Prediction

- Two methods, the SF_{ag} and SF_{aging} , were utilized to model and incorporate binder oxidative aging effects in the CMSE fatigue analysis.

- The SF_{ag} method is based on the binder DSR_f and assumes that N_f decline due to aging is predominantly due to binder oxidative aging. Although this approach provides a rapid and simple approach for incorporating aging effects in N_f analysis, it does not account for mix design and other mixture effects.
- The SF_{aging} method utilizes Miners' cumulative damage hypothesis and incorporates traffic loading, the binder DSR_f function, and HMAC mixture N_f (unaged and aged). It is a more fundamental approach but requires aged HMAC mixture data as input.
- Although further validation and modification is necessary, the SF_{ag} and SF_{aging} methods provided an initial and promising means to incorporate aging effects in the CMSE analysis. The results produced were reasonable. Integration into a single aging shift factor was suggested as a possible means to address their limitations. Another alternative is to use binder-HMAC mixture relationships to address aging effects in the CMSE analysis, but this approach equally needs further investigation.

Surrogate Fatigue Test Protocols

While the CMSE fatigue analysis approach can be rationally utilized for characterizing HMAC mixture fatigue resistance based on fundamental material properties and is ideal for structural design analysis and N_f performance prediction, a surrogate fatigue test protocol is required for rapid mix-design checks and HMAC mixture screening for fatigue resistance. In this regard, the following recommendations were made:

- For simplicity and practicality, the TS test was proposed as a surrogate fatigue test protocol with a limiting fatigue threshold value of $\epsilon_f \geq 3180 \mu\epsilon$. The test time is at most 5 minutes at an ambient test temperature or 20 °C (68 °F). This test protocol did not, however, give the best correlation with N_f .

- In terms of providing a good correlation with the HMAC mixture fatigue resistance based on the SF_{ag} concept, the RDT test (test time: $\cong 20$ minutes [test temperature \cong ambient or $20\text{ }^{\circ}\text{C}$ ($68\text{ }^{\circ}\text{F}$)] was proposed (as the second choice) with a limiting fatigue threshold value of $b \leq 0.65$. The RDT b criterion is recommended for a comprehensive analysis or when the TS ϵ_f criterion produces inconclusive results or is considered insufficient. The RDT's major limitation is its dependence on the TS test, which needs to be further investigated.
- In consideration of the RDT dependence on the TS test in the current CMSE approach, both the TS and RDT can be used as one comprehensive TS-RDT surrogate fatigue test protocol (total test time $\cong 25$ minutes, test temperature \cong ambient or $20\text{ }^{\circ}\text{C}$ [$68\text{ }^{\circ}\text{F}$]). The TS-RDT surrogate fatigue test protocols were initially validated and correlated well with BB, OT, and MEPDG results for three HMAC mixtures.

RECOMMENDATIONS

The following recommendations were made based on the results presented in this report:

- Additional laboratory validation and sensitivity analysis of the CMSE/CM approaches with additional HMAC mixtures and laboratory aging exposure conditions are needed to:
 - populate the N_f database;
 - further validate the CMSE/CM concepts and analysis models;
 - discretely explore other shift factors such as traffic wander;
 - formulate realistic reliability and statistical analysis models;
 - provide additional data for quantifying the N_f -aging relationship and develop more realistic aging shift factors that incorporate mixture volumetrics (binder content, AV, VMA), effects of temperature variations, and traffic loading;
 - further investigate and improve the SF_{ag} and SF_{aging} methods for incorporating aging effects in CMSE N_f analysis;
 - further explore the binder-HMAC mixture relationships as an alternative to using aging shift factors (SF_{ag} and SF_{aging});

- explore the possibilities of incorporating multiple distress analyses (e.g., moisture sensitive and rutting) in the CMSE approach; and
 - further explore and validate the proposed the surrogate fatigue test protocols.
- Field validation with pilot trial HMAC pavement sections and/or implementation projects to investigate the practical application of the CMSE/CM approaches is suggested.
 - Formulation and possible integration of the CMSE/CM fatigue analysis models with HMAC pavement structure design and analysis is recommended.
 - CMSE/CM software development is needed for a faster and more reliable computing methodology that will also aid and facilitate a comprehensive sensitivity analysis of the models.

CLOSURE AND PRODUCT DELIVERABLES

Within the framework of this research project, a limited N_f database based on various mix-design parameters and field conditions was established. This N_f database is presented in tabular format and is included as appendices in this report ([Appendix D](#)) and in Report 0-4468-2 (Appendix G) ([Walubita et al., 2005b](#)). To meet the project objectives, a fatigue analysis system (Chapters 1, 3, and 7 of this report and Report 0-4468-2) and surrogate fatigue test protocols (Chapters 6 and 7 of this report) were established and recommended. A workshop presenting the results of the project for TxDOT personnel was also conducted on March 6, 2006, in Austin, Texas.

REFERENCES

AASHTO PP6-94, Standard Practice for Grading or Verifying the Performance Grade of an Asphalt Binder. AASHTO Standards, Washington, D.C., 1996.

AASHTO Designation: PP2. Standard Practice for Short and Long Term Aging of Hot Mix Asphalt, *AASHTO Provisional Standards*, Washington, D.C., June Edition, 1994.

AASHTO TP5-98, Standard Test Method for Determining the Rheological Properties of Asphalt Binder Using a Dynamic Shear Rheometer (DSR). AASHTO Standards, Washington, D.C., 1998.

AASHTO TP8-94. Standard Test Method for Determining the Fatigue Life of Compacted Hot-Mix Asphalt (HMA) Subjected to Repeated Flexural Bending. AASHTO Standards, Washington, D.C., 1996.

AASHTO 2002 (NCHRP 1-37A) Pavement Design Guide. Pocket Facts, AASHTO 2002 (NCHRP 1-37A) Pavement Design Guide. <http://trb.org/mepdg> Accessed November, 2004

Al-Azri, N. A., S. H. Jung, K. M. Lusford, A. Ferry, J. A. Bullin, R. R. Davison, and C. J. Glover. Binder Oxidative Aging in Texas Pavements: Hardening Rates, Hardening Susceptibilities, and the Impact of Pavement Depth. Paper accepted for presentation at the 2006 TRB January conference, Washington, D.C., 2006.

Burr, B. L., R. R. Davison, C. J. Glover, and J. A. Bullin. Solvent Removal from Asphalt. In *Transportation Research Record: Journal of the Transportation Research Board*, No. 1269, TRB, National Research Council, Washington, D.C., 1990, pp. 1-8.

Burr, B. L., R. R. Davison, C. J. Glover, and J. A. Bullin. Softening of Asphalts in Dilute Solutions at Primary Distillation Conditions. In *Transportation Research Record: Journal of the Transportation Research Board*, No. 1436, TRB, National Research Council, Washington, D.C., 1994, pp. 47-53.

Burr, B. L., R. R. Davison, H. B. Jemison, C. J. Glover, and J. A. Bullin. Asphalt Hardening in Extraction Solvents. In *Transportation Research Record: Journal of the Transportation Research Board*, No. 1323, TRB, National Research Council, Washington, D.C., 1991, pp. 70-76.

Burr, B. L., C. J. Glover, R. R. Davison, and J. A. Bullin. New Apparatus and Procedure for the Extraction and Recovery of Asphalt Binder from Pavement Mixtures. In *Transportation Research Record: Journal of the Transportation Research Board*, No. 1391, 1993, pp. 20-29.

Cheng, D. Surface Free Energy of Asphalt-Aggregate System and Performance Analysis of Asphalt Concrete Based on Surface Free Energy. Ph.D. Dissertation. Texas A&M University, College Station, Texas, 2002.

Christensen, D.W., Jr., T. Pellinen, and R.F. Bonaquist, Hirsch Model for Estimating the Modulus of Asphalt Concrete, *Journal of Association of Asphalt Paving Technologists*, Vol 72, 2003, pp. 97-121.

Cipione, C. A., R. R. Davison, B. L. Burr, C. J. Glover and J. A. Bullin. Evaluation of Solvents for Extraction of Residual Asphalt from Aggregates. In *Transportation Research Record: Journal of the Transportation Research Board*, No. 1323, TRB, National Research Council, Washington, D.C., 1991, pp. 47-52.

Coons, R. F. and P. H. Wright. An Investigation of the Hardening of Asphalt Recovered from Pavements of Various Ages. *Journal of Association of Asphalt Paving Technologists*, Vol. 37, 1968, pp. 510-528.

Ferry, J.D., *Viscoelastic properties of polymers*, 3rd ed., Wiley, New York, 1980.

Glover, C. J., R. R. Davison, C. H. Domke, Y. Ruan, P. Juristyarini, D. B. Knorr, and S. H. Jung. *Development of New Method for Assessing Asphalt Binder Durability with Field Validation*. Report FHWA/TX-05/1872-2, Texas Transportation Institute (TTI), College Station, Texas, 2005.

Huang, Y. H. *Pavement Analysis and Design*. Prentice Hall, Englewood Cliffs, N.J., 1993.

Jemison, H. B., B. L. Burr, R. R. Davison, J. A. Bullin, and C. J. Glover. Application and Use of the ATR, FT-IR Method to Asphalt Aging Studies. In American Chemical Society Symposium on Chemistry and Characterization of Asphalts. *Fuel Science & Technology International*, Vol. 10, No. 4, 1992, pp. 795-808.

Juristyarini, P. Asphalt modification and testing of performance-related cracking failure properties, Ph.D. Dissertation, Texas A&M University, College Station, 2003.

Kandhal, P.S. Low-Temperature Ductility in Relation to Pavement Performance. In ASTM STP 628: Low-Temperature Properties of Bituminous Materials and Compacted Bituminous Paving Mixtures. American Society for Testing and Materials, Philadelphia, PA, 1977, pp. 95-106.

Kandhal, P. S. and S. Chakraborty. Effect of Asphalt Film Thickness on Short- and Long-Term Aging of Asphalt Paving Mixtures. In *Transportation Research Record: Journal of the Transportation Research Board*, No. 1535, TRB, National Research Council, Washington, D.C., 1996, pp. 83-90.

Kim, Y. R., H. J. Lee, Y. Kim, and D. N. Little. Mechanistic Evaluation of Fatigue Damage Growth and Healing of Asphalt Concrete: Laboratory and Field Experiments. In *Eighth International Conference on Asphalt Pavements*, University of Washington, Seattle, WA, 1997a, pp. 1089-1107.

Kim, Y. R., H. J. Lee, and D. N. Little. Fatigue Characterization of Asphalt Concrete Using Viscoelasticity and Continuum Damage Theory (with Discussion). *Journal of the Association of Asphalt Paving Technologists*, Vol. 66, 1997b, pp. 520-569.

Lee, H. J. Uniaxial Constitutive Modeling of Asphalt Concrete Using Viscoelasticity and Continuum Damage Theory. Ph.D. Dissertation. North Carolina State University, Raleigh, North Carolina, 1996.

Leicht, S. E., P. Juristyarini, R. R. Davison and C. J. Glover. An Investigation of Oxidative Curing on the Properties of High Cure Asphalt Rubber. *Petroleum Science and Technology*, Vol. 19, Nos. 3 and 4, 2001, pp. 317-334.

Liu, M., M. A. Ferry, R. R. Davison, C. J. Glover and J. A. Bullin. Oxygen Uptake as Correlated to Carbonyl Growth in Aged Asphalts and Asphalt Corbett Fractions. *Industrial & Engineering Chemistry Research*, Vol. 37, No. 12, 1998, pp. 4669-4674.

Lytton, R. L., J. Uzan, E. G. Fernando, R. Roque, D. Hiltunen, and S. M. Stoffels, *Development and Validation of Performance Prediction Models and Specifications for Asphalt Binders and Paving Mixes*. Report SHRP-A-357. Strategic Highway Research Program, Washington, D.C., 1993.

Marek, C. R. and M. Herrin. Tensile Behavior and Failure Characteristics of Asphalt Cements in Thin Films. *Journal of Association of Asphalt Paving Technologists*, Vol. 37, 1968, pp. 386-421.

Medani, T. O., Huurman, M., and A. A. A. Molenaar. "On the Computation of Master Curves for Bituminous Mixes." EuroBitumen, 2004.

Miner, M.A. "Cumulative damage in fatigue," Transactions of ASME, 67, A159-A164, 1945.

Mirza, M. W. and M. W. Witzak. Development of a Global Aging System for Short and Long Term Aging of Asphalt Cements (with Discussion). *Journal of Association of Asphalt Paving Technologists*, Vol. 64, 1995, pp. 393-430.

Montgomery, Elizabeth A. Peck, and G. Geoffrey. Introduction to Linear Regression Analysis. John Wiley, New York, c2001, 2001.

Park, D. W. Characterization of Permanent Deformation in Asphalt Concrete Using a Laboratory Prediction Method and an Elastic-Viscoplastic Model. Ph.D. Dissertation. Texas A&M University, College Station, Texas, 2004.

Ofori-Abebrese, K, E. Fatigue Resistance of Hot-Mix Asphalt Concrete Mixtures (HMAC) Using the Calibrated Mechanistic with Surface Energy Measurements (CMSE) Approach. Masters Thesis. Texas A&M University, College Station, Texas, 2006.

Ruan, Y., R.R. Davison, and C.J. Glover, An investigation of asphalt durability: Relationships between ductility and rheological properties for unmodified asphalts, *Petroleum Science and Technology*, Vol 21 (1-2), 2003, pp. 231-254.

Schapery, R. A. Correspondence Principles and a Generalized J Integral for Large Deformation and Fracture-Analysis of Viscoelastic Media. *International Journal of Fracture*, Vol. 25, No. 3, 1984, pp. 195-223.

Si, Z. Characterization of Microdamage and Healing of Asphalt Concrete Mixtures. Ph.D. Dissertation." Texas A&M University, College Station, Texas, 2001.

Tseng, K. H. and R. L. Lytton. Fatigue Damage Properties of Asphaltic Concrete Pavements. In *Transportation Research Record: Journal of the Transportation Research Board*, No. 1286, TRB, National Research Council, Washington, D.C., 1990, pp. 150-163.

TxDOT. *Standard Specifications for Construction and Maintenance of Highways, Streets, and Bridges*, Austin, Texas, 2004.

TxDOT. Condition of Texas Pavements. PMIS Annual Report, FY 2001 – 2003, TxDOT, Construction Division, Materials & Pavement Section, Austin, Texas, 2003.

TxDOT. *Pocket Facts*, TxDOT Test Specification Manuals
<http://manuals.dot.state.tx.us>. Accessed January, 2005.

Vassiliev, N. Y., R. R. Davison and C. J. Glover. Development of a Stirred Airflow Test Procedure for Short-Term Aging of Asphaltic Materials. *Bituminous Binders 2002*, No. 1810, 2002, pp. 25-32.

Walubita, L. F. Comparison of Fatigue Analysis Approaches for Predicting Fatigue Lives of Hot-Mix Asphalt Concrete (HMAC) Mixtures. PhD Dissertation, Texas A&M University, College Station, Texas, 2006.

Walubita, L.F., A. Epps Martin, H. S. Sung, C. J. Glover, E. S. Park, A. Chowdhury, and R. L. Lytton. *Comparison of Fatigue Analysis Approaches for Two Hot Mix Asphalt Concrete (HMAC) Mixtures*. TxDOT Technical Report FHWA/TX-05/0-4468-1, TTI, College Station, Texas, 2005a.

Walubita, L.F., A. Epps Martin, H. S. Sung, C. J. Glover, E. S. Park, and A. Chowdhury. *Comparison of Fatigue Analysis Approaches for Two Hot Mix Asphalt Concrete (HMAC) Mixtures*. TxDOT Technical Report FHWA/TX-05/0-4468-2, TTI, College Station, Texas, 2005b.

Walubita, L.F., A. Epps Martin, and G. S. Cleveland. *Application of the New M-E Pavement Design Guide Software for Fatigue Characterization of Three Texas Asphalt Mixtures*. Paper accepted for presentation at the 10th ICAP 2006 Conference in Quebec, Canada, August 12-17, 2006.

Williams, D.J., *Polymer science and engineering*. Prentice-Hall, Englewood Cliffs, N.J., 1971.

Zhou, F., and T. Scullion. *Overlay Tester: A Simple And Rapid Screening Test For Characterizing the Crack Resistance of Asphalt Mixes*. Paper accepted for presentation at the 10th ICAP 2006 Conference in Quebec, Canada, August 12-17, 2006.

APPENDICES

APPENDIX A

CMSE FATIGUE ANALYSIS MODELS

Parameter	Report 0-4468-2 (Walubita et al., 2005b)	After Sensitivity Analysis
Shift factor due to HMAC anisotropy, SF_a	$SF_a = \left(\frac{E_z}{E_x}\right)^{1.75} \cong 2.0$	$SF_a = 2.0$
Shift factor due to healing, SF_h	$SF_h = 1 + g_5 \left(\frac{\Delta t_r}{a_{TSF}}\right)^{g_6}$	$SF_h = 1 + g_5 \left(\frac{\Delta t_r}{a_{TSF}}\right)^{g_6}$
Shift factor due to aging, SF_{ag}	$SF_{ag} = u[\chi(t)]^w$, $\chi(t) = \left(\frac{m'@t_i}{m'@t_0}\right) \left(\frac{DSR_{f(1)}@t_0}{DSR_{f(1)}@t_i}\right)$	$SF_{ag} = u[\chi(t)]^w \cong u_1[t]^{w_1}$
Load cycles to crack initiation, N_i	$N_i = \left(\frac{C_{max}^{(1+2n)}}{A}\right) \left(\left[\frac{4\pi A_c}{b}\right]^n\right) (C_D)^n$	$N_i = 1 \times 10^{-5} \left(\frac{0.0075^{(1+2n)}}{A}\right) \left([2.366 \times 10^5 b^{-1}]^n\right)$
Number of load cycles to crack propagation, N_p	$N_p = \left(\frac{d^{\left(\frac{1-n}{2}\right)}}{[A(2r)^n (SG)^n (1-nq)]}\right) \left(1 - \left[\frac{C_{max}}{d}\right]^{(1-nq)}\right) \left(\frac{1}{\gamma}\right)^n$	$N_p = 1 \times 10^3 \gamma^{-n} \left(\frac{d^{\left(\frac{1-n}{2}\right)}}{\left[(1-1.18n)A \left(\frac{4.397E_1(1-\nu)}{(1+\nu)(1-2\nu)}\right)^n\right]}\right) \left(1 - [0.0075d^{-1}]^{(1-1.18n)}\right)$
Paris' Law fracture coefficient, A & n	$A = \frac{k}{\sigma_i^2 I_i} \left[\left[\frac{D_1^{(1-m_i)} E_i}{\Delta G_f} \right]^{\left[\frac{1}{m_i} \left[\frac{1}{(n_{BD}+1)}\right]\right]} \right] \int_0^{\Delta r} w^n(t) dt$, $n = 1/m$	$A = 0.165 \sigma_i^{-2} [0.5042 - (0.1744 \ln(n))] \left[\frac{E_1^m}{\Delta G_f} \left(\frac{\sin(m\pi)}{m\pi}\right)^{(1-m)} \right]$
HMAC mixture fatigue resistance, N_f	$N_f = SF_i (N_i + N_p) = 2SF_{ag} (SF_h) (N_i + N_p) \geq Q \times TrafficDesign_{ESALs}$	

APPENDIX A (Continued)
CM FATIGUE ANALYSIS MODELS

Parameter	Report 0-4468-2 (Walubita et al., 2005b)	After Sensitivity Analysis
Shift factor due to HMAC anisotropy, SF_a	$SF_a = \left(\frac{E_z}{E_x}\right)^{1.75} \cong 2.0$	$SF_a = 2.0$
Shift factor due to healing, SF_h	$SF_h = 1 + g_5 \left(\frac{\Delta t_r}{a_{TSF}}\right)^{g_6}$	$SF_h = 1 + g_5 \left(\frac{\Delta t_r}{a_{TSF}}\right)^{g_6}$
Shift factor due to aging, SF_{ag}	$SF_{ag} = u[\chi(t)]^w$, $\chi(t) = \left(\frac{m' @ t_i}{m' @ t_0}\right) \left(\frac{DSR_{f(1)} @ t_0}{DSR_{f(1)} @ t_i}\right)$	$SF_{ag} = u[\chi(t)]^w \cong u_1 [t]^{w_1}$
Load cycles to crack initiation, N_i	$N_i = \left(\frac{C_{max}^{(1+2n)}}{A}\right) \left(\left[\frac{4\pi A_c}{b}\right]^n\right) (C_D)^n$	$N_i = 1 \times 10^{-5} \left(\frac{0.0075^{(1+2n)}}{A}\right) \left([2.366 \times 10^5 b^{-1}]^n\right)$
Number of load cycles to crack propagation, N_p	$N_p = \left(\frac{d^{\left(\frac{1-n}{2}\right)}}{[A(2r)^n (SG)^n (1-nq)]}\right) \left(1 - \left[\frac{C_{max}}{d}\right]^{(1-nq)}\right) \left(\frac{1}{\gamma}\right)^n$	$N_p = 1 \times 10^3 \gamma^{-n} \left(\frac{d^{\left(\frac{1-n}{2}\right)}}{\left[(1-1.18n)A \left(\frac{4.397E_1(1-\nu)}{(1+\nu)(1-2\nu)}\right)^n\right]}\right) \left(1 - [0.0075d^{-1}]^{(1-1.18n)}\right)$
Paris' Law fracture coefficients, A & n	$A = 10^{1 + \left\{g_2 + \frac{g_3}{m_t} \log\left(\frac{\sin(m\pi)}{m\pi E_t}\right) + g_4 \log(\sigma_t)\right\}}$, $n = g_o + \left(\frac{g_1}{m_t}\right)$	
HMAC mixture fatigue resistance, N_f	$N_f = SF_i (N_i + N_p) = 2SF_{ag} (SF_h) (N_i + N_p) \geq Q \times TrafficDesign_{ESALS}$	

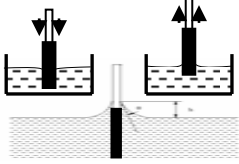
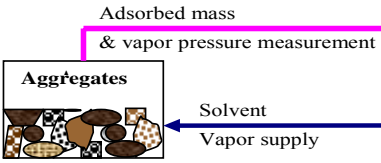
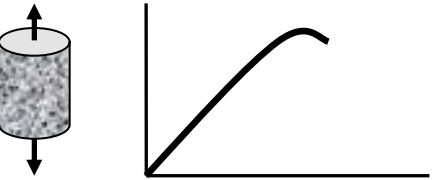
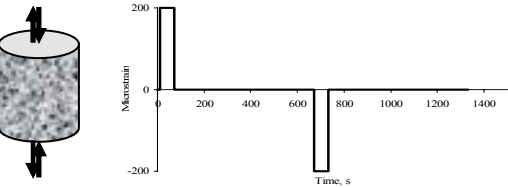

APPENDIX A (Continued)
DEFINITION OF PARAMETERS

Parameter	Definition
SF_a	Shift factor due to HMAC anisotropy (unitless)
E_z, E_x	Vertical and lateral elastic moduli (psi)
SF_h	Shift factor due to healing (unitless)
g_i	Fatigue field calibration constants (unitless)
Δt_r	Rest period between major traffic loads (s)
a_{TSF}	Temperature shift factor for field conditions ($\cong 1.0$)
SF_{ag}	Shift factor due to binder oxidative aging (unitless)
u, w	Material regression constants
$\chi(t)$	Material property ratio that relates the aged to the unaged binder shear properties
m'	Slope of the plot of binder $DSR_f(\omega)$ versus frequency (ω) within a reduced angular frequency range of 1 E-06 to 1 E+02 rad/s at 20 °C (68 °F)
$DSR_{f(1)}$	The value of $[G' / (\eta' / G')]$ at 1 rad/s (Pa·s)
t_i	Aging exposure period at time t_i in years

Parameter	Definition
N_i	Number of load cycles to crack initiation
A, n	Paris' Law fracture coefficients (unitless)
N_p	Number of load cycles to crack propagation
γ	Shear strain computed at the edge of loaded tire
ν	Poisson's ratio
d	HMAC layer thickness
E_l	Elastic relaxation modulus at 1.0 s in tension (_t) (or compression (_c))
m_i	Stress relaxation rate from RM master-curve (subscript t = tension, c = compression)
σ_t	Tensile strength
ΔG_i	Surface energy (subscript f = fracture, h = healing)
D_l	Tensile creep compliance
k, I_b, n_{BD}	Material coefficients

APPENDIX B

CMSE/CM LABORATORY TESTS

Test	Loading Configuration	Test Parameters and Output Data
Wilhelmy Plate (WP) [Not required in CM approach]		Automatic immersion and withdrawal of binder coated glass plates into/from liquid solvents up to approx. 5 mm depth @ 20±2 °C. Test time: ≈45 minutes. Measurable parameter is the dynamic contact angle (θ) and final output data is the surface energy (SE) components for the binder ($\Gamma_{i, binder}$) used to compute mixture fracture (ΔG_f) and healing (ΔG_h) energies, respectively.
Universal Sorption Device (USD) [Not required in CM approach]		50 g (washed & oven dried) aggregate of fractional size (4.75 mm < aggregate size < 2.63 mm). Measurable parameters are vapor pressure & adsorbed gas mass of liquid solvents @ 25±2 °C. Test time: 60 to 70 hrs. Output data is SE components for the aggregates ($\Gamma_{j, aggregate}$) used to compute mixture fracture (ΔG_f) and healing (ΔG_h) energies, respectively.
Tensile Strength (TS) [CMSE approach]		Tensile loading until break @ 0.05 in/min (1.27 mm/min) @ 20 °C. Test time: ≈ 5 minutes. Output data is HMAC mixture tensile strength (σ) and failure strain (ϵ_f). [See page 10-7 for full details]
Uniaxial Relaxation Modulus (RM)		Trapezoidal shaped strain-controlled @ 200 microstrain (tension and compression), 60 s loading & 600 s rest period @ 10, 20, & 30 °C. Test time: ≈ 25 minutes. Output data is HMAC mixture elastic relaxation modulus ($E(t)$), stress relaxation rate (m), and temperature correction factors (a_T). [See page 10-15 for full details]
Uniaxial Repeated Direct-Tension (RDT)		Haversine strain-controlled (tension) @ 1 Hz, 30 °C, & 350 microstrain for 1000 load cycles. Test time: ≈20 minutes. Output data is dissipated pseudo strain energy (DPSE) and rate of fracture damage accumulation (b). [See page 10-24 for full details]

APPENDIX B (Continued)

THE TENSILE STRENGTH (TS) TEST

Section 1. Overview

Use this test method to characterize the tensile strength and ductility potential of compacted hot-mix asphalt concrete (HMAC) mixtures. The measured fundamental material properties from this test are the tensile strength and the tensile failure strain at break under direct-tensile loading.

Units of Measurements

The values given in parentheses (if provided) are not standard and may not be exact mathematical conversions. Use each system of units separately. Combining values from the two systems may result in nonconformance with the standards.

Section 2. Apparatus

Use the following apparatus:

- Loading mechanism capable of applying a continuous axial tensile load at a constant elongation (deformation) rate of 0.05 inches/min (1.27 mm/min) or any specified elongation rate for up to 5 minutes. See [Figure TS-1](#) for the TS loading configuration.
 - The axial load measuring device (load cell) must be capable of measuring the axial load to an accuracy of $\pm 2\%$ of the applied axial load.
 - The load cell must be calibrated and/or checked prior to initiation of any program of testing, rechecked monthly thereafter, and recalibrated semiannually.
- Temperature control system (if required) capable of controlling temperature with a range of 50 to 100 °F (10 to 30 °C). The recommended TS test temperature is ambient (room) or 68 °F (20 °C). A temperature control system may be used for this test but is unnecessary if the test is run at ambient temperature and the temperature does not fluctuate significantly.

- The temperature must be held to within ± 2 °F (± 1 °C) of the specified test temperature.
- The system must include a temperature-controlled cabinet or chamber large enough to hold at least three specimens.
- The specimens should be pre-conditioned to the test temperature for a minimum period of 2 hr prior to testing.
- Loading platens
 - Two loading platens must be used for the upper and lower ends of the specimen.
 - Both loading platens must be of the same diameter as the specimen being tested to provide for positive centering of the specimen under load.
 - The upper loading platen provides attachment to the load cell.
 - The loading platens must be thoroughly cleaned and wiped dry prior to use. The sides of the loading platens attaching to the specimen must preferably be rough to provide an effective attaching surface to the specimen. The other sides of loading platens must have provisions to attach to the load cell and base plate, respectively.
- LVDT attachments
 - Use three LVDTs for deformation measurements.
 - Attach the LVDTs at three radial equi-distances around the specimen. The vertical distance between the LVDT holders should be 4 inches (100 mm) center to center and 1 inch (25 mm) from the specimen end. See [Figure TS-2](#) for the setup.
- Measurement and recording system
 - Measure the vertical deformation with Linear Variable Differential Transducers (LVDT), resolution of each LVDT must be better than 0.0001 inches (0.0025 mm).
 - Measure load with an electronic load cell capable of measuring vertical loads of up to 5000 lbs (22241 N) with an accuracy of $\pm 2\%$ of the load level being applied.
 - The temperature should be monitored and recorded via a thermocouple probe inserted inside a dummy HMAC specimen also placed in the temperature chamber (if a temperature chamber is used).
 - Continuously monitor and record the load and axial deformations during the test at least every 0.1 s. Temperature should also be continuously monitored and recorded at least every 5 s.

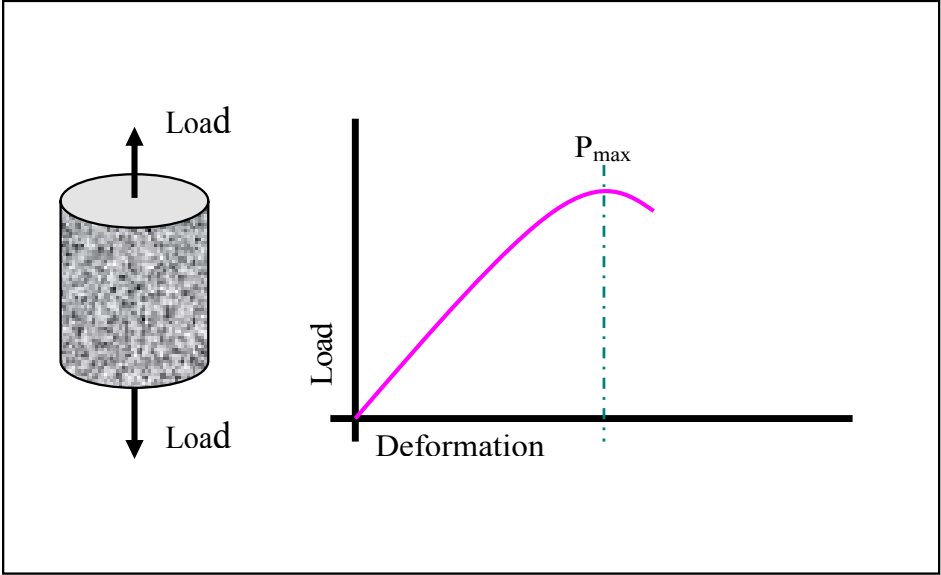


Figure TS-1. TS Loading Configuration.

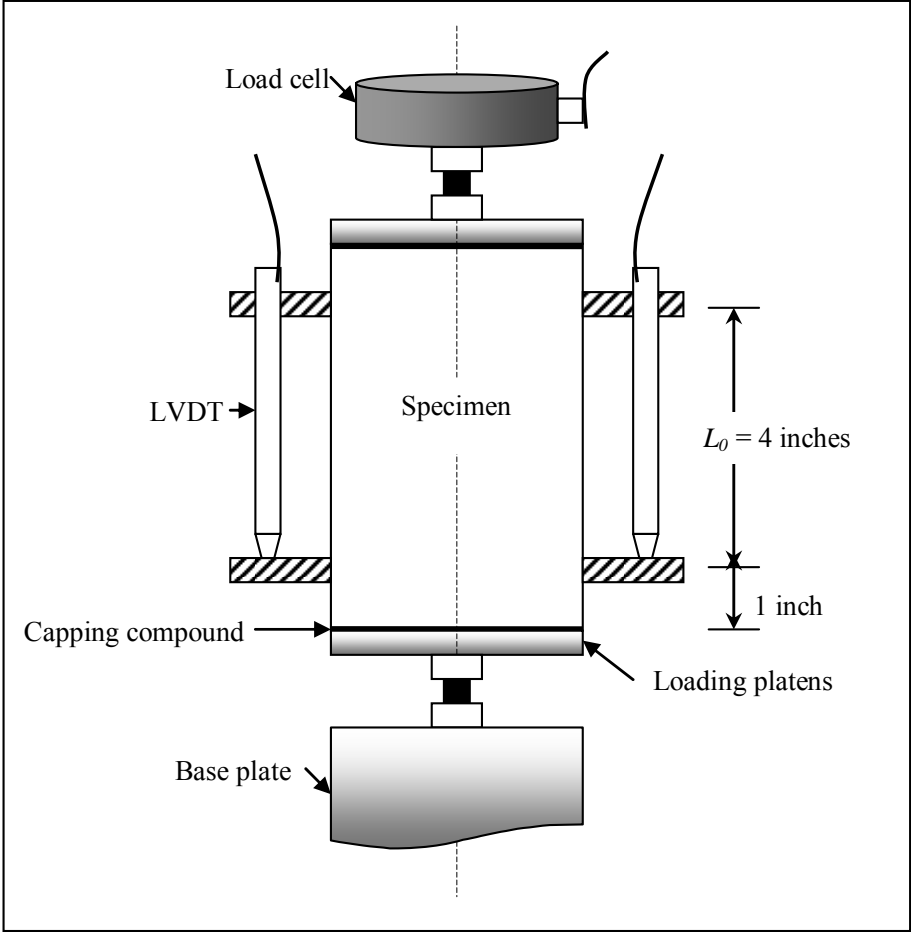


Figure TS-2. Specimen Setup and Measurement Configuration.

Section 3. Materials

- Capping compound (such as 2 ton Epoxy) able to withstand at least 1000 lbs (5000 N) load without cracking for attaching the loading platens to the specimen.
- Gluing compound (such as Pro CA Cyanoacrylate and an accelerator) for attaching the LVDT fixtures to the specimen.
- CO₂ (as needed for maintaining the temperature of the test chamber if required).

Section 4. Specimen

- Laboratory Molded Specimen
 - Prepared according to test methods “Tex-205-F, Laboratory Method of Mixing Bituminous Mixtures,” and or “Tex-241-F, Superpave Gyrotory Compacting of Test Specimens of Bituminous Mixtures”.
 - The cylindrical specimen diameter must be 4 inches (100 mm) and specimen height must be 6 inches (150 mm) to a tolerance of ± 0.1 inches (± 2 mm).
 - Specimens may initially be molded to 6 inches diameter by 7 inches height and then sawn/cored to final dimensions of 4 inches diameter by 6 inches height.
 - Specimen end surfaces must be sawn smooth and parallel.
 - Density of test specimens must be $93 \pm 0.5\%$ (i.e., $7 \pm 0.5\%$ air voids). However, a $\pm 1\%$ tolerance may also be acceptable.
- Core Specimen
 - Cylindrical specimen of diameter of 4 inches (100 mm) and height of 6 inches (150 mm) with ± 0.1 inches (± 2 mm) tolerance.
 - End surfaces must be smooth and parallel.

Section 5. Procedure

Follow the following procedure to perform the TS test:

Step 1: Specimen Dimensions and Density

- Fabricate at least two specimens as described in [Section 4](#).
- Measure and record the diameter and height of the specimens.
- Measure and record the relative density and air voids of specimens according to test methods Tex-207-F, "Determining Density of Compacted Bituminous Mixtures" and Tex-227-F, "Theoretical Maximum Specific Gravity of Bituminous Mixtures".

Step 2: Attaching Loading Platens and LVDT Fixtures

- Mix the capping compound and use it to attach the loading platens to the end surfaces of the specimen. Two loading platens are required for each specimen.
- Apply some pressure (such as extra weights) to the loading platens and allow the capping compound to dry for about 24 hr.
- Using the gluing compound, attach the LVDT fixtures to the specimen as described in Section 2.
- Pre-condition the specimen (s) to the test temperature for a minimum period of 2 hr prior to testing.

Step 3: Specimen Setup and Testing

- Attach the specimen to the loading mechanism and load cell as shown in [Figure TS-2](#). Make sure to align the specimen along the central axis of loading so as to minimize the induction of undesirable moments that can lead to erroneous results.
- Put the LVDTs in the LVDT fixtures and make sure that they are all zeroed prior to testing.

- In a load-controlled mode, apply a continuously increasing tensile load at a deformation rate of 0.05 inches/min (1.27 mm/min) or any specified loading rate for approximately 5 minutes or when the specimen breaks.
- The test terminates automatically after 5 minutes. However, the test can also be set to terminate automatically when the specimen breaks (i.e., when the maximum load is reached and begins to progressively decline) before 5 minutes is reached. In fact, it is recommended to set the TS test to terminate automatically at some point after the maximum load is reached instead of going all the way to 5 minutes. One way to achieve this is to code the TS control program with a code such as “stop the test when the peak load drops by 25% or 50%” for example.
- During the entire testing period, monitor and record all the necessary data. The measurable data from this test are the load (P [lbs or kips]), deformation (ΔL [inches]), time (t [s]), and temperature (T [°F]).
- When testing is complete, disconnect and remove the specimen from the machine setup.

Section 6. Calculations

- Calculate the tensile strength and failure strain at break as follows:

- Tensile strength

$$\sigma_t = \frac{P_{\max}}{\pi r^2} \quad \text{Equation (TS-1)}$$

- Failure tensile strain

$$\varepsilon_f = 10^6 \frac{\Delta L @ P_{\max}}{L_0} \quad \text{Equation (TS-2)}$$

- Where :

- ◆ σ_t = Tensile strength, psi (or MPa)
- ◆ P_{\max} = Maximum tensile load at break, lbs (or kN)
- ◆ r = Radius of the cylindrical HMAC specimen, inches (or mm)
- ◆ ε_f = Failure tensile strain at break (at P_{\max}) in microns, in/in (or mm/mm)
- ◆ ΔL = Maximum deformation at P_{\max} , inches (mm)
- ◆ L_0 = Initial distance between the LVDT holders (see [Figure TS-2](#)), inches (or mm)

- For each specimen, ε_f should be calculated as the average of the three LVDTs.
- [Figure TS-3](#) is a typical plot of tensile stress versus strain, where:

- $Tensile\ stress = \frac{Load}{Specimen\ X - Area} = \frac{P}{\pi r^2}$, psi
- $Tensile\ microstrain = 10^6 \frac{Deformation}{L_0} = 10^6 \frac{\Delta L}{4} = 2.50 \times 10^5 \Delta L$, in/in

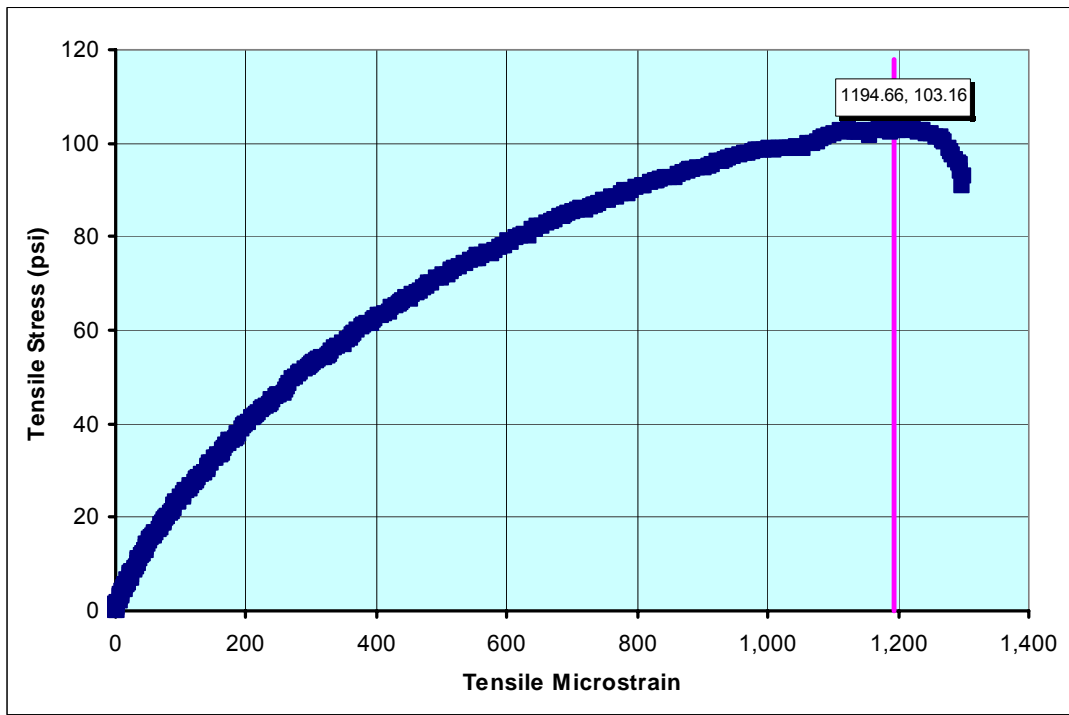


Figure TS-3. Typical Plot of Tensile Stress versus Strain.

- From this plot, obtain:
 - The tensile strength, σ_t (psi) as the maximum tensile stress (maximum load) at break, e.g., $\sigma_t = 103.16$ psi in [Figure TS-3](#).
 - The failure tensile strain at break, ε_f , e.g., $\varepsilon_f = 1194.66 \mu\varepsilon$ in [Figure TS-3](#).
- Based on the HMA mixtures evaluated in this project, the following threshold value was preliminarily proposed as an indicator of good fatigue resistance: $\varepsilon_f \geq 3180 \mu\varepsilon$

A modifiable Excel spreadsheet is available to numerically perform the calculations.

Section 7. Replicates and Statistical Variability

- A minimum of two replicate specimens are recommended for the TS test.
- If the computed coefficient of variation for the σ_t of the two specimens differs by more than 15 percent, it is recommended to test a third specimen. Note that 15 percent is a typically acceptable COV for HMAC mixtures/specimens due to HMAC heterogeneity and test variability.

Section 8. Report

- The final results and data to be reported for subsequent analyses include:
 - (1) the air void content (and density)
 - (2) the binder content
 - (3) the (average) tensile strength (σ_t)
 - (4) the (average) failure tensile strain (ε_f) in microns
 - (5) the loading rate
 - (6) the test temperature
 - (7) the COV of σ_t and ε_f

APPENDIX B (Continued)

THE RELAXATION MODULUS (RM) TEST

Section 1. Overview

Use this test method to characterize the elastic relaxation modulus and potential to relax applied loads for HMAC mixtures. The measurable fundamental material properties from the RM test are the elastic relaxation modulus and the stress relaxation rate denoted as m .

Units of Measurements

The values given in parentheses (if provided) are not standard and may not be exact mathematical conversions. Use each system of units separately. Combining values from the two systems may result in nonconformance with the standards.

Section 2. Apparatus

Use the following apparatus:

- Loading mechanism capable of applying a tensile and compressive load to maintain a constant axial strain (deformation or displacement) in tension or compression mode for a specified loading time period. See [Figure RM-1](#) for the RM loading configuration.
 - The axial load measuring device (load cell) must be capable of measuring the axial load to an accuracy of $\pm 2\%$ of the applied axial load.
 - The load cell must be calibrated and/or checked prior to initiation of any program of testing, rechecked monthly thereafter, and recalibrated semiannually.
- Temperature control system capable of controlling temperature with a range of 50 to 100 °F (10 to 30 °C). The RM test must at least be run at three temperatures to facilitate generation of a master-curve. The three recommended RM test temperatures are 50, 68, and 86 °F (10, 20, and 30 °C), respectively.

- The temperature must be held to within ± 2 °F (± 1 °C) of the specified test temperature.
- The system must include a temperature-controlled cabinet or chamber large enough to hold at least three specimens.
- The specimens should be pre-conditioned to the test temperatures (in the temperature chamber) for a minimum period of 2 hrs prior to testing.
- Loading platens
 - Two loading platens must be used for the upper and lower ends of the specimen.
 - Both loading platens must be of the same diameter as the specimen being tested to provide for positive centering of the specimen under load.
 - The upper loading platen provides attachment to the load cell.
 - The loading platens must be thoroughly cleaned and wiped dry prior to use. The sides of the loading platens attaching to the specimen must preferably be rough to provide an effective attaching surface to the specimen. The other sides of loading platens must have provisions to attach to the load cell and base plate, respectively.
- LVDT attachments
 - Use three LVDTs for deformation measurements.
 - Attach the LVDTs at three radial equi-distances around the specimen. The vertical distance between the LVDT holders should be 4 inches (100 mm) center to center and 1 inch (25 mm) from the specimen end. See [Figure RM-2](#) for the setup.
- Measurement and recording system
 - Measure the vertical deformation with Linear Variable Differential Transducers (LVDT), resolution of each LVDT must be better than 0.0001 inches (0.0025 mm).
 - Measure load with an electronic load cell capable of measuring vertical loads of up to 5000 lbs (22241 N) with an accuracy of $\pm 2\%$ of the load level being applied.
 - The temperature should be monitored and recorded via a thermocouple probe inserted inside a dummy HMAC specimen also placed in the temperature chamber.
 - Continuously monitor and record the load and axial deformations during the test at least every 0.5 s. Temperature should also be continuously monitored and recorded at least every 5 s.

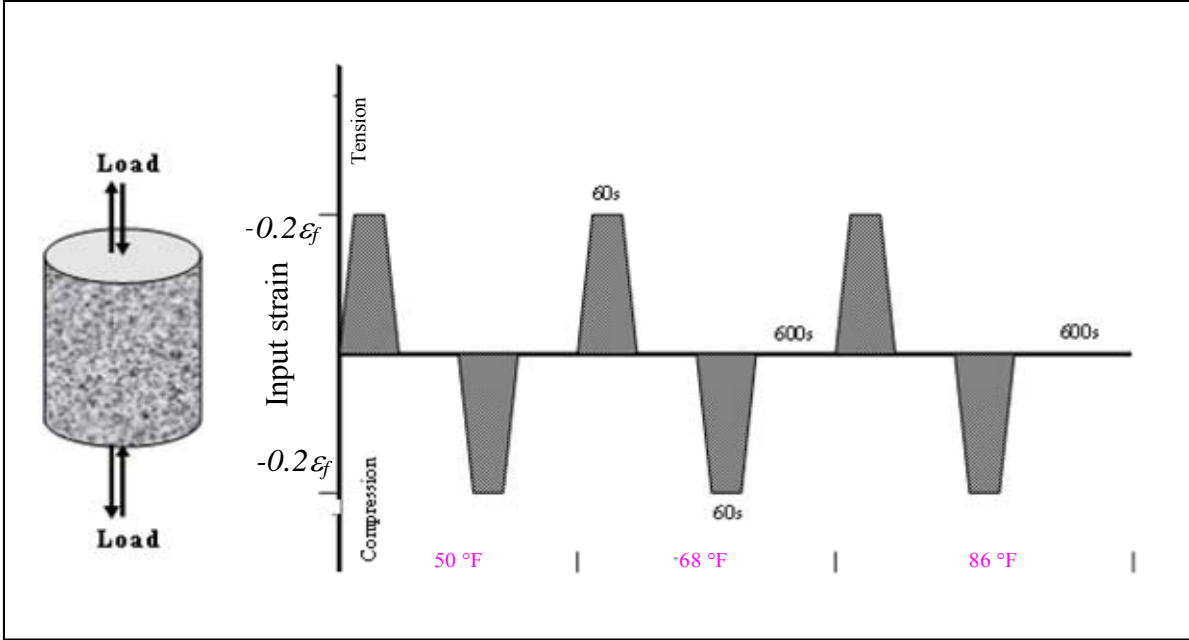


Figure RM-1. RM Loading Configuration.

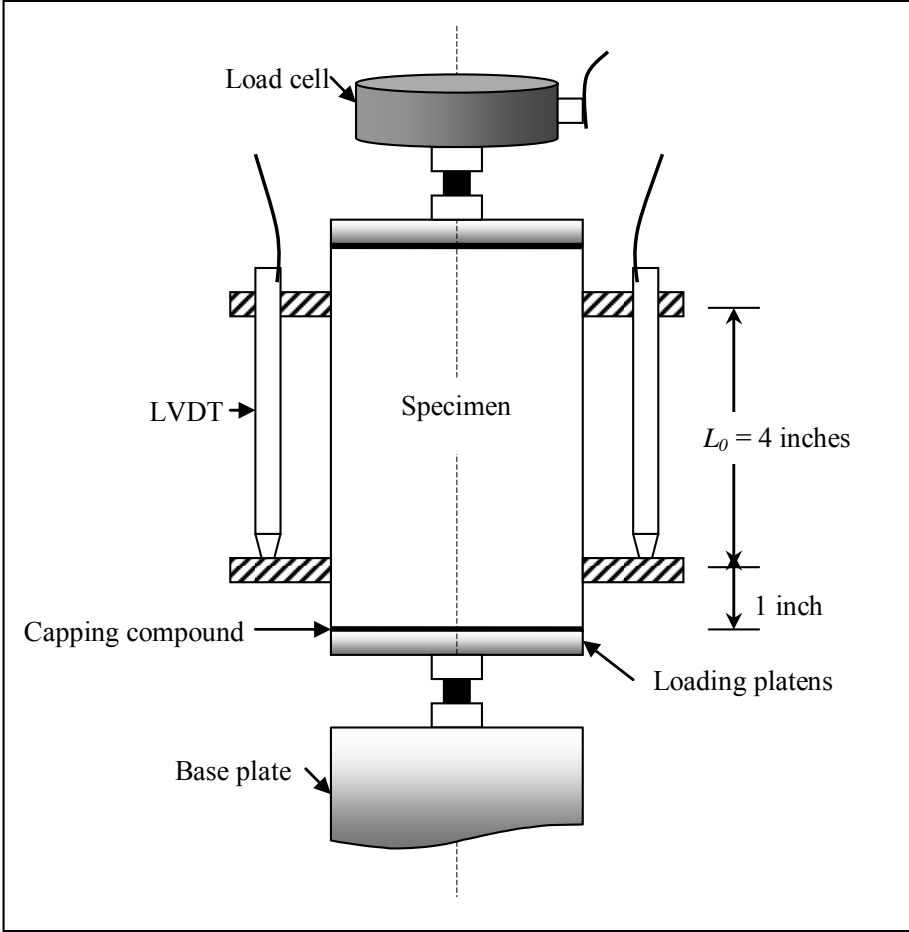


Figure RM-2. Specimen Setup and Measurement Configuration.

Section 3. Materials

- Capping compound (such as 2 ton Epoxy) able to withstand at least 1000 lbs (5000 N) load without cracking for attaching the loading platens to the specimen.
- Gluing compound (such as Pro CA Cyanoacrylate and an accelerator) for attaching the LVDT fixtures to the specimen.
- CO₂ (as needed for maintaining the temperature of the test chamber).

Section 4. Specimen

- Laboratory Molded Specimen
 - Prepared according to test methods "Tex-205-F, Laboratory Method of Mixing Bituminous Mixtures," and or "Tex-241-F, Superpave Gyrotory Compacting of Test Specimens of Bituminous Mixtures".
 - The cylindrical specimen diameter must be 4 inches (100 mm), and specimen height must be 6 inches (150 mm) to a tolerance of ± 0.1 inches (± 2 mm).
 - Specimens may initially be molded to 6 inches in diameter by 7 inches in height and then sawn/cored to a final dimension of 4 inches in diameter by 6 inches in height.
 - Specimen end surfaces must be sawn smooth and parallel.
 - Density of test specimens must be $93 \pm 0.5\%$ (i.e., $7 \pm 0.5\%$ air voids). However, a $\pm 1\%$ tolerance may also be acceptable.
- Core Specimen
 - Cylindrical specimen with a diameter of 4 inches (100 mm) and a height of 6 inches (150 mm) with ± 0.1 inches (± 2 mm) tolerance.
 - End surfaces must be smooth and parallel.

Section 5. Procedure

To perform the RM test, follow the following procedures:

Step 1: Specimen Dimensions and Density

- Fabricate at least two specimens as described in [Section 4](#).
- Measure and record the diameter and height of the specimens.
- Measure and record the relative density and air voids of specimens according to test methods "Tex-207-F, Determining Density of Compacted Bituminous Mixtures" and "Tex-227-F, Theoretical Maximum Specific Gravity of Bituminous Mixtures".

Step 2: Attaching Loading Platens and LVDT Fixtures

- Mix the capping compound and use it to attach the loading platens to the end surfaces of the specimen. Two loading platens are required for each specimen.
- Apply some pressure (such as extra weights) to the loading platens and allow the capping compound to dry for about 24 hrs.
- Using the gluing compound, attach the LVDT fixtures to the specimen as described in Section 2.
- Pre-condition the specimen(s) to the test temperature for a minimum period of 2 hrs prior to testing.

Step 3: Specimen Setup and Testing

- Attach the specimen to the loading mechanism and load cell as shown in [Figure RM-2](#). Make sure to align the specimen along the central axis of loading so as to minimize the induction of undesirable moments that can lead to erroneous results.
- Put the LVDTs in the LVDT fixtures and make sure that they are all zeroed prior to testing.
- In a displacement-controlled (strain-controlled) mode, apply a load equivalent to 20% of the failure tensile strain from the TS test (i.e., $0.2\varepsilon_f$) for the specified time period.

- The RM test basically involves applying a constant axial strain (displacement) to a cylindrical HMAC specimen either in tension or compression for a given time period and then releasing the strain (or displacement) for another given time period, thereby allowing the specimen to rest or relax (elastic recovery). The input strain waveform is trapezoidal shaped (see [Figure RM-1](#)).
- For a given test temperature, e.g., 50 °F (10 °C), the loading sequence should basically consist of applying a $0.2\varepsilon_f$ tensile strain (or equivalent displacement) for a period of 60 s, followed by a 600 s rest period and then application of a $0.2\varepsilon_f$ compressive strain for 60 s, followed by another 600 s rest period. The time interval for the strain load application from 0 to $+0.2\varepsilon_f$ (tension) or 0 to $-0.2\varepsilon_f$ (compression) strain is 0.6 s.
- The RM test should be run in strain-controlled (displacement or LVDT mode) and one of the three LVDTs, preferably the LVDT designated as LVDT 1 should be used as the control.
- The total test time for both the tensile and compressive loading cycle for a given test temperature is approximately 25 minutes, so the test terminates automatically after 25 minutes. However, the test can also be set to terminate automatically when the compressive loading cycle is completed because data captured during the 600 s rest period is not necessarily used in the calculations.
- Repeat the loading process for all the three specified test temperatures.
- During the entire testing period, monitor and record all the necessary data. The measurable data from this test include the time (t [s]), load (P [lbs or kips]), deformation (ΔL [inches]), and temperature (T [°F]).
- When all testing cycles have been completed, disconnect and remove the specimen from the machine setup.

Section 6. Calculations

- Calculate the time-dependent elastic relaxation modulus as follows:

$$E(t) = \frac{P(t)}{\pi r^2 \varepsilon} = \frac{5P(t)}{\pi r^2 \varepsilon_f} \quad \text{Equation (RM-1)}$$

○ Where :

- ◆ $E(t)$ = Time-dependent elastic relaxation modulus, psi (or MPa)
 - ◆ $P(t)$ = Load, lbs (or kN)
 - ◆ r = Radius of the cylindrical HMAC specimen, inches (or mm),
 - ◆ ε_f = Failure tensile strain at break (at P_{max}) from the TS test
- Using the time-temperature superposition principle, generate a master curve of $E(t)$ versus reduced time ξ (s) in the form of simple power function illustrated below:

$$E(t) = E_1 \xi^{-m} \quad \text{Equation (RM-2)}$$

○ Where :

- ◆ $E(t)$ = Time-dependent elastic relaxation modulus, psi (MPa)
 - ◆ E_1 = Elastic relaxation modulus at a reduced loading time of 1 s, psi (MPa)
 - ◆ ξ = Reduced loading time, s
 - ◆ m = Stress relaxation rate ($0 \leq m < 1$)
- Reduced time is determined as a function of the actual loading time (t) and temperature correction factors (a_T)

$$\xi = \frac{t}{a_T} \quad \text{Equation (RM-3)}$$

- The reference temperature for the master curve should be 68 °F (20 °C) and should be generated for both tension and compression loading modes.
- [Figure RM-3](#) is a typical plot of the RM master-curve for tension loading mode at a reference temperature of 68 °F (20 °C).

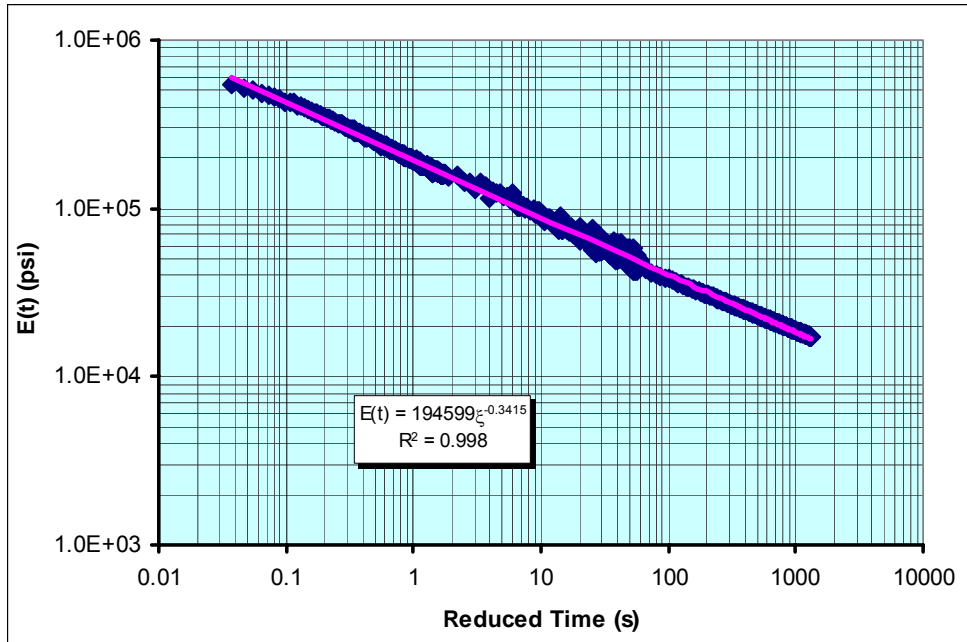


Figure RM-3. Typical Plot of a RM Master Curve (Tension, $T_{ref} = 68\text{ }^{\circ}\text{F}$).

- From this master curve, obtain:
 - The elastic relaxation modulus, E_I (psi) (in tension) as the $E(t)$ at a reduced loading time of 1 s, e.g., $E_I = 194,599$ psi in [Figure RM-3](#).
 - The stress relaxation rate (m) (in tension), which is the slope of the RM master-curve, e.g., $m = 0.3415$ in [Figure RM-3](#).

A modifiable Excel spreadsheet is available to numerically perform the calculations. Note that the consistency of the RM master-curve is highly dependent on the consistency of the laboratory test data, the raw data reduction process, and the time-temperature superposition model used.

Section 7. Replicates and Statistical Variability

- A minimum of two replicate specimens are recommended for this test.
- If the computed coefficient of variation for the σ_t of the two specimens differs by more than 15 percent, it is recommended to test a third specimen. Note that 15 percent is a typically acceptable COV for HMAC mixtures/specimens due to HMAC heterogeneity and test variability.

Section 8. Report

- The final results and data to be reported for subsequent analyses include:
 - (1) the air void content (and density)
 - (2) the binder content
 - (3) the (average) elastic relaxation modulus (E_I), both tension ($E_{I(t)}$), and compression ($E_{I(c)}$)
 - (4) the (average) stress relaxation rate (m), both tension (m_t) and compression (m_c)
 - (5) the temperature correction factors (a_T), both tension and compression
 - (6) the reference temperature for the master-curve (T_{ref})
 - (7) the COV of E_I and m , both tension and compression

APPENDIX B (Continued)

THE UNIAXIAL REPEATED DIRECT-TENSION (RDT) TEST

Section 1. Overview

Use this test method to characterize the fracture damage potential of hot-mix asphalt concrete (HMAC) mixtures under repeated direct tensile loading. The measurable fundamental material property from the RDT test is the rate of accumulation of fracture damage under repeated direct tensile loading, a parameter denoted as b .

Units of Measurements

The values given in parentheses (if provided) are not standard and may not be exact mathematical conversions. Use each system of units separately. Combining values from the two systems may result in nonconformance with the standards.

Section 2. Apparatus

Use the following apparatus:

- Loading mechanism capable of applying a uniaxial repeated direct-tensile loading to a cylindrical HMAC specimen at a given strain level for a specified number of load cycles. See [Figure RDT-1](#) for the RDT loading configuration.
 - The axial load measuring device (load cell) must be capable of measuring the axial load to an accuracy of $\pm 2\%$ of the applied axial load.
 - The load cell must be calibrated and/or checked prior to initiation of any program of RDT testing, rechecked monthly thereafter, and recalibrated semiannually.
- Temperature control system (if required) capable of controlling temperature with a range of 50 to 100 °F (10 to 30 °C). The recommended RDT test temperature is ambient (room) or 68 °F (20 °C). A temperature control system may be used for this test but is unnecessary if the test is run at ambient temperature and the temperature does not fluctuate significantly.

- The temperature must be held to within ± 2 °F (± 1 °C) of the specified test temperature.
- The system must include a temperature controlled cabinet or chamber large enough to hold at least three specimens.
- The specimens should be pre-conditioned to the test temperatures (in the temperature chamber) for a minimum period of 2 hrs prior to testing.
- Loading platens
 - Two loading platens must be used for the upper and lower ends of the specimen.
 - Both loading platens must be of the same diameter as the specimen being tested to provide for positive centering of the specimen under load.
 - The upper loading platen provides attachment to the load cell.
 - The loading platens must be thoroughly cleaned and wiped dry prior to use. The sides of the loading platens attaching to the specimen must preferably be rough to provide an effective attaching surface to the specimen. The other sides of loading platens must have provisions to attach to the load cell and base plate, respectively.
- LVDT attachments
 - Use three LVDTs for deformation measurements.
 - Attach the LVDTs at three radial equi-distances around the specimen. The vertical distance between the LVDT holders should be 4 inches (100 mm) center to center and 1 inch (25 mm) from the specimen end. See [Figure RDT-2](#) for the setup.
- Measurement and recording system
 - Measure the vertical deformation with Linear Variable Differential Transducers (LVDT), resolution of each LVDT must be better than 0.0001 inches (0.0025 mm).
 - Measure load with an electronic load cell capable of measuring vertical loads of up to 5000 lbs (22241 N) with an accuracy of $\pm 2\%$ of the load level being applied.
 - The temperature should be monitored and recorded via a thermocouple probe inserted inside a dummy HMAC specimen also placed in the temperature chamber.
 - Continuously monitor and record the load and axial deformations during the test at least every 0.005 s. Temperature should also be continuously monitored and recorded at least every 5 s.

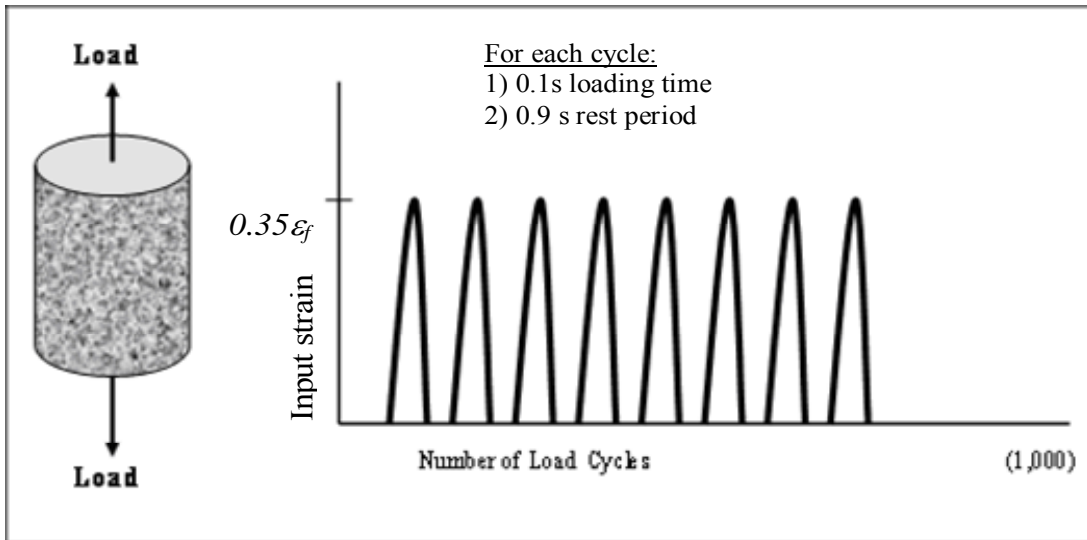


Figure RDT-1. RDT Loading Configuration

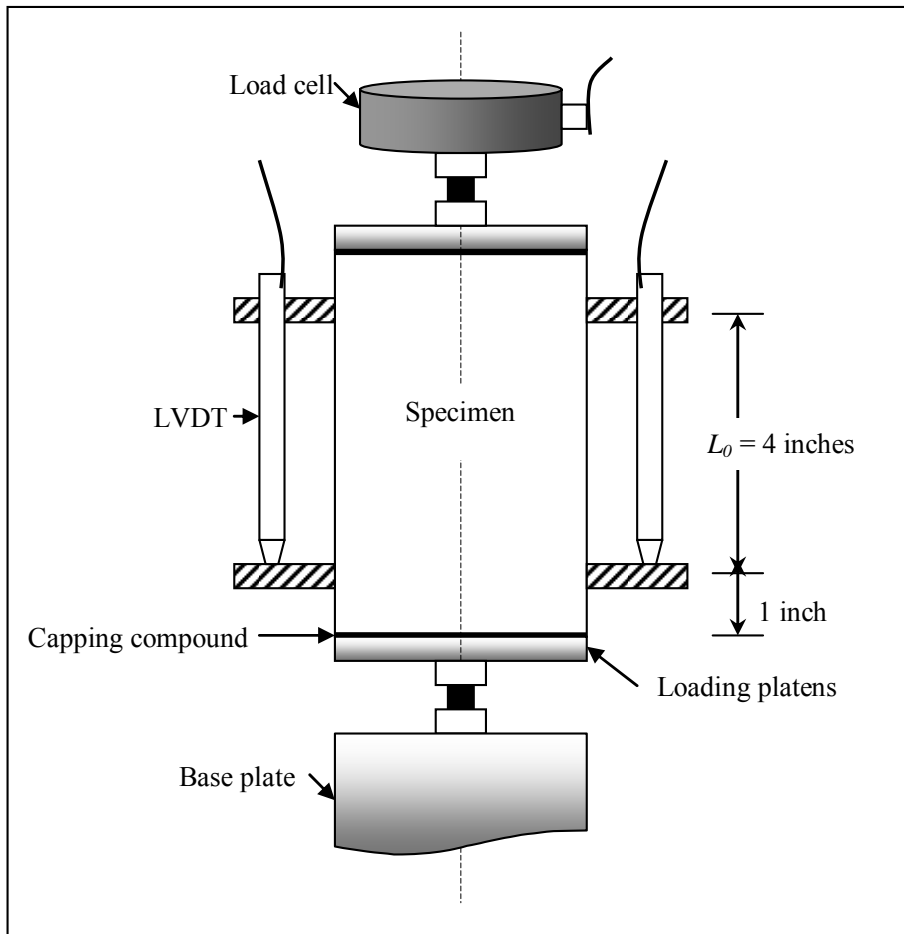


Figure RDT-2. Specimen Setup and Measurement Configuration

Section 3. Materials

- Capping compound (such as 2 ton Epoxy) able to withstand at least 1000 lbs (5000 N) load without cracking for attaching the loading platens to the specimen.
- Gluing compound (such as Pro CA Cyanoacrylate and an accelerator) for attaching the LVDT fixtures to the specimen.
- CO₂ (as needed for maintaining the temperature of the test chamber).

Section 4. Specimen

- Laboratory Molded Specimen
 - Prepared according to test methods "Tex-205-F, Laboratory Method of Mixing Bituminous Mixtures," and or "Tex-241-F, Superpave Gyrotory Compacting of Test Specimens of Bituminous Mixtures".
 - The cylindrical specimen diameter must be 4 inches (100 mm) and specimen height must be 6 inches (150 mm) to a tolerance of ± 0.1 inches (± 2 mm).
 - Specimens may initially be molded to 6 inches diameter by 7 inches height and then sawn/cored to final dimensions of 4 inches diameter by 6 inches height.
 - Specimen end surfaces must be sawn smooth and parallel.
 - Density of test specimens must be $93 \pm 0.5\%$ (i.e., $7 \pm 0.5\%$ air voids). However, a $\pm 1\%$ tolerance may also be acceptable.
- Core Specimen
 - Cylindrical specimen of diameter of 4 inches (100 mm) and height of 6 inches (150 mm) with ± 0.1 inches (± 2 mm) tolerance.
 - End surfaces must be smooth and parallel.

Section 5. Procedure

Follow the following procedure to perform the RDT test:

Step 1: Specimen Dimensions and Density

- Fabricate at least two specimens as described in [Section 4](#).
- Measure and record the diameter and height of the specimens.
- Measure and record the relative density and air voids of specimens according to test methods "Tex-207-F, Determining Density of Compacted Bituminous Mixtures" and "Tex-227-F, Theoretical Maximum Specific Gravity of Bituminous Mixtures".

Step 2: Attaching Loading Platens and LVDT Fixtures

- Mix the capping compound and use it to attach the loading platens to the end surfaces of the specimen. Two loading platens are required for each specimen.
- Apply some pressure (such as extra weights) to the loading platens and allow the capping compound to dry for about 24 hrs.
- Using the gluing compound, attach the LVDT fixtures to the specimen as described in Section 2.
- Pre-condition the specimen (s) to the test temperature for a minimum period of 2 hrs prior to testing.

Step 3: Specimen Setup and Testing

- Attach the specimen to the loading mechanism and load cell as shown in [Figure RDT-2](#). Make sure to align the specimen along the central axis of loading so as to minimize the induction of undesirable moments that can lead to erroneous results.
- Put the LVDTs in the LVDT fixtures and make sure that they are all zeroed prior to testing.

- In a displacement-controlled (strain-controlled) mode, repeatedly apply a tensile load equivalent to 35% of the failure tensile strain from the TS test (i.e., $0.35\varepsilon_f$) up to a specified number of load cycles.
- The RDT loading sequence basically consists of repeatedly applying an axial direct tensile strain of $0.35\varepsilon_f$ (or equivalent displacement) to a cylindrical HMAC specimen at a frequency of 1 Hz for a total of 1,000 load cycles. The actual loading time per cycle is 0.1 s with a 0.9 s rest period between load pulses. A complete load cycle including the rest period is 1.0 s. The input strain waveform is haversine shaped (see [Figure RDT-1](#)).
- The RDT test should be run in strain-controlled (displacement or LVDT mode) and one of the three LVDTs preferably the LVDT designated as LVDT 1 should be used as the control.
- A complete RDT test takes at most 20 minutes. The test terminates automatically when 1 000 load cycles have been completed.
- During the entire testing period, monitor and record all the necessary data. The measurable data from this test include the time (t [s]), load (P [lbs or kips]), deformation (ΔL [inches]), number of load cycles (N), loading frequency (Hz), and temperature (T [°F]).
- When testing is completed, disconnect and remove the specimen from the machine setup.

Section 6. Calculations

- Calculate the stress as follows:

$$\sigma_c(t) = \int_0^t E(t-\tau) \frac{\partial \varepsilon(\tau)}{d\tau} d\tau \quad \text{Equation (RDT-1)}$$

$$\sigma_m(t) = \frac{P(t)}{\pi r^2} \quad \text{Equation (RDT-2)}$$

- Where :

- ◆ $\sigma_c(t)$ = Calculated time-dependent tensile stress, psi (or MPa)
- ◆ $E(t-\tau)$ = Tensile relaxation modulus (undamaged condition) at time $t-\tau$, psi (or MPa)
- ◆ $\sigma_m(t)$ = Physically measured time-dependent tensile stress, psi (or MPa)
- ◆ $P(t)$ = Load, lbs (or kN)
- ◆ r = Radius of the cylindrical HMAC specimen, inches (or mm)

- Calculate the modulus as follows:

$$E_R = \frac{\sigma_m(t)_1}{\varepsilon_m(t)_1} \quad \text{Equation (RDT-3)}$$

- Where :

- ◆ E_R = Reference modulus, psi (or MPa)
- ◆ $\sigma_m(t)_1$ = Physically measured time-dependent tensile stress, psi (or MPa) at the first RDT load cycle,
- ◆ $\varepsilon_m(t)_1$ = Physically measured time-dependent tensile strain (in/in [mm/mm]) at the first RDT load cycle

- Calculate the pseudo strain as follows:

$$\varepsilon_R(t) = \left[\frac{\sigma_c(t)}{E_R} \right] \quad \text{Equation (RDT-4)}$$

- Where $\varepsilon_R(t)$ is the pseudo strain, in/in (mm/mm).

- Calculate the non-linearity correction factor as follows:

$$\Psi(t) = \frac{\sigma_c(t)_1}{\sigma_m(t)_1} \quad \text{Equation (RDT-5)}$$

- Where $\psi(t)$ is the non-linearity correction factor.

- Using the double meridian distance method (DMD) for traverse area determination, determine the dissipated pseudo strain energy (DPSE) as the area enclosed within a hysteresis loop of each load cycle using the following expression:

$$DPSE = \sum \psi(t) (\varepsilon_R(t) \times \sigma_m(t)) \quad \text{Equation (RDT-6)}$$

- DPSE is simply the area in the pseudo hysteresis loop of the measured stress versus the calculated pseudo strain as shown in the example in [Figure RDT-3](#).

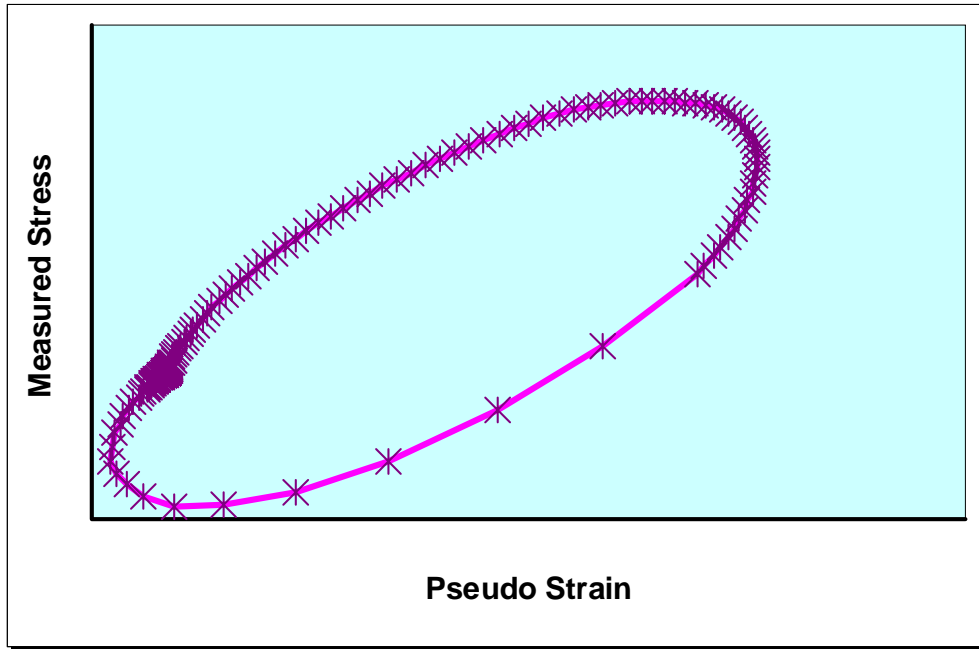


Figure RDT-3. Example of Hysteresis Loop.

- Determine the rate of fracture damage accumulation (parameter b) as the slope of the plot of DPSE versus the number of RDT load cycles (N) on a semi log scale. The DPSE- N relationship yields a linear expression of the following form:

$$W_R = a + b \text{Log}(N) \quad \text{Equation (RDT-7)}$$

- Where:
 - $W_R = \text{DPSE (J/m}^3\text{)}$
 - $a = \text{Constant or DPSE at the first RDT load cycle}$
 - $b = \text{Slope of } W_R\text{-log } N \text{ plot}$
 - $N = \text{RDT load cycle}$
- [Figure RDT-4](#) shows a typical plot of DPSE versus Log N .

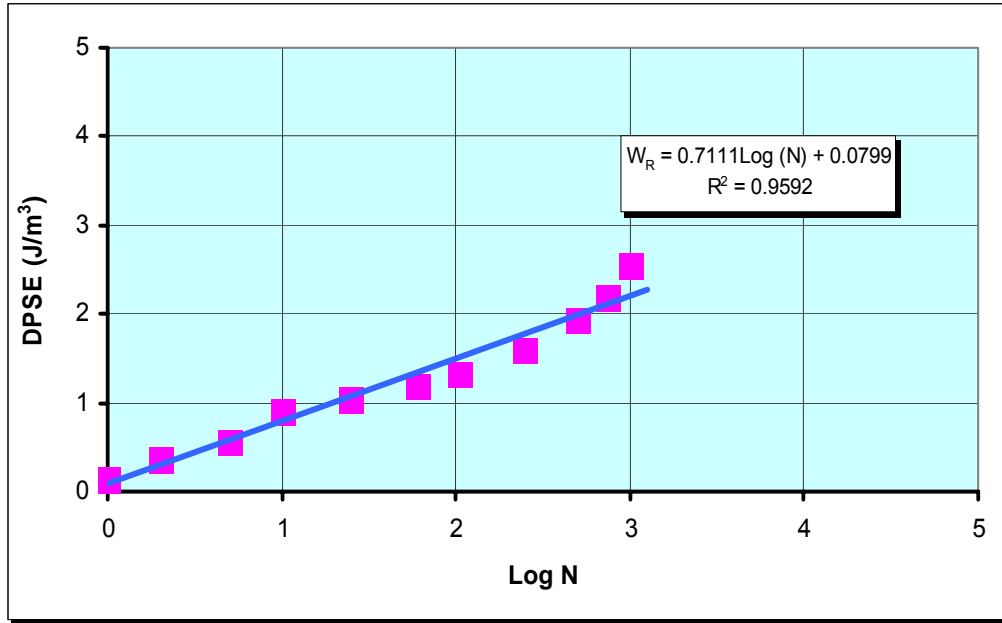


Figure RDT-4. Typical Plot of DPSE versus Log N.

- From this plot, obtain the rate of fracture damage accumulation, b as the slope of the plot of DPSE versus Log N, e.g., $b = 0.71$ in [Figure RDT-4](#).
- Based on the HMAC mixtures evaluated in this project, the following threshold value was preliminarily proposed as an indicator of good fatigue resistance: $b \leq 0.65$.

A modifiable Excel spreadsheet is available to numerically perform the calculations. Note that the value of the coefficient of correlation (R^2) in [Figure RDT-4](#) is a function of the consistency of the laboratory test data.

Section 7. Replicates and Statistical Variability

- A minimum of two replicate specimens are recommended for this test.
- If the computed coefficient of variation for the σ_f of the two specimens differs by more than 15 percent, it is recommended to test a third specimen. Note that 15 percent is a typically acceptable COV for HMAC mixtures/specimens due to HMAC heterogeneity and test variability.

Section 8. Report

- The final results and data to be reported for subsequent analyses include:
 - (1) the air void content (and density)
 - (2) the binder content
 - (3) the (average) b value
 - (4) the test temperature
 - (5) the COV of b

APPENDIX C
MATERIAL PROPERTIES

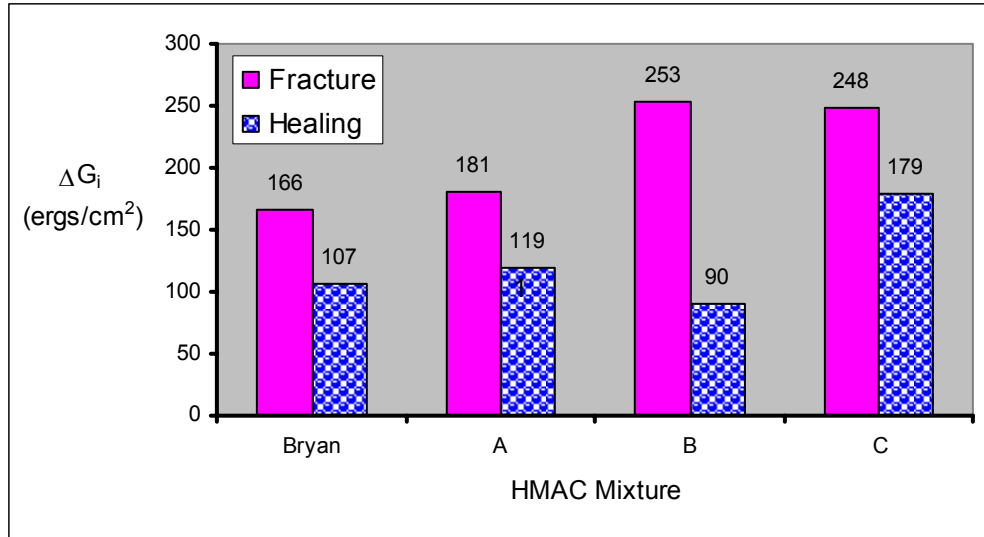


Figure C1. HMAC Mixture Adhesive Bond Strengths (0 Months).

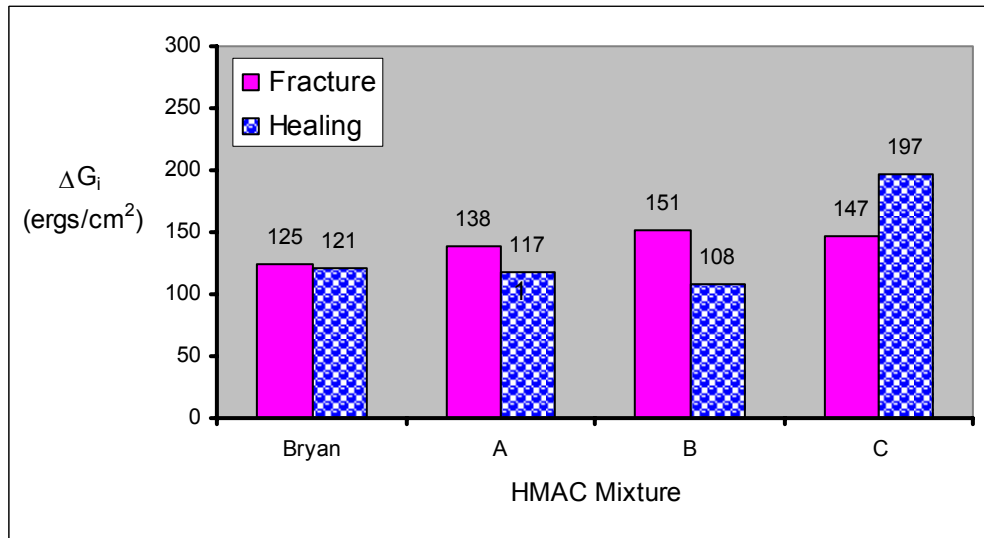


Figure C2. HMAC Mixture Adhesive Bond Strengths (6 Months).

APPENDIX C (Continued)
MATERIAL PROPERTIES

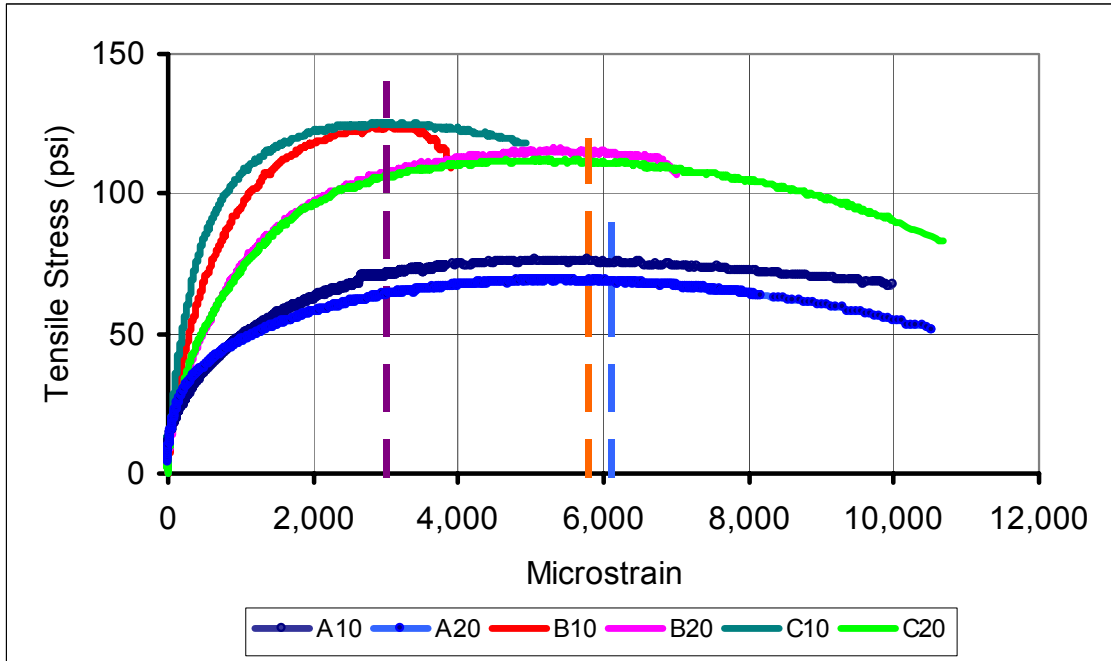


Figure C3. HMAC Mixture Tensile Strength (0 Months).

APPENDIX C (Continued)
MATERIAL PROPERTIES

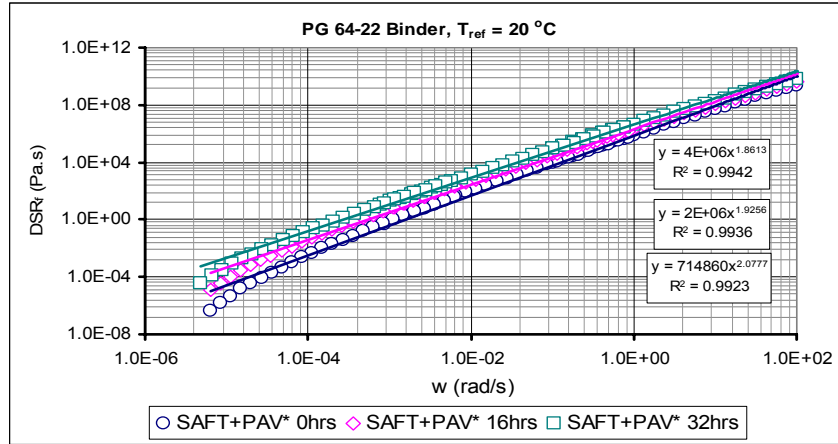


Figure C4. PG 64-22 Binder DSR Master Curve.

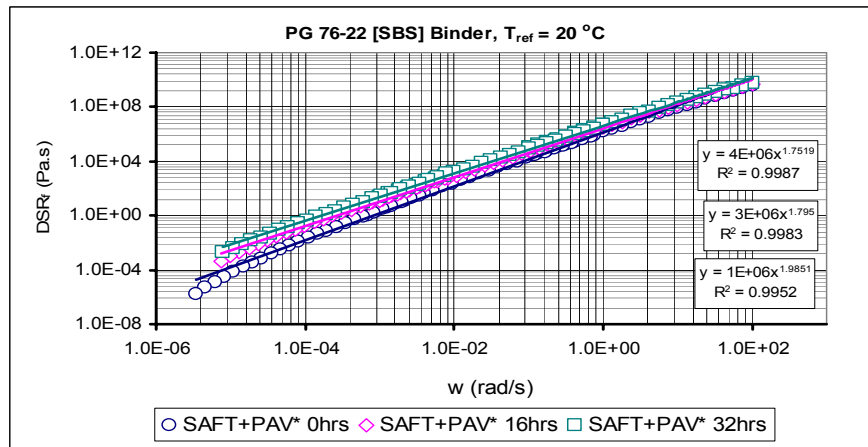


Figure C5. PG 76-22 (SBS) Binder DSR Master Curve.

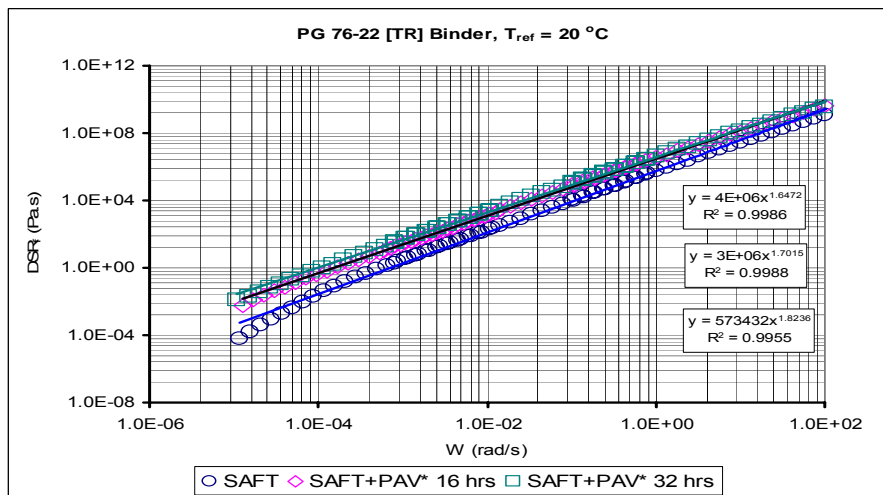


Figure C6. PG 76-22 (TR) Binder DSR Master Curve.

APPENDIX D
HMAC MIXTURE FATIGUE LIFE

Table D1. CMSE Approach (Wet-Warm Environment).

HMAC Mixture	PS1	PS2	PS3	PS4	PS5
Bryan	3.82E+06	2.13E+06	2.18E+06	1.96E+06	5.49E+06
A10	8.37E+06	5.72E+06	5.87E+06	5.25E+06	1.58E+07
A20	9.74E+06	6.65E+06	6.83E+06	6.11E+06	1.72E+07
B10	8.01E+06	6.56E+06	6.57E+06	4.45E+06	1.98E+07
B20	9.23E+06	6.91E+06	6.91E+06	4.69E+06	1.01E+07
C10	1.63E+06	1.03E+06	1.03E+06	7.01E+05	1.51E+06
C20	2.29E+06	1.71E+06	1.72E+06	1.16E+06	2.50E+06

10-37

Table D2. CM Approach (Wet-Warm Environment).

HMAC Mixture	PS1	PS2	PS3	PS4	PS5
Bryan	3.10E+06	2.38E+06	2.06E+06	1.96E+06	5.38E+06
A10	7.88E+06	6.40E+06	5.56E+06	5.30E+06	1.45E+07
A20	1.10+07	7.45E+06	6.47E+06	6.16E+06	1.69E+07
B10	7.77E+06	5.55E+06	6.23E+06	4.59E+06	1.93E+07
B20	8.33E+06	6.33E+06	7.10E+06	5.23E+06	1.07E+07
C10	1.98E+06	9.46E+05	1.06E+06	7.81E+05	1.60E+06
C20	2.00E+06	1.57E+06	1.76E+06	1.30E+06	2.66E+06

APPENDIX D (Continued)
HMAC MIXTURE FATIGUE LIFE

Table D3. CMSE Approach (Dry-Cold Environment).

HMAC Mixture	PS1	PS2	PS3	PS4	PS5
Bryan	4.42E+06	2.46E+06	2.52E+06	2.26E+06	6.34E+06
A10	9.69E+06	6.61E+06	6.79E+06	6.05E+06	1.71E+07
A20	1.13E+07	7.68E+06	7.90E+06	7.05E+06	1.99E+07
B10	8.65E+06	6.78E+06	6.79E+06	4.61E+06	2.05E+07
B20	9.97E+06	7.14E+06	7.14E+06	4.86E+06	1.05E+07
C10	1.70E+06	1.06E+06	1.06E+06	7.26E+05	1.56E+06
C20	2.47E+06	1.77E+06	1.78E+06	1.20E+06	2.59E+06

Table D4. CM Approach (Dry-Cold Environment).

HMAC Mixture	PS1	PS2	PS3	PS4	PS5
Bryan	3.59E+06	2.75E+06	2.38E+06	2.26E+06	6.21E+06
A10	9.69E+06	7.39E+06	6.43E+06	6.11E+06	1.67E+07
A20	1.13E+07	8.60E+06	7.48E+06	7.10E+06	1.95E+07
B10	8.46E+06	5.80E+06	6.51E+06	4.79E+06	2.01E+07
B20	1.00E+07	6.62E+06	7.42E+06	5.46E+06	1.12E+07
C10	1.75E+06	9.89E+05	1.11E+06	8.15E+05	1.67E+06
C20	2.49E+06	1.64E+06	1.84E+06	1.36E+06	2.78E+06

APPENDIX E

LIMITING FATIGUE THRESHOLD VALUES: PAVEMENT SERVICE LIFE (X_{PSL}) AND THE SF_{aging} METHOD

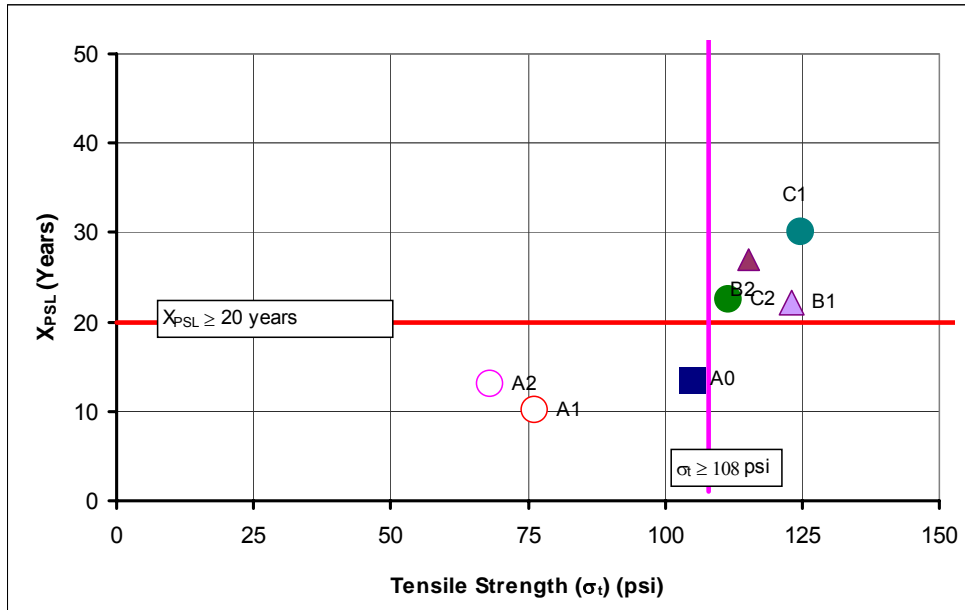


Figure E1. Tensile Strength (σ_t) versus X_{PSL} .

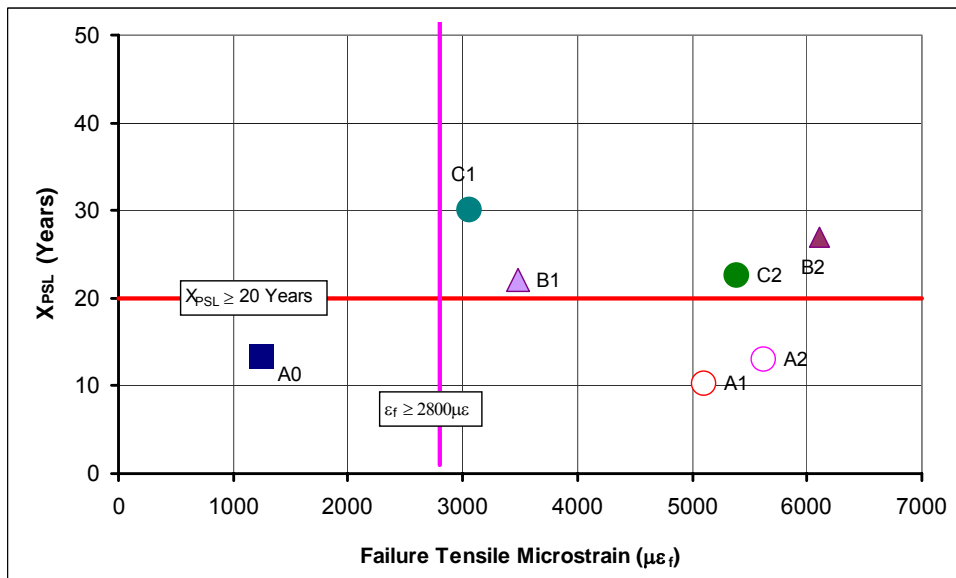


Figure E2. Failure Strain (ϵ_t) versus X_{PSL} .

APPENDIX E (Continued)
LIMITING FATIGUE THRESHOLD VALUES:
PAVEMENT SERVICE LIFE (X_{PSL}) AND THE SF_{aging} METHOD

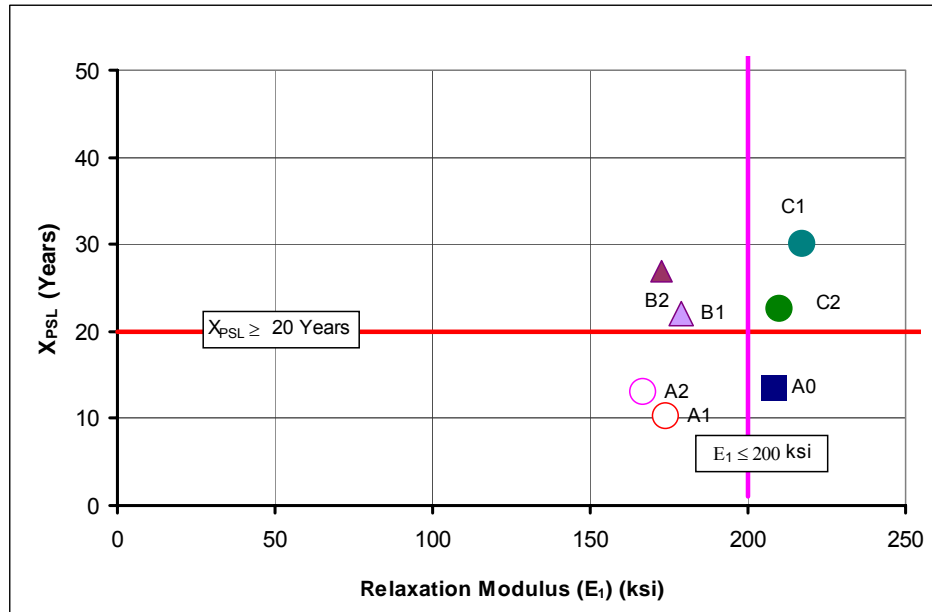


Figure E3. Relaxation Modulus (Tension) (E_1) versus X_{PSL} .

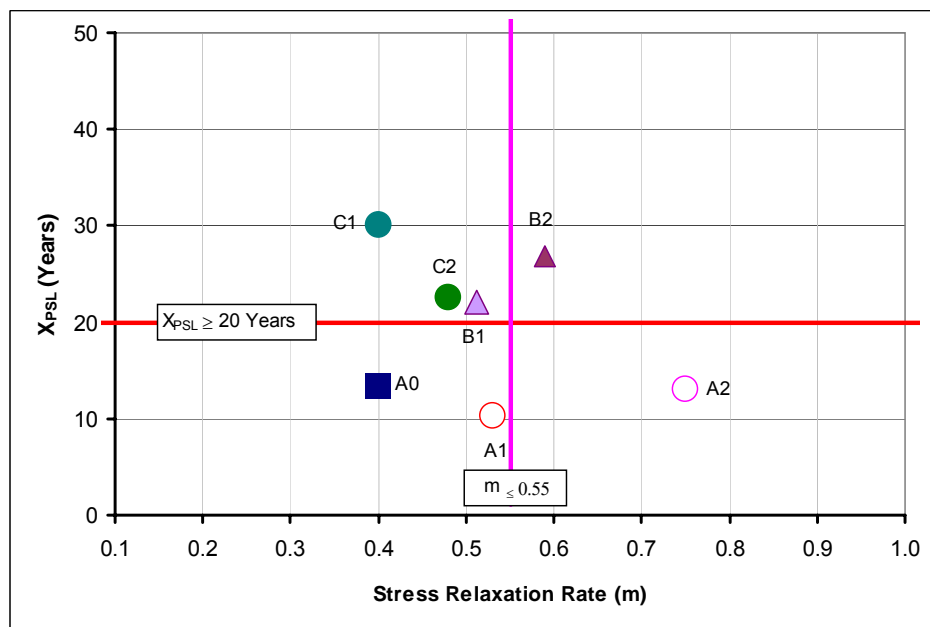


Figure E4. Stress Relaxation Rate (m) versus X_{PSL} .

APPENDIX E (Continued)
LIMITING FATIGUE THRESHOLD VALUES:
PAVEMENT SERVICE LIFE (X_{PSL}) AND THE SF_{aging} METHOD

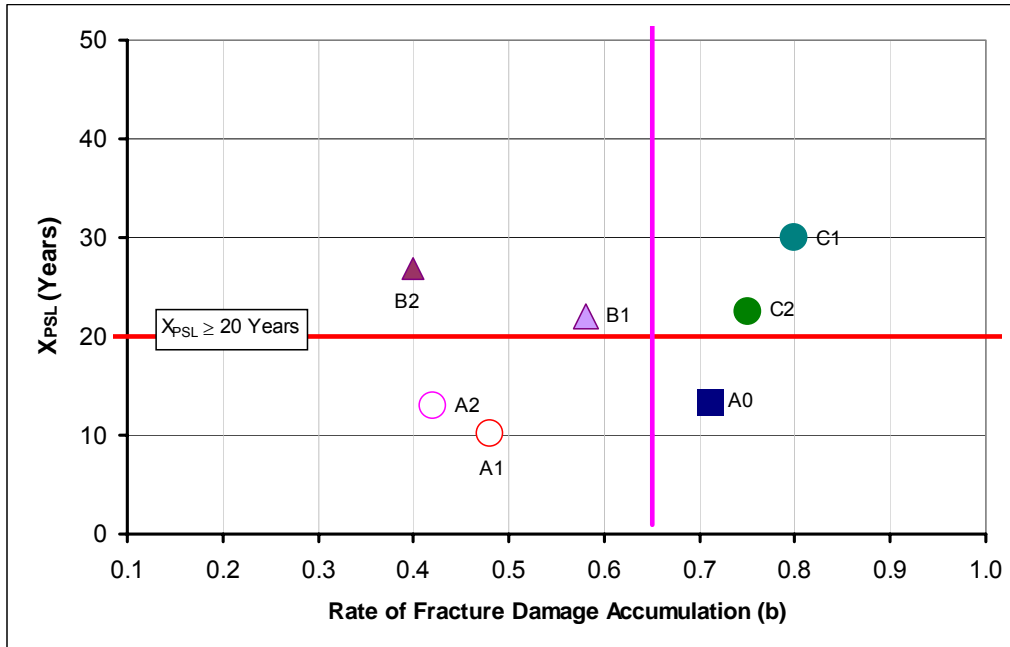


Figure E5. Rate of Fracture Damage Accumulation (b) versus X_{PSL} .